DEFORMATION BEHAVIOUR AND MARTENSITIC TRANSFORMATIONS IN METASTABLE AUSTENITIC STEELS AND LOW ALLOYED MULTIPHASE STEELS

DISSERTATION

Approved for the award of the degree of
Doktor-Ingenieur
Dr. -Ing.

Department of Materials Science and Technology
Freiberg University of Mining and Technology

By MSc. Musa Omollo Onyuna
Born 28.08.68 in Homa-Bay, Kenya

Referees: Prof. Dr.-Ing. habil. Heinrich Oettel, Freiberg
Prof. Dr.-Ing. habil. Horst Biermann, Freiberg
Prof. Dr.-Ing. Gudrun Lange, Dresden

Date of submission: 04.04.2003
Date of award: 27.06.2003

ACKNOWLEDGEMENTS

I would like to acknowledge the “Deutscher Akademischer Austausch Dienst (DAAD)” for the award of scholarship that enabled me to undertake this research work in Germany. My very special thanks to my supervisor, Prof. Dr.-Ing. habil. Heinrich Oettel for the support, astute professional and technical advice, and encouragement during the period of this work. Special thanks to Prof. Dr.-Ing. habil. Horst Biermann and Prof. Dr.-Ing Gudrun Lange for accepting to be referees for this work.

I would like to remember with warm affection the people that I worked with on a day to day basis; the laboratory staff at the Institute of Physical Metallurgy (TEM laboratory staff, the X-ray laboratory staff, and Optical Micrography staff), and the laboratory staff at the “Institut für Werkstofftechnik”, TU Bergakademie Freiberg.

Many people contributed in one way or another during the preparation of this work and it would be a monumental task to name them all and what exactly each did. To all, I say thank you very much.

I owe a great debt of gratitude to Prof. Dr.-Ing. habil. Ulrich Martin and Dr.-Ing Andreas Weiß for their invaluable professional and constructive advice that proved indispensable to me during the course of this research work.

Many thanks to my wife, Jane Omollo and children, Emmanuel C.B. Omollo and Shalom Andesia Omollo, the people that make my life worth what it is and who give the impetus for the next day and struggle.

To my Mum, Doris Arot Opondo, and Dad, Charles Riaga Onyuna, to whom I owe my very self, I dedicate this work.

To God be the glory for in this, I see his wonderful work:

Isaiah 40:18, 26, 31

To whom then will you liken God?
Or what likeness will you compare to him?
Lift up your eyes on high,
And see who has created these things...,
But those who wait on the Lord
Shall renew their strength;
They shall mount up with wings like Eagles,
They shall run and not be weary,
They shall walk and not faint.

ABSTRACT

The major aim of this research work was to study how the deformation induced martensite in metastable austenitic steels and low alloyed ferritic-bainitic steels with retained austenite affect the flow curves and the accompanying transformation plasticity. These steels exhibit attractive combinations of strength, weldability and formability. In particular, the target was to quantify the effect of various phases, the austenite-martensite transformation as they impact on the flow curves.

Commercially available metastable austenitic steel, AISI 304 (X5CrNi18.10), and specially laboratory prepared Mn-Si-Al steel were used for the experiments. Tensile specimens prepared from the metastable austenitic steel were heat treated; heated to 1050°C, held for 30 minutes and subsequently quenched in water to room temperature. The Mn-Si-Al steel was prepared from scrap, poured into ingots and cold rolled to round bars. A CCT and TTT diagram using deformation dilatometer were constructed for the Mn-Si-Al steel. This was done to help obtain optimal amounts of the microstructural components in the final structure after suitable processing conditions. On the basis of the results from the CCT diagram, a special heat treatment cycle to obtain metastable retained austenite at room temperature was prepared for the tensile specimens. Uniaxial tensile tests were carried out at different temperatures and to different levels of straining for the two steels. After testing, metallographic, X-ray, and TEM specimens were prepared from these tensile specimens for further microstructural characterisation.

Simulation of the flow curves and the effect of deformation induced martensite formed during deformation were carried out using a commercially available Finite Element Software, ANSYS56/57, from Swanson International and a modified law of mixture. This dual approach using simulation augmented with experimental data and microstructural characterisation helped improve the understanding of transformation induced plasticity in the two investigated steels.

The results of FEM simulation showed that the flow curves in AISI 304 (X5CrNi18.10) depend not only on the amount of deformed martensite but is also influenced by the constitutive relationships of the different phases, and variant conversions. Taking into consideration the extra dislocation generated during the austenite-martensite transformation using the modified law of mixture improved the agreement of experimental and simulated results but also demonstrated that other factors such as variant conversions can play a significant role in enhancing ductility and strength.

Phase transformation paths of $\gamma \rightarrow \alpha'$, $\varepsilon \rightarrow \alpha'$, and $\gamma \rightarrow \varepsilon$ which affects the rate of strain hardening and rate of decay of work hardening was shown to be vital in enhancing ductility and strength. It is also possible that the enhancement of ductility is due to the effect of phase transformation on fracture kinetics for the AISI 304 steel. For the Mn-Si-Al steel, the enhanced elongation was found to depend not only on the stability which affects the rate of transformation and amount of the transformed austenite but also on the position of the retained austenite in relationship to other phases in the microstructure which affects composite deformation. The deformation behaviour of the major phases that constitute the microstructure was found to be critical in enhancing the good mechanical properties.

The tensile properties of the Mn-Si-Al steel were promising and an overall improvement of 4-8% in maximum uniform elongation attained was attributed to phase transformations, strain hardening and composite deformation behaviour in the temperature range -80°C to 120°C.

TABLE OF CONTENTS

NOMENCLATURE AND ABREVIATIONS

a	[m^2]	Area
$\dot{a}$	[m^2/s]	Rate of phase boundary movement
A	[-]	Constant
A	[-]	Constant
A_f	[-]	Constant
Δa	[m^2]	Change in area
α	[-]	Constant, rate of shear band formation
α'	[-]	Deformation induced martensite
B	[-]	Constant
B_1	[-]	Partitioning parameter for inclusion
B_0	[-]	Partitioning parameter for matrix
B_f	[-]	Constant
β	[-]	Constant
β^s_o	[-]	Eshelby's tensor for spherical inclusion
c	[-]	Constant
C	[-]	Constant
C_c	[-]	Constant
e_c	[-]	Engineering strain
ε	[-]	True strain, hcp martensite
ε_c	[-]	Composite strain
ε_m	[-]	Matrix strain
$\bar{\varepsilon}^{o'}$	[-]	Overall plastic strain
ε^{tr}	[-]	Transformation strain
${}^g\varepsilon_V$	[-]	Local shape change
E	[MPa]	Young's modulus
f	[m^3]	Volume fraction of inclusion
F	[N]	Force
g	[-]	Normalized net thermodynamic driving force

$\bar{g}$ [-] Dimensionless mean of a given probability distribution function

g_1 [-] Dimensionless constant

g_2 [-] Dimensionless constant

G [MPa] Bulk modulus, Shear modulus

$H(\dot{\Sigma})$ [-] Heaviside function

I [-] Identity tensor

k [-] Constant

K [-] Constant

κ [-] Effective bulk modulus

M_B [K] Burst martensite start temperature

n [-] Constant

N [-] Unit deviatoric tensor

p [MPa] Pressure

P [-] Probability parameter

$\dot{p}$ [MPa/s] Rate of change of pressure

$\rho^*_{d\gamma}$ [-] Average dislocation density in deformed austenite zone due to strain-induced martensite at any composite strain

q [-] Constant

r [-] Constant that models the random orientation of shear-bands

s [-] Constant

S_g [-] Standard deviation

t [s] Time

Δt [s] Change in time

T [K] Temperature

$\overset{\nabla}{T}$ [MPa] Jaumann derivative of stress

$\bar{v}_m$ [-] Average volume of martensitic embryos per austenite volume

$\bar{v}_I$ [-] Average volume of shear band intersection

σ [MPa] Applied stress

σ_c [MPa] Composite stress

$\bar{\sigma}'$ [MPa] Equivalent stress

σ_m	[MPa]	Matrix stress
σ_y	[MPa]	Yield stress
$\dot{\gamma}_a$	[-]	Plastic shear strain rate in austenite
γ	[-]	Austenite
$\dot{\bar{\gamma}}^P$	[-]	Equivalent plastic shear strain rate
$\dot{\gamma}^T$	[-]	Total equivalent shear strain rate
$\bar{\tau}$	[MPa]	Equivalent shear stress
$\dot{\Sigma}$	[-]	Measure of the triaxiality of state of stress
ν	[-]	Poisson's ratio
$V_{d\gamma}$	[m^3]	Volume fraction of deformed austenite zone due to strain-induced martensite
$\dot{V}_\alpha$	[m^3 /s]	Rate of martensite volume evolution
$V(t)$	[m^3 /s]	Volume transformed as function of time
ΔV	[m^3]	Change in volume
V	[m^3]	Volume
V_α	[m^3]	Volume fraction of martensite (Ludwigson and Berger equation), volume fraction of ferrite
$V_{\gamma R}$	[m^3]	Volume fraction of retained austenite
V_γ	[m^3]	Volume fraction of retained austenite
$V_{\gamma o}$	[m^3]	Volume fraction of retained austenite before deformation
$V_{\alpha'}$	[m^3]	Volume of deformed martensite
V_α	[m^3]	Volume of ferrite
V_{sb}	[m^3]	Volume fraction of shear band
FEM		Finite element method

CHAPTER 1

1 INTRODUCTION

1.1 MOTIVATION AND AIM

Since 1970, the automotive industry has been faced with increasing pressure from environmental groups to increase automobile efficiencies and reduce emissions [Cut99, Mat02]. To date the most effective methods of reducing automobile emissions have been improving the combustion cycle (generally raising the temperature of combustion), introducing post-combustion processes (such as catalytic converters), and making vehicles lighter [Cut99].

In the 1970s, the first significant reduction in emissions came because of fundamental improvements in engine design. This resulted in reduction of nitrogen oxides and hydrocarbon vapours content in exhaust gases. The next major milestone in vehicle emissions control technology came in 1980 and 1981 with the introduction of control systems utilizing catalysts to convert carbon monoxide and hydrocarbons to carbon dioxide and water [Cut99].

The automotive manufacturers have now turned to new technologies to make vehicles lighter. A significant part of this effort includes the substitution of Al and Mg alloys for engine, chassis, and body components, which have traditionally been formed or cast in ferrous alloys. The challenge for the steel industry is to develop steels with enhanced strength without compromising formability and performance so that thin sheets can be used for various components.

The steel industry responded to this demand for new steels in the last 20 years by introducing new steel categories as the high strength low alloy steels (HSLA), the interstitial free high strength steels (IF-HS), and the dual phase steels (DP-steels) [Vas02]. The HSLA steels gain their strength from precipitation hardening and grain refinement.

DP steels gain their strength from the two-phase microstructure (70-95% ferrite and 5-30% martensite). The IF-HS steels gain their strength and their good formability from solid solution strengthening and precipitation hardening [Vas02]. However, in the last 10 years, there has been a great focus on low alloy multiphase steels with metastable retained austenite. These steels exhibit enhanced strength and ductility which promises to be pivotal in cold formability of automotive components to reduce weight.

The favourable mechanical properties of these steels due to transformation of metastable retained austenite to martensite during deformation have so far been realized under restricted working environments [Mat02]. It is desirable, however, to obtain the favourable mechanical properties under arbitrary working environments and to utilize these properties of the phase transformations in designing new alloys and to be able to predict the mechanical behaviour of materials undergoing such phase transformations. It is also important to know the transformation strengthening mechanisms in order to control and predict strength/formability balance. The new interest in deformation induced martensitic transformations in low alloy multiphase steels centres on the mechanical properties of the transformation as a deformation mechanism [Mar97]. In non-thermoelastic systems, this can provide enhanced ductility, toughness, formability and deep-drawability. These properties are very desirable to the automotive industry.

The main aim of this work was, therefore, to study how transformation induced plasticity accompanying deformation induced martensitic transformations in metastable austenitic steel and in low alloyed Mn-Si-Al multiphase steel affect the flow curves. The different microstructures that results from different processing and loading conditions were been investigated and characterised. Special considerations have been given to the appearance of ε-martensite and α'-martensite so that the transformation reaction paths: $\gamma \rightarrow \varepsilon \rightarrow \alpha'$, $\gamma \rightarrow \varepsilon$, $\varepsilon \rightarrow \alpha'$, $\gamma \rightarrow \alpha'$, could be ordered and the possible transformation path and mechanism determined. A central theme in this work was the investigation of Transformation Plasticity phenomenon in low alloy Mn-Si-Al multiphase steel and in metastable austenitic steel, AISI 304 (X5CrNi18.10). The steel AISI 304 offers an opportunity to study deformation induced martensitic transformation where only metastable austenite is present while in low alloy Mn-Si-Al multiphase steel the retained austenite exists together with other phases.

The possibilities to compare and apply the results of AISI 304 in the case of low alloy Mn-Si-Al multiphase steel necessitated the selection of these two steels. The transformation plasticity mechanisms in the selected steels have been investigated and factors that favour improved properties pointed out. The transformation plasticity phenomenon has been related to microstructural features and its strengthening mechanisms investigated.

The resulting flow curves have been simulated using finite element method and a modified law of mixture. The numerical simulations in the case of non-thermoelastic martensitic transformation presented here serve as a tool to study the role of various phases in terms of their stress-strain relationships, and hardening as they impact on the flow stresses. A better understanding of transformation plasticity mechanism and strengthening was obtained by combining the finite element method and the modified law of mixtures.

In particular, to investigate the intractability of transformation induced plasticity, the following have been done;

- Melting and hot rolling of low alloy Mn-Si-Al multiphase steel at the Institute of Iron and Steel Technology and the Institute of Metal Forming at TU Bergakademie Freiberg. Heat treatment of metastable austenitic stainless steel and Mn-Si-Al multiphase steel.
- Characterisation of the microstructure before and after uniaxial tensile testing for the two selected steels.
- Characterisation of deformation induced martensite.
- Characterisation of the flow curves.
- Simulation of the flow curves using finite element method and a modified law of mixture.

1.2 OUTLINE

The research work is presented in seven chapters. The first chapter contains the background, motivation and aim of this research work. The second chapter gives a brief overview of low alloy high strength steels in terms of processing, transformation kinetics, microstructure, fatigue behaviour and how retained austenite affects their properties. Chapter 3 gives an overview of some important transformation plasticity models documented in literature.

These models are discussed and their suitability in capturing, understanding, and predicting the transformation plasticity phenomenon are presented. The possibility of using these models to predict the flow curves of metastable austenitic and high strength multiphase steels have also been discussed. Finally a modified Goel model (law of mixture model) has been proposed to help in understanding the mechanism of transformation plasticity and in predicting the flow curves.

Chapter 4 gives an overview of the experimental work carried out. Details of the experiments carried out and equipments used are presented in this chapter.

To help in microstructural characterisation, optical microscopy, magnetic measurements, transmission electron microscopy, micro-hardness measurements, and X-ray diffraction analysis experiments were performed. Dilatometer tests were carried out to help in design of heat treatment process that could guarantee retained austenite in the low alloy high strength Mn-Si-Al multiphase steel. The flow curves were generated by uniaxial testing at different temperatures for the two tested steels.

In Chapter 5, the results of these experiments are presented and discussed. In Chapter 6, the results of simulation of the flow curves with special consideration of transformation plasticity are presented and discussed. In applying the finite element method and the modified law of mixture, we sought to apply continuum mechanics principles to the continuum length scale of heterogeneities of multiphase materials, thus placing the microstructure-mechanics relationship on a quantitative basis. The main emphasis was on the predictive capability of microstructural variations on the ductility and strength of multiphase materials. Since flow stress and ductility are often accepted as the main parameters controlling cold-formability, therefore, there is a great desire to model combination of properties which will respond with required precision in engineering service using the microstructure-mechanics paradigm. Chapter 7 gives a summary of this work chapter by chapter, recapitulating the major points in each.

CHAPTER 2

2 TECHNOLOGICAL ASPECTS OF MULTIPHASE HIGH STRENGTH STEELS

2.1 INTRODUCTION

Martensitic transformations in solids have been known for a long time. Because of its enormous potential applications, research on it has been sustained with great interest over the years. A martensitic transformation involves the coherent formation of one phase from another without change in composition by a diffusionless, homogeneous lattice shear [Sin89]. Different types of martensitic transformation in both ferrous and nonferrous alloys have been recognised which may be distinguished from one another by kinetics, morphology, and crystallography or internal structure.

Some typical characteristics of martensitic transformation are outlined below:

- Athermal martensitic transformation - In this type of transformation, the reaction proceeds only while the temperature is changing and the nucleation process occurs without thermal activation.
- Isothermal martensitic transformation - The transformation occurs at constant temperature characterised by slow nucleation but extremely rapid growth. The number of nuclei of martensite formed depends on both temperature and time, increasing with time at a particular reaction temperature.
- Burst martensitic transformation - In this type, the transformation starts suddenly (at M_B) and a large volume fraction of martensite gets formed in a single event (within milliseconds), a burst.
- Mechanically induced martensitic transformation - The deformation-induced martensitic transformation has been classified into two modes, namely stress-assisted martensite and strain-assisted martensite based on the origin of nucleation sites that initiate the transformation.

The transformation induced plasticity (TRIP) which depends of the thermodynamic stability of austenite phase was first investigated in high alloyed Chromium Nickel steels by Zackay and co-workers [Zac67]. Transformation induced plasticity has been defined as a significantly increased plasticity during a phase change [Fis00]. The phenomenon of transformation induced plasticity has been observed in steels and other alloys [Fis00]. When a martensitic transformation occurs under applied stress, a macroscopic strain, termed transformation plasticity, accompanies the transformation. This strain has been attributed to a biasing of the martensitic-plate variants which form under stress [Ols82].

Low alloy multiphase steels that have metastable austenitic phase possess favourable mechanical properties such as high strength, ductility and toughness due to deformation induced martensitic transformation. The deformation behaviour of such steels depends among other things strongly on the deformation induced martensitic transformation and the deformation behaviours of the individual micro-constituents. When martensitic transformation takes place in the elastic region, it does not always result in improved properties. This is very often the case in heat treatment and quenching of steel. After heat treatment most component are normally tempered to improve toughness. However, when the martensitic transformation occurs in the plastic region, it may result in enhanced ductility and hence better formability.

Martensitic transformation in solids is considered as a first order phase transition occurring without diffusion and is accompanied by an inelastic strain called the transformation strain which results from two contributions: the lattice variant Bain strain and the lattice invariant strain which may be slip or twinning [Sin89, Fis00]. The Bain strain describes the geometrical transformation from the parent fcc lattice (austenite) to the product bct or bcc lattice (martensite). The lattice invariant strain is an accommodation step relaxing the internal stresses generated by the Bain strain through a shear along an invariant plane resulting in the formation of a habit plane. Due to the high symmetry of the austenitic lattice, several Bain strain components are possible so that different martensitic variants may be formed with the corresponding habit planes and transformation strains. To minimise the strain energy the martensite forms as thin plates on particular crystallographic planes known as the habit plane. In the absence of hydrostatic stress state, a preferred orientation in Bain strain components will take place.

2.2 PROCESSING OF HIGH STRENGTH STEELS

The attractive properties of transformation-induced plasticity steels have generated considerable scientific and industrial interest since it was first reported by Zackay and co-workers [Zac67]. The transformation-induced plasticity steels developed by Zackay and co-workers is processed by solution treatment (1120°C), ausforming (450°C, 80%), and subzero cooling. Currently, two principal thermomechanical methods have been developed and industrially tested. The first method involves intercritical annealing of a cold rolled product combined with a holding period in the bainite field for obtaining cold rolled high strength multiphase steels. The other method involves austenite hot rolling combined with a holding period in the ferrite field followed by deformation in the bainitic range to obtain hot rolled high strength multiphase steel [Ble98, Jac98]. The final structure is composed of bainite, ferrite, retained austenite and may be ausformed martensite. For the first method, during stage one annealing process, two distinct transformations take place: the deformed ferrite matrix recrystallises and austenite forms. During stage two, bainite is formed and only a part of the austenite is retained at room temperature as metastable austenite while the other part transforms into martensite [Ble98, Jac98]. However, difficulties in actual production of low alloy high strength multiphase steels still exist. In general, higher levels of Si and Mn are required to manufacture hot rolled multiphase steels. The high levels of Si present casting difficulties, affect the surface quality by the appearance of “red scale” defects and present difficulties during hot dip galvanising by lack of wetting and formation of a fragile intermetallic layer. Several modifications of thermomechanical methods have been proposed [Pic98, Jac98, Ebe98, Par98].

2.3 TRANSFORMATION KINETICS

The stress-strain relationship accompanying the martensitic transformation during deformation was first analysed by Ludwigson and Berger [Lud69]. The amount of deformation-induced martensite was proposed to be a function of strain. The observed work hardening was proposed to be a summation of the work hardening of austenite and the hardening due to martensite.

The following expression was given by Ludwigson and Berger:

$$V_{\alpha'} = A e^{B} V_{\gamma} \tag{2.1}$$

where $V_{\alpha'}$ is the volume fraction of martensite, e is the engineering strain, V_{γ} is the instantaneous volume fraction of austenite, A is a constant and the exponent B is ≈ 3 for stainless steels.

Two views have been proposed on the role of plastic deformation of austenite on the deformation-induced martensitic transformation. One view proposed by Olson and Cohen [Ols75] is that the kinetics of deformation-induced martensitic transformation is a function of strain. The following expression was given:

$$V_{\alpha'} = 1 - \exp\left\{-\beta\left[1 - \exp(-\alpha\varepsilon)\right]^{n}\right\} \tag{2.2}$$

where $V_{\alpha'}$ the volume fraction of martensite, ε is the strain and α, β, n are constants.

The expression (Equation (2.2)) was modified by Stringfellow, Parks and Olson [Str91] to take into account the stress state at the shear band intersections. They gave the rate of martensitic volume evolution as:

$$\dot{V}_{\alpha'} = (1 - V_{\alpha'})\left(A_f \dot{\gamma}_a + B_f \dot{\Sigma}\right) \tag{2.3}$$

where $\dot{V}_{\alpha'}$ is the rate of martensite volume formed, $V_{\alpha'}$ is the volume of martensite formed and

$$A_f = \alpha\, \beta_0\, r(1 - V_{sb})(V_{sb})^{r-1} P \tag{2.4}$$

$$B_f = \frac{g_2}{\sqrt{2\pi}} \beta_0 (V_{sb})^{r} \exp\left[-\frac{1}{2}\left(\frac{g - \overline{g}}{s_g}\right)^2\right] H(\dot{\Sigma}) \tag{2.5}$$

where $\beta_0 = C\,\overline{v}_m / \overline{v}_I$, V_{sb} is the volume fraction of shear bands, $\dot{\gamma}_a$ is the plastic shear strain rate in austenite, α is the rate of shear band formation, $\overline{v}_m$ is the average volume of martensitic embryos per austenite volume, $\overline{v}_I$ is the average volume of a shear band intersection, C is a geometric constant, g is the normalised net thermodynamic driving force, $\overline{g}$ is a dimensionless mean of a given probability distribution function, s_g is the standard deviation, $H(\dot{\Sigma})$ is the Heaviside step function, $\dot{\Sigma}$ is a measure of the “triaxiality” of state of stress given by $\Sigma\left(\frac{\dot{p}}{p} - \frac{\dot{\tau}}{\tau}\right)$ and $\Sigma = \frac{-p}{\sqrt{3}\dot{\tau}}$, r is a constant that models a random orientation of shear-bands.

P is a probability parameter (probability of a shear band intersection acting as a nucleus). $\dot{p}$ and p are pressure rate and pressure respectively. $\dot{\tau}$ and τ are equivalent shear stress rate and equivalent shear stress respectively. The transformation kinetic equation proposed by Stringfellow, Parks and Olson contains very many parameters that need to be known beforehand and this limits its practical application.

The second view proposed by Tamura and co-workers [Tam82] is that the kinetics of deformation-induced martensitic transformation is a simple function of stress. The volume fraction martensite transformed was suggested to be proportional to the increase in the mechanical driving force. Tamura explained the decrease of critical applied stress to initiate martensitic transformation on the fact that austenite deforms plastically thus concentrating stress at obstacles and grain boundaries, twin boundaries and this concentration of stress becomes equivalent to the critical stress to initiate martensitic transformations. The transformation kinetic reaction from austenite to α'-martensite has been extensively studied compared to austenite-ε-martensite phase transformation. To the knowledge of the author, the only study devoted to the kinetics of strain-induced fcc-hcp martensitic transformation was done by Remy [Rem77].

2.4 MICROSTRUCTURE OF MULTIPHASE HIGH STRENGTH STEELS

Dual phase and multiphase high strength steels can be classified into three types according to the microstructure as shown in Figure 2.1 [Tsu00]. In type I, the microstructure is composed of austenite and martensite formed during deformation. In type II, the microstructure is composed of retained austenite in tempered martensite matrix and type III where the microstructure is composed of bainite, retained austenite and ferrite. The deformation behaviour is very much dependent on the microstructure as well as the deformation induced martensitic transformation. Bleck et al. [Ble98] in their review of TRIP Steels pointed out that it is the phase dependent fine microstructure difference in different areas with local chemical composition and local mechanical properties that is responsible for the favourable cold formability in TRIP Steels. The carbon content in retained austenite before and after straining has been reported to remain relatively constant [Lun02].

For alloyed high strength steels with high amounts of chromium and Nickel, strength and strain values were reported to increase with increased amount of martensite transformed. It has also been pointed out that different martensitic transformations can take place i.e. fcc austenite can transform to hcp martensite, hcp martensite can transform to bcc martensite and austenite can transform straight to bcc martensite [Wei01]. The retained austenite decreases with increase in strain during transformation. The parameters for quantitative microstructural characterisation have been given as grain size, phase volume fraction, local chemical compositions and phase stability. For low alloy high strength multiphase steels, the author has not come across M_s^{σ} that have been experimentally determined.

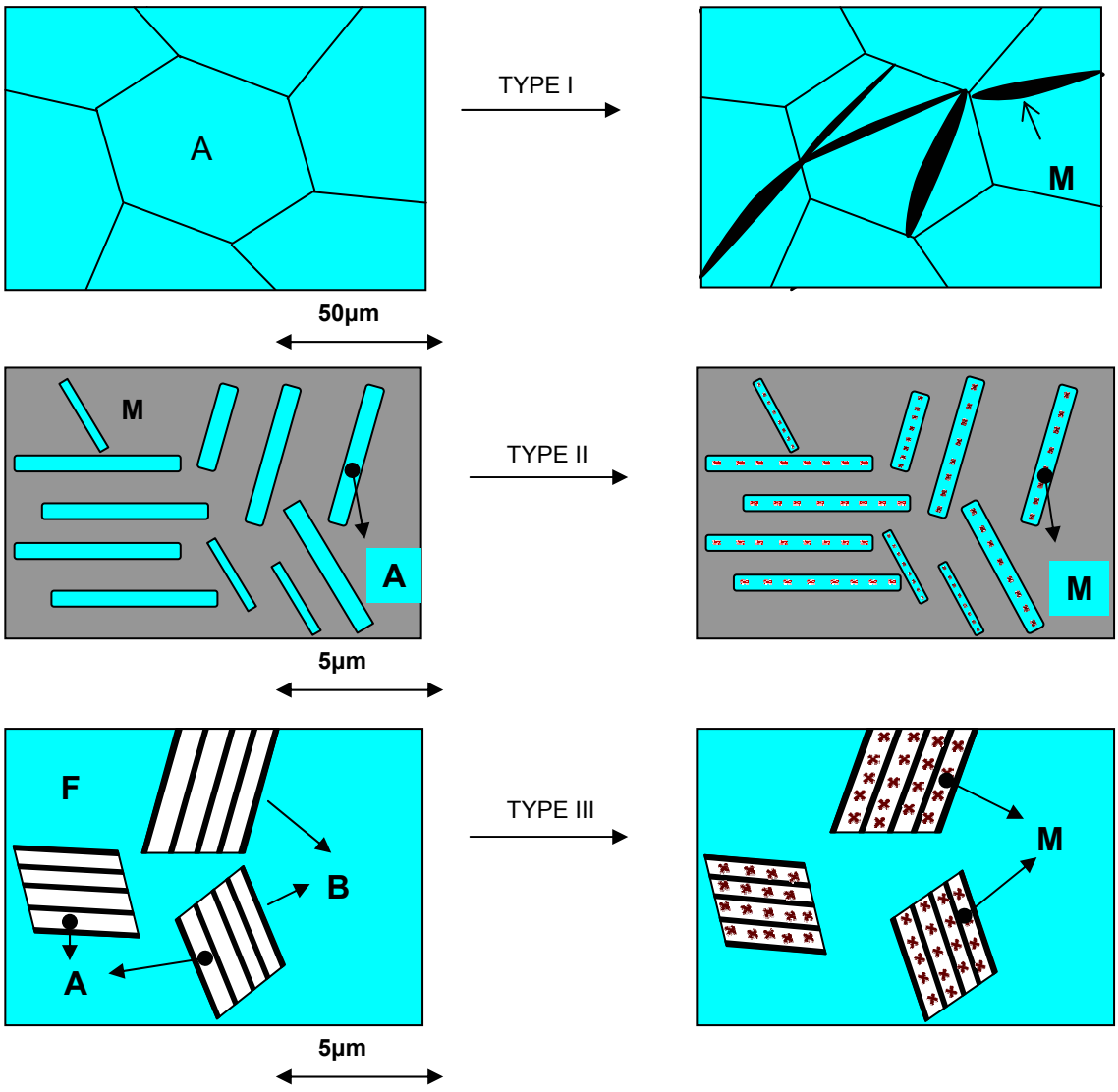

Figure 2.1 Types of TRIP Steels, adapted from [Tsu00]; A, B, F, and M are retained austenite, bainite, ferrite and martensite phases respectively.

2.5 FATIGUE BEHAVIOUR OF MULTIPHASE HIGH STRENGTH STEELS

On strain rate, it is generally accepted that when specimens are deformed in air or in gas atmosphere, transformation plasticity occurs less readily with increased strain rate. Studies have been made on fatigue behaviour of metastable austenitic steels accompanying the martensitic transformation during cyclic stressing [Tam82, Sch00]. Under conditions of controlled stress amplitude, metastable austenitic steels exhibit superior fatigue properties than stable austenitic steels [Sch00]. This is because strength is increased by deformation-induced martensite. Under controlled strain-amplitude conditions, the fatigue life is reduced by deformation-induced martensite because of gradual increase in the stress applied. The high triaxiality of the stress state at the crack tip promotes the martensitic transformation.

On low temperature fatigue of high nitrogen austenitic steel, Vogt et al [Vog90] found out that the deformation mechanisms of austenitic stainless steel are planar in nature. Both α'-martensite and ε-martensite were observed. It was suggested that ε-martensite forms as a transition phase when austenite transforms to α'-martensite. For low temperature fatigue of 316L and 316LN austenitic stainless steels, a decrease in temperature was observed to favour planar slip. ε-phase has been reported to be relatively stable at low temperature. α'-martensite forms at the intersections of bands of ε-martensite.

TRIP Steels containing 10% retained austenite and having elongation of about 34% have been reported to have a better fatigue strength than Dual-Phase steel containing ferrite and martensite and precipitation-hardened low alloy high strength steels (HSLA) [Yok96].

2.6 EFFECT OF RETAINED AUSTENITE AND ALLOYING ELEMENTS ON MULTIPHASE HIGH STRENGTH STEELS

Relation between transformation plasticity and retained austenite has been studied by several workers [Tam82, Zar97, Kru02] in terms of volume fraction, effect of prior deformation, mechanical stability, composition, morphology, size and distribution. It is generally agreed that retained austenite affects press-formability, stretch-formability, deep drawability and absorbed impact energy.

Elongation has been reported to be marked decreased with increase in the degree of prior deformation of austenite. However, the transformation plasticity phenomenon is clearly independent of the amount of prior deformation if a comparison is made between the difference between peak elongation and austenite elongation above M_d.

Niobium bearing multiphase steels has been studied by several workers [Par97, Chi97]. The element Nb has been reported to enable Mn-Si TRIP Steels to be processed by a variety of thermomechanical processing routes. It has been reported that more than 30% retained austenite is necessary to obtain a marked increase in strength and ductility in Fe-Ni-C alloys. Park et al. [Par97] reported that continuous cooling is not effective to form adequate amount of retained austenite and that bulky granular type retained austenite transforms more easily during tensile test. This type of grain was reported to be easily obtained when final rolling is performed in the temperature range 800°C-850°C followed by water cooling. Chiro et al. [Chi97] varied the state of retained austenite; volume fraction, solute enrichment and mechanical stability by varying the isothermal bainite hold conditions (temperature and time).

The highest volume fraction of retained austenite (9.5%) with optimum mechanical properties was obtained at a holding temperature of 400°C for a holding time of 5 minutes. Hanzaki et al [Han97a] reported that the volume fraction of retained austenite depends very much on bainite transformation temperature and holding time in Si-Mn TRIP Steels with and without Nb alloying. Several researchers [Tra02, Mah02, Tim02] have also looked into the possibility of replacing silicon with other elements like aluminium, copper, phosphorus, molybdenum and niobium. Aluminium [Mah02] has been reported to increase uniform elongation while tensile strength remains unaffected. Phosphorus and copper have been reported to increase tensile strength by increasing the ferrite hardness and the amount of bainite formed [Tra02]. Aluminium helps in the formation of acicular ferrite and granular bainite which helps in increasing the tensile strength. Molybdenum (Mo) additions have been reported to increase the ultimate tensile strength [Tim02].

CHAPTER 3

3 TRANSFORMATION PLASTICITY MODELS

3.1 INTRODUCTION

The study of the constitutive equations for multiphase high strength steels is much less developed as compared with shape memory alloys [Che00]. A lot of work has been carried out on prediction of the kinetics of the strain induced martensitic transformation for various loading cases. Dynamics of phase transformations considering the movement of interfaces has also been attempted by several workers on thermoelastic and non-thermoelastic martensitic transformations [Che00, Rei97]. Attempts have been made to relate stress and strain for materials undergoing phase transformations and to account for the accompanying transformation-induced plasticity over the years. Studies of plastic flow at different strain levels have been carried out extensively for single phase materials (apart from dispersion hardening alloys where the volume fraction of the second phase is small). An overview of some models in literature on this subject is presented below.

3.1.1 Anderson and Bishop Model

Anderson and Bishop [Wer87] investigated transformation plasticity in Uranium when subjected to Neutron rays. They proposed the following relationship relating stress and strain:

$$\varepsilon \approx \frac{5}{4}\frac{\sigma}{\sigma_y} g_{\varepsilon_v} \tag{3.1}$$

where σ_y is the yield stress, σ is the applied stress, and g_{ε_v} is the local shape change due to neutron rays.

Yielding was assumed to occur according to von Mises criterion. The material was taken to be ideal plastic with equally distributed orientation under homogeneous deformation. This model is useful when the applied stresses are small compared to the yield stress.

3.1.2 Greenwood and Johnson Model

Greenwood and Johnson [Gre65] investigated deformation of metals under small stresses during phase transformations. They deduced that, for a complete cycle through the transformation temperature, the resultant deformation varies linearly with the applied stress (provided the stress is small), the fractional volume change on transformation and inversely as the flow stress of the weaker phase. The total permanent strain per complete cycle was given as:

$$\varepsilon = \left\{5\sigma\left(\frac{\Delta V}{V}\right)\right\} \Big/ 3\sigma_y \tag{3.2}$$

where σ is applied stress, $\frac{\Delta V}{V}$ is volume dilatation, σ_y is the yield stress of the weaker phase and ε is the strain developed. This model does not consider the orientation distribution of the new phase. This model is applicable to thermoelastic transformations when the temperature is changing. Direct application of this model in the case of non-thermoelastic transformations involving large stresses may not yield reasonable results.

3.1.3 Abrassart Model

Abrassart [Wer87] assumed an equally distributed square lattice as shown in Figure 3.1 below.

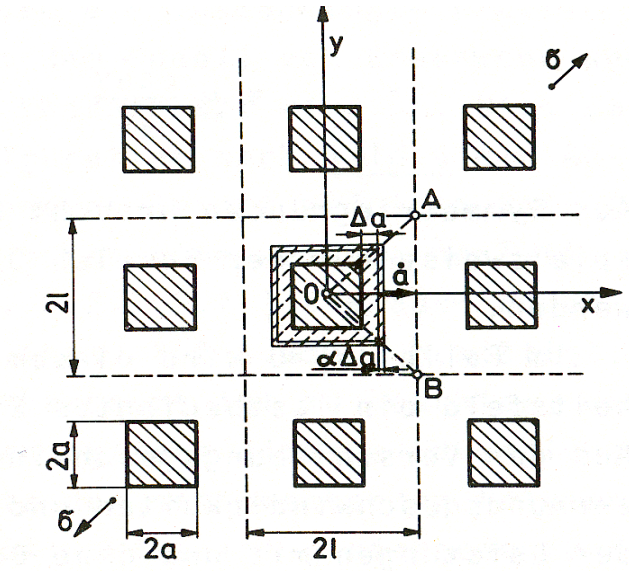

Figure 3.1 Schematic representation of Abrassart model [Wer87].

where $\dot{a}$ is the rate of phase boundary movement, same in x and y directions, ε^{tr} is the transformation strain and Δa is the transformed area

The Displacement rate is given as $\approx \varepsilon^{tr} \frac{\Delta a}{\Delta t}$, after time t.

Displacement in the x and y directions are given respectively as:

$$u = \varepsilon^{tr} \frac{a\dot{a}}{x} \tag{3.3}$$

$$v = \varepsilon^{tr} \frac{a\dot{a}y}{x^2} \tag{3.4}$$

The total plastic strain in loading direction, which is diagonal direction, is given as,

$$\varepsilon = \frac{3}{4} \frac{\Delta V}{\sigma_y} \left(V(t) - \frac{2}{3} V(t)^{3/2} \right) \sigma \tag{3.5}$$

where ΔV is the volume change due to transformation plasticity, σ_y is the yield stress of the matrix, and $V(t)$ is the transformed volume fraction as a function of time. This model may not be used for diffusionless transformations like martensitic transformations because of the time factor.

3.1.4 Magee Model

The model presented by Magee [Wer87] considered the effect of all orientations during transformation. Diagrammatically, the model is shown in Figure 3.2 below;

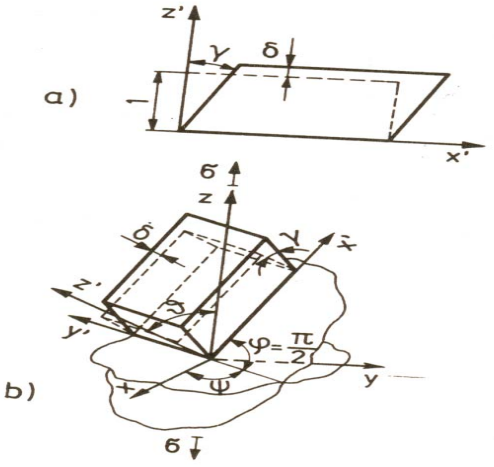

Fig 3.2 Schematic representation Magee Model [Wer87].

The local shape distortion due to transformation is given by the tensor T.

$$T = \begin{pmatrix} 0 & 0 & \gamma/2 \\ 0 & 0 & 0 \\ \gamma/2 & 0 & \delta \end{pmatrix} \tag{3.6}$$

where γ and δ are invariant shear and dilatation respectively.

Strain in the loading direction according to tensor transformation rules is given by:

$$\varepsilon_{ZZ}(\vartheta,\varphi) = \frac{1}{2}\left[\gamma \sin 2\vartheta \sin\varphi + \delta(1+\cos 2\vartheta)\right] \tag{3.7}$$

For complete martensite transformation in the loading direction considering all orientations, the global strain is given as:

$$\varepsilon = \frac{\int_0 \varepsilon_{ZZ}{}^{\sigma} f(\vartheta) d\vartheta}{\int_0 {}^{\sigma} f(\vartheta) d\vartheta} \tag{3.8}$$

where ε is the strain and ${}^{\sigma} f(\vartheta)$ is the partition function proportional to the work done.

In this model, the transformation strain is independent of external applied stress and the effect of plastic accommodation during martensite formation is neglected.

3.1.5 Werner and Fischer Model

Werner and Fisher [Wer87] assumed a beam model in which the austenite transformed to martensite as spheres evenly distributed throughout the specimen. Solid-ideal plastic behaviour was assumed with constant strain in all the micro-regions. The applied load was assumed constant as the transformation takes place.

For plastic transformation accompanied by volume change, the following equation was proposed as:

$$\varepsilon = \varepsilon_{IA} + \varepsilon_{IB} \approx C_G \Delta V \left(\frac{C_I}{\sigma_{YA}} + \frac{C_{II}}{\sigma_{YB}} \right) \sigma \tag{3.9}$$

where ε is the strain, ΔV is the volume change, C_G is the factor determining the orientation distribution of phase boundaries, and A, B are the phases involved.

For plastic transformation accompanied by shape change, the following equation was proposed:

$$\frac{\sigma}{\sigma_y} = \frac{\int_{\varphi=0}^{2\pi}\int_{\vartheta=0}^{\pi}\omega(\vartheta,\varphi)g(\vartheta,\varphi,\sigma)\sin\vartheta d\vartheta d\varphi}{\int_{\varphi=0}^{2\pi}\int_{\vartheta=0}^{\pi}g(\vartheta,\varphi,\sigma)\sin\vartheta d\vartheta d\varphi} \tag{3.10}$$

where σ is the applied stress, σ_y is the yield stress of the matrix, $g(\vartheta,\varphi,\sigma)$ is a weighting function that determines the orientation distribution of the local co-ordinate system, and $\omega(\vartheta,\varphi)$ is a function that gives the strain.

This model allows the effect of special orientations to be considered (Magee Effect) but in case these orientations do not occur, this model is equivalent to Greenwood-Johnson model with an additional shear term. The model does not consider the case where the applied load is changing and the temperature is constant throughout the transformation.

3.1.6 Stringfellow-Parks-Olson Model

The constitutive model proposed by Stringfellow-Parks-Olson [Str92] consists of two parts; a transformation kinetics law describing the evolution of the volume fraction of martensite and a constitutive law defining the flow strength of the evolving two-phase composite. The rate of increase in the volume fraction of martensite is given in Chapter 2 (Equations. (2.3), (2.4), and (2.5)) as:

$$\dot{V}_{\alpha'} = (1-V_{\alpha'})(A_f\dot{\gamma}_a + B_f\dot{\Sigma})$$

where,

$$A_f = \alpha\,\beta_0 r(1-V_{sb})(V_{sb})^{r-1}P$$

$$B_f = \frac{g_2}{\sqrt{2\pi}}\beta_0(V_{sb})^r \exp\left[-\frac{1}{2}\left(\frac{g-\bar{g}}{s_g}\right)^2\right]H(\dot{\Sigma})$$

where,

$$\beta_0 = C\,\bar{\nu}_m/\bar{\nu}_I$$

V_{sb} is the volume fraction of shear bands, $\dot{\gamma}_a$ is the plastic shear strain rate in austenite, α is the rate of shear band formation, $\bar{v}_m$ is the average volume of martensitic embryos per austenite volume, $\bar{v}_I$ is the average volume of a shear-band intersection, and C is a geometric constant.

The stress rate invariants are given constitutively by,

$$\dot{\bar{\tau}} = \frac{1}{2}\overset{\nabla}{T}.N = G\left(\beta\dot{\gamma}^T - \dot{\bar{\gamma}}^P\right) \tag{3.11}$$

$$\dot{P} = -\frac{1}{3}\overset{\nabla}{T}.I = -K\left(\dot{e}_V^T - \dot{e}_V^P\right) \tag{3.12}$$

where $\overset{\nabla}{T}$ is the Jaumann derivative of stress, N is a unit deviatoric tensor coaxial with the stretching tensor, I is an identity tensor, $\dot{\gamma}^T$ is the total equivalent shear strain rate, and $\dot{\bar{\gamma}}^P$ is the equivalent plastic shear strain rate.

The evolution of stress with strain is given as,

$$\dot{\bar{\tau}} = G'\left[\beta\dot{\gamma}^T - \left\{V\dot{\gamma}_m + (1-V)\dot{\gamma}_a\right\} - A(1-V)\left(A_f\dot{\gamma}_a + K'C_f\dot{e}^T\right)\right] \tag{3.13}$$

$$\dot{p} = -K'\left[\dot{e}^T - \Delta V(1-f)\left(A_f\dot{\gamma}_a + D_f\dot{\bar{\tau}}\right)\right] \tag{3.14}$$

where,

$$C_f = B_f/\sqrt{3}\,\dot{\tau}$$
$$D_f = B_f P/\sqrt{3}\,\dot{\tau}^2$$
$$G' = G/\left[1 + G(1-V)A\,D'_f\right]$$
$$K' = K/\left[1 + K(1-V)\Delta V\,C_f\right]$$
$$A'_f = A_f\left[1 - K'(1-V)\Delta V\,C_f\right]$$
$$D'_f = D_f\left[1 - K'(1-V)\Delta V\,C_f\right]$$

This model is excellent because it gives the evolution of stress with strain with consideration of transformation kinetics. It may be observed, however, that there are other nucleation processes that function in addition to the main shear-band intersection mechanism. The actual strain in the austenite might be less than the measured total strain. This is because shape change of the transformation contributes to the overall plastic strain. The influence of stress on spontaneous nucleation may not apply to nucleation by the shear-band intersection mechanisms and the local stress may not be equal to the macro or measured total stress. This model has many constants which require careful experimentation for their determination and thus hinders straightforward application.

3.1.7 Tsuchida-Tomota Model

Tsuchida and Tomota [Tsu00] presented a micromechanical model combining the Eshelby inclusion theory, the Mori-Tanaka mean field theory and the Weng secant method that could capture the behaviour of the three types of TRIP steels. In the Tsuchida-Tomota model (hereby referred to as TT model) the stress-induced transformation kinetics is given as a function of overall plastic strain by the equation:

$$V_\gamma = \frac{V_{\gamma 0}}{1+\left(k/q\right)V_{\gamma 0}\left(\bar{\varepsilon}^{p*}\right)^q} \tag{3.15}$$

where V_γ is the volume fraction of retained austenite, $V_{\gamma 0}$ is the volume fraction of retained austenite before deformation, $\bar{\varepsilon}^{p*}$ is the overall plastic strain, and k,q are constants. The stress-strain curves for austenite and martensite in metastable austenitic steel were approximated by the experimental tensile properties obtained at 353 K and 77 K respectively and approximated by the Swift equation:

$$\bar{\sigma}' = a\left(b+\bar{\varepsilon}^{0'}\right)^N \tag{3.16}$$

where $\bar{\sigma}'$ is the equivalent stress, $\bar{\varepsilon}^{0'}$ is the equivalent plastic strain, and a,b,N are constants. Stress or strain partition parameter was given by the equation:

$$B_0^s = \frac{\beta_0^s\left(\mu_1-\mu_0^s\right)+\mu_0^s}{\left(f+(1-f)\beta_0^s\left(\mu_1-\mu_0^s\right)\right)+\mu_0^s} \tag{3.17}$$

where f is the volume fraction of inclusion, β_0^s is Eshelby's tensor for spherical inclusions, μ is the shear modulus, and ν^s is the Poisson ratio. Eshelby's tensor is given as:

$$\beta_0^s = 2\left(4-5\nu^s\right)/15\left(1-\nu^s\right) \tag{3.18}$$

where $0,1,s$ are subscripts indicating the matrix, inclusion and values for the secant modulus. The TT model supposes that the partitioning parameter varies with deformation and therefore, three stages of deformation were presented with three different equations as below;

Stage I - Elastic deformation

In this stage the matrix and inclusion deform elastically and the effective bulk(κ), shear(μ), and Young Modulus (E) are given as:

$$\frac{\kappa}{\kappa_0} = 1 + \frac{f(\kappa_1 - \kappa_0)}{(1-f)\alpha_0(\kappa_1 - \kappa_0) + \kappa_0} \tag{3.19}$$

$$\frac{\mu}{\mu_0} = 1 + \frac{f(\mu_1 - \mu_0)}{(1-f)\beta_0(\mu_1 - \mu_0) + \mu_0} \tag{3.20}$$

$$E = 9\kappa\mu/3\kappa + \mu \tag{3.21}$$

Stage II- Elastoplastic deformation

If the matrix yields first, the equivalent stress is given as below,

$$\bar{\sigma}' = \frac{a_0\left(b_0 + \varepsilon^{p*(0)}\right)^{N_0}}{B_0^s} \tag{3.22}$$

If the inclusion yields first, the equivalent stress is given as below,

$$\bar{\sigma}' B_1 = a_1\left(b_1 + \frac{\bar{\varepsilon}^{p*}}{f B_1}\right)^{N_1} + \frac{3\mu_0(1-\beta_0)(1-f)}{f\,\bar{\varepsilon}^{0'}} \tag{3.23}$$

where $\bar{\varepsilon}^{p*}$ is the overall plastic strain and B_1, B_0 are partitioning parameter for matrix and inclusion respectively.

Stage III- Plastic deformation

In this stage both constituents deform plastically. The equivalent stress is given by simultaneous equations as:

$$\bar{\sigma}' B_1^s + 3\mu_0^s\left(1-\beta_0^s\right) f B_1^s \varepsilon^{p*(1)} = a_0\left(b_0 + \varepsilon^{p*(0)}\right)^{N_0} \tag{3.24}$$

$$\bar{\sigma}' B_1^s - 3\mu_0^s\left(1-\beta_0^s\right)(1-f) B_1^s \varepsilon^{p*(1)} = a_1\left(b_1 + \varepsilon^{p*(1)}\right)^{N_1} \tag{3.25}$$

where $\varepsilon^{p*(1)}$ is the plastic strain in the inclusion and β_0^s is the Eshelby tensor under the Weng secant method. Internal stresses usually develop as a result of plastic deformation which is inherently heterogeneous due to the heterogeneity of the constituent medium. To effectively predict the macroscopic plastic properties, it is important to find a way to relate the internal stresses with the applied stress. In this model, the internal stresses that are yielded from plastic difference between the constituents are said to be relaxed partially by dislocation motion in the vicinity of the interface and that the Weng method gives the stress or strain partitioning after plastic relaxation mathematically. The practical application of this model in prediction of flow curves requires that the various stages be clearly known and separable which is very difficult.

3.1.8 Goel Model

Goel et al [Goe85] proposed a semi-mechanistic model to describe the flow behaviour of commercial dual-phase steels containing a minimum of 20.0 volume pct of 'as quenched' martensite and varying amounts of retained austenite in a ferrite matrix. They derived the composite flow stress and strain incorporating various contributions to flow stress due to the following:

- Normal work-hardening of ferrite, retained austenite and martensite
- Extra work-hardening of ferrite by accommodation dislocations generated around the as quenched as well as the strain –induced martensite
- Load transfer between the individual phases using an intermediate law of mixtures.

The composite flow stress was given as:

$$\sigma_c = \left(V_\alpha + V_{\gamma R}\right)\sigma_m + K_{\alpha'}\left\{V^0_{\alpha'} + V^0_{\gamma R}\left(1 + \frac{e_C^{-B}}{A}\right)^{-1}\right\} \bullet \left\{\ln\left(1 + e_{\alpha'}\right)\right\}^{n_{\alpha'}} \tag{3.26}$$

The composite flow strain was given as:

$$\varepsilon_c = \left(V_\alpha + V_{\gamma R}\right)\ln\left(1 + e_m\right) + V^T_{\alpha'}\ln\left(1 + e_{\alpha'}\right) \tag{3.27}$$

where $V_\alpha, V^0_{\alpha'}, V^0_{\gamma R}$ are volume fractions of ferrite, as quenched martensite, and retained austenite, $V^T_{\alpha'}$ is the total martensite volume at any strain, $V_{\gamma R}$ is the instantaneous volume fraction of retained austenite at any strain, σ_c, ε_c are composite stress and strain, e_c is composite engineering strain, σ_m is matrix stress, e_m is matrix engineering strain, $n_{\alpha'}$ is strain-hardening exponent of martensite; $K_{\alpha'}$ is strength factor for martensite, and A, B are constants. This model was chosen because it is flexible and can easily be extended to other steels. The model gives the flow stresses while incorporating various important contributions mentioned above in the plastic range.

3.2 MODIFICATION OF THE GOEL MODEL FOR MULTIPHASE STEELS

Multiphase steels can be considered to be heterogeneous materials at the micro-level. To determine the overall macroscopic characteristics of heterogeneous media is an essential problem in many engineering applications. To perform experiments on a number of material samples for various phase properties, volume fractions and loading histories is a formidable task. Several questions still remain unanswered:

- Is it possible to quantify the transformation plasticity in relationship to macroscopic stress and strain during plastic deformation?
- Is it possible to quantify the transformation plasticity in relationship to the known amount of retained austenite and known amounts of transformed products?
- What is the role played by the variant conversions and interphase boundaries in transformation plasticity?

An important aim of theoretical descriptions of composites is the prediction of their overall properties from the material behaviour of their constituents. It is assumed that macroscale and microscale are sufficiently different to allow the stress and strain fields to be split into contributions corresponding to each length scale. The microscale variations of the stress and strain fields are assumed to influence the macroscale behaviour via their averages.

For a general multiphase material assuming constant strain during stressing, the composite stress is given by:

$$\sigma_c = V_i \sigma_i \tag{3.28}$$

where i represents the phases present, V_i is the volume fraction of each of the phases, and σ_i is the true stress in each of the phases.

The composite strain assuming constant stress is given as:

$$\varepsilon_c = V_i \varepsilon_i \tag{3.29}$$

where ε_i is the true strain in each of the phases.

However, conditions of constant stress and strain do not exist in reality. The above equations (3.28 and 3.29) do not indicate anything about the absolute amounts of the stress and strain transfer. Therefore, amount of stress and strain transfer is determined by defining a slope q or partition coefficient. We define q, such that

$$q = \frac{\Delta \sigma_i}{\Delta \varepsilon_i} \tag{3.30}$$

where q is the ratio of stress to strain transfer between the phases. When $\Delta \varepsilon_i \to 0$, then iso-strain condition exits, q is very large. When $\Delta \sigma_i \to 0$, iso-stress condition exits. $|q|$ is a factor that depends on volume fractions, flow stress ratios of the constituent phases, strain hardening, geometry, and applied strain. From the work of Goel et al. [Goe85] the value of q varies from 3000 to 11,000 MPa.

3.2.1 TRANSFORMATION KINETICS

The amount of martensite formed during stressing of a specimen in the temperature range M_s and M_s^{σ} is increased with increase in stress and strain. The kinetics of deformation-induced martensitic transformation is traditionally treated as a function of strain. Only Tamura and co-workers have proposed an equation indicating that the volume fraction of martensite formed during stressing is proportional to the increase in mechanical driving force [Tam82].

Following the treatment of Ludwigson and Berger [Lud69], the volume fraction of martensite formed due to strain induced transformation (SIT) of austenite is given in Chapter 2 (Equation (2.1)) as:

$$V_{\alpha'} = A e_C^B V_{\gamma R}$$

where e_C is the total (composite) applied engineering strain, and A, B are constants describing the rate of transformation with increasing strain. These constants are obtained from curve fitting the equation with the experimental data.

After time t during deformation:

$$V_{\gamma R} = V_{\gamma R}^0 - V_{\alpha'} \tag{3.31}$$

where $V_{\gamma R}$ is the current volume fraction of austenite, $V_{\gamma R}^0$ is the original volume fraction of austenite, and $V_{\alpha'}$ is the volume of martensite formed.

Substituting (Equation (2.1)) in (3.31) we get,

$$V_{\alpha'} = A e_C^B \left(V_{\gamma R}^0 - V_{\alpha'}\right) = V_{\gamma R}^0 \left\{1 + \frac{e_C^{-B}}{A}\right\}^{-1} \tag{3.32}$$

Substituting (Equation (3.32)) in (Equation (3.31)) we get,

$$V_{\gamma R} = V_{\gamma R}^0 \left\{1 - \left(1 + \frac{e_C^{-B}}{A}\right)^{-1}\right\} \tag{3.33}$$

3.2.2 DEFORMATION OF INDIVIDUAL MICROCONSTITUENTS

The stress-strain behaviour of the individual micro-constituent is given by the power law,

$$\sigma = k\,\varepsilon^{n} \tag{3.34}$$

where σ is the true stress, ε is the true strain, and k, n are strength factor and strain-hardening exponent respectively.

Now consider a composite with retained austenite transforming to martensite in an equally distributed framework shown in Figure 3.3 below [Bou85]:

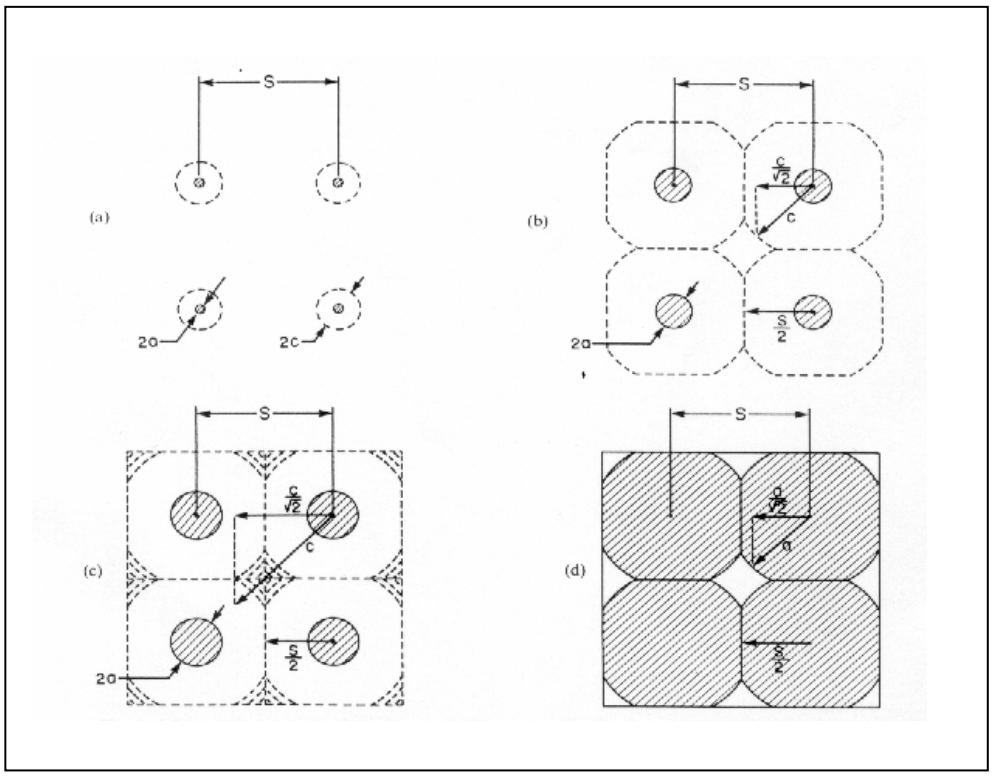

Figure 3.3 Schematic orientation of the austenite/ferrite plastic zones (dotted lines) around martensite particles of spacing s (shaded area). (a) When $V_{\alpha'}$ is small the plastic zones do not contact one another. (b) For larger $V_{\alpha'}$, there is contact with adjacent plastic zones. (c) As $V_{\alpha'}$ increases further, the undeformed matrix becomes disconnected geometrically. (d) At the largest range of $V_{\alpha'}$, adjacent martensite particles contact one another.

For fully austenitic steel, flow stress is given by the power law:

$$\sigma_{\gamma} = k\,\varepsilon_{\gamma}^{n} \tag{3.35}$$

If we have retained austenite in the microstructure, the total contribution of work-hardened austenite and its volume fraction to flow stress at any strain is given by:

$$V_{\gamma R}\sigma_{\gamma R} = V_{\gamma R}^{0} k_{\gamma R}\left\{1-\left(1+\frac{e_C^{-B}}{A}\right)^{-1}\right\}\varepsilon_{\gamma R}^{n_{\gamma R}} \tag{3.36}$$

where $\varepsilon_{\gamma R}$ is the true strain in austenite, and $k_{\gamma R}, n_{\gamma R}$ are strength factor and strain hardening exponent for pure austenite respectively.

Total contribution of martensite α' to flow stress is given as:

$$V_{\alpha'}\sigma_{\alpha'} = k_{\alpha'}\left\{V_{\gamma R}^{0}\left(1+\frac{e_C^{-B}}{A}\right)^{-1}\right\}\varepsilon_{\alpha'}^{n_{\alpha'}} \tag{3.37}$$

Goel and co-workers [Goel85] considered the hardening due to dislocations generated in ferrite because of austenite to martensite transformation during quenching. For pure austenitic steel this aspect cannot be considered. Hardening in the austenite in metastable austenitic steels and low alloy multiphase steels will be considered.

HARDENING DUE TO DISLOCATION GENERATION IN AUSTENITE DURING THE STRAIN INDUCED TRANSFORMATION IN METASTABLE AUSTENITIC STEELS

Following the work of Goel [Goel85, Bou83], if the strain-induced martensitic transformation is continuous as per the kinetics of transformation, then the extra dislocations generated continuously as a result of this transformation will further contribute to austenite strengthening throughout the plastic deformation.

The volume fraction of α' formed over the strain interval e_c to $e_c+\Delta e$ can be written as:

$$\Delta V_{\alpha'} = V_{\gamma R}^{0}\left\{\left[1+\frac{\left(e_C+\Delta e\right)^{-B}}{A}\right]^{-1} - \left[1+\frac{e_C^{-B}}{A}\right]^{-1}\right\} \tag{3.38}$$

The volume fraction of the deformed austenite zone around the strain-induced martensite, α′, over the strain interval e to $e_c+\Delta e$ can be given by the three equations given below depending on how much strain induced martensite has formed.

$$\Delta V_{d\gamma} = \Delta V_{\alpha'}\left[\left(\frac{c}{a}\right)^3 - 1\right] \tag{3.39}$$

where a is the radius of formed martensite and c is the radius of the plastic zone after transformation (see Figure 3.3).

For volume of martensite given by,

$$0 < V_{\alpha'} < \frac{\pi}{2}\left(\frac{a}{c}\right)^3 \tag{3.40}$$

and

$$\Delta V_{d\gamma} = 2\pi\frac{\Delta V_{\alpha'}}{V_{\alpha'}}\left\{\frac{2}{3}\left(\frac{c}{s}\right)^3\left[1-\left(\frac{a}{c}\right)^3\right]-\left(\frac{c}{s}-\frac{1}{2}\right)^2\left(2\frac{c}{s}+\frac{1}{2}\right)\right\} \tag{3.41}$$

For volume of martensite given by,

$$\frac{\pi}{2}\left(\frac{a}{c}\right)^3 < V_{\alpha'} < \frac{\sqrt{2}}{3}\pi\left(\frac{a}{c}\right)^3 \tag{3.42}$$

and

$$\Delta V_{d\gamma} \cong 1 - \Delta V_{\alpha'} \tag{3.43}$$

For volume of martensite given by,

$$\frac{\sqrt{2}}{3}\pi\left(\frac{a}{c}\right)^3 < V_{\alpha'} \tag{3.44}$$

The dislocation density in the deformed austenite zone due to strain-induced martensite will be given as:

$$\rho^*_{d\gamma} = \rho(e) + \frac{3C\left[\frac{2}{3}\sigma_\gamma\left(\frac{1}{2G}+2k\right)\right]^g}{\left(\frac{R}{c}\right)^3-\left(\frac{a}{c}\right)^3} \bullet \int_{a/c}^{R/c}\left[\left(\frac{c}{r}\right)^3 - 1\right]^g\left(\frac{r}{c}\right)^2 d\left(\frac{r}{c}\right) \tag{3.45}$$

where $\rho(e)$ is the average dislocation density at the current strain given by:

$$\rho(e) = C\,\varepsilon^{g} \tag{3.46}$$

And C, g are material constants, R is the outer radius of the plastic zone (this depends on the volume of martensite), G is the shear modulus of austenite, and k is coefficient of volumetric compression.

The average increase in the austenite dislocation density due to strain induced martensite transformation is given as:

$$\rho^{*}_{d\alpha'} = \frac{\rho^{*}_{d\gamma}\,\Delta V_{d\gamma}}{V_{\gamma}} \tag{3.47}$$

If $\Delta\varepsilon_{d\alpha'}$ is the effective true plastic strain in austenite developed due to the strain induced transformation over the strain interval e_c to $(e_c+\Delta e)$, then:

$$\Delta\varepsilon_{d\alpha'} = \left(\frac{\rho^{*}_{d\alpha'}}{C}\right)^{1/g} \tag{3.48}$$

The total true plastic strain in austenite developed due to strain induced transformation from strain 0 to strain e_c, can be given as a summation,

$$\varepsilon^{T}_{d\alpha'} = \sum_{e_c} \Delta\varepsilon_{d\alpha'} \tag{3.49}$$

The total contribution of this strain to the composite stress is given as,

$$V_{\gamma}\sigma_{\gamma} = V_{\gamma}\,k\left(\varepsilon^{T}_{\gamma}\right)^{n} \tag{3.50}$$

where $\varepsilon^{T}_{\alpha'}$ is the true plastic strain due to dislocations in austenite, k, n are constants, and $\varepsilon^{T}_{d\alpha'} = \varepsilon^{T}_{\alpha'}$.

HARDENING DUE TO DISLOCATION GENERATION IN FERRITE DURING THE STRAIN INDUCED TRANSFORMATION IN MULTIPHASE STEELS

The dislocations generated in ferrite during the strain induced transformation in high strength multiphase steels contribute to the overall composite strength. This contribution is given as,

$$V_{\alpha}\sigma_{\alpha} = V_{\alpha}\,k\left(\varepsilon^{T}_{\alpha}\right)^{n} \tag{3.51}$$

where ε^{T}_{α} is the true plastic strain due to dislocations in ferrite, k, n are constants, $\varepsilon^{T}_{d\alpha'} = \varepsilon^{T}_{\gamma}$, and V_{α} is the volume fraction of ferrite.

3.2.3 COMPOSITE FLOW STRESS AND STRAIN

The composite flow stress from Equation (3.28) for metastable austenitic steels is given as:

$$\sigma_c = V_i \sigma_i = V_{\gamma R}^0 k_{\gamma R} \left\{ 1 - \left(1 + \frac{e_C^{-B}}{A} \right)^{-1} \right\} \varepsilon_T^{n_{\gamma R}} + k_{\alpha'} \left\{ V_{\gamma R}^0 \left(1 + \frac{e_C^{-B}}{A} \right)^{-1} \right\} \varepsilon_\alpha^{n_{\alpha'}} \tag{3.52}$$

where $\varepsilon_T = \varepsilon_{\gamma R} + \varepsilon_\gamma^T$.

The composite flow strain from Equation (3.29) is given as:

$$\varepsilon_C = V_{\gamma R} \varepsilon_T + V_{\alpha'} \varepsilon_{\alpha'} \tag{3.53}$$

The stress-strain partition is given as:

$$q = \left(\frac{k_{\alpha'} \varepsilon_\alpha^{n_{\alpha'}} - \sigma_m}{\varepsilon_{\alpha'} - \varepsilon_m} \right) \tag{3.54}$$

with austenite as the matrix.

The composite flow stress from Equation (3.28) for high strength multiphase steels as:

$$\sigma_c = V_i \sigma_i = V_\alpha \sigma_\alpha + V_{\gamma R} \sigma_{\gamma R} + V_b \sigma_b + V_{\alpha'} \sigma_{\alpha'}$$

$$\sigma_c = \left(V_\alpha + V_b + V_{\gamma R} \right) \sigma_m + k_{\alpha'} \left\{ V_{\gamma R}^0 \left(1 + \frac{e_C^{-B}}{A} \right)^{-1} \right\} \varepsilon_\alpha^{n_{\alpha'}} \tag{3.55}$$

where σ_m is the matrix stress, σ_α is the stress in ferrite, $\sigma_{\gamma R}$ is the stress in retained austenite, and σ_b is the stress in bainite. V_b is the volume fraction of bainite, V_α is the volume fraction of ferrite, $V_{\gamma R}$ is the volume fraction of retained austenite, and $V_{\alpha'}$ is the volume fraction of martensite.

It is assumed that bainite and ferrite have the same constants. Therefore,

$$k_\alpha = k_b$$
$$n_a = n_b$$

The composite strain is given by:

$$\varepsilon_c = \left(V_\alpha + V_b + V_{\gamma R} \right) \varepsilon_m + V_{\alpha'} \varepsilon_{\alpha'} \tag{3.56}$$

where ε_m is the matrix strain and $\varepsilon_m = \varepsilon_\alpha = \varepsilon_{\gamma R} = \varepsilon_b$.

The stress-strain partition is given by:

$$q = \left(\frac{k_{\alpha'} \varepsilon_{\alpha'}^{n_{\alpha'}} - \sigma_m}{\varepsilon_{\alpha'} - \varepsilon_m} \right)$$

with ferrite, bainite and retained austenite as matrix. We have assumed that ferrite and retained austenite are equal in strength; therefore, the expressions that give the dislocations generated are the same in both cases.

Total contribution of the martensite to the flow stress is given as below:

$$V_{\alpha'} \sigma_{\alpha'} = k_{\alpha'} \left\{ V_{\gamma R}^0 \left(1 + \frac{e_C^{-B}}{A} \right) \right\} \varepsilon_{\alpha'}^n \tag{3.57}$$

If we assume the matrix is composed of ferrite, bainite and retained austenite then, contribution of the matrix is given as:

$$\left(V_\alpha + V_b + V_{\gamma R} \right) \sigma_m = \left(V_\alpha + V_b \right) k_\alpha \left\{ \varepsilon_m + \varepsilon_\alpha^T \right\}^{n_\alpha} + V_{\gamma R}^0 k_{\gamma R} \left\{ 1 - \left(1 + \frac{e_C^{-B}}{A} \right)^{-1} \right\} \bullet \left\{ \varepsilon_m^{n_{\gamma R}} \right\} \tag{3.58}$$

Expressions for the composite flow stress and strain have been derived incorporating various contributions to flow stress due to normal work-hardening of ferrite, bainite, and retained austenite. Extra work-hardening of ferrite, bainite and austenite due to accommodation of dislocations inside the phases as a result of deformation induced martensite transformation has been incorporated. The temperature dependence is assumed to be captured mainly by the constants A while constant B takes into consideration the autocatalytic nature of martensitic transformation in Ludwigson and Berger's transformation kinetics expression.

CHAPTER 4

4 EXPERIMENTAL DETAILS

4.1 TEST MATERIALS

Two types of steels were selected for this study. The first type of steel selected was commercial available metastable austenitic steel (High alloy high strength steel) AISI 304 (German Grade X5CrNi18.10) and the second type of steel selected was low alloyed high strength Mn-Si-Al multiphase steel. The chemical composition the steels are presented in the Table 4.1 below:

Table 4.1 Chemical composition of the investigated steels in wt-%.

	Fe	C	Cr	Ni	Mn	N	Mo	Si	Al	Cu	V
X5CrNi18.10	69.71	0.043	19.19	9.03	1.15	0.096	0.23	0.38	-	-	0.18
Mn-Si-Al Steel	93.97	0.19	0.49	0.26	1.57	-	-	1.18	1.64	0.70	-

For the Mn-Si-Al Steel, the melt was prepared at the Institute of Iron and Steel Technology, TU Bergakademie Freiberg, using normal production methods and the final round bars were produced via cold rolling at the Institute of Metal Forming, TU Bergakademie Freiberg. The AISI 304 (German Grade X5CrNi18.10) steel was sourced from the market.

4.2 MICROSTRUCTURE

4.2.1 MICROSCOPY

Optical microscopy was done at the Institute of Physical metallurgy, TU Bergakademie Freiberg. Initial microstructures and grain sizes were estimated before any testing was done on the specimens. Extreme care was taken during preparation to avoid martensite formation that could falsify the results. Etching martensite, bainite, and retained austenite for quantitative metallography normally presents complex problems. This is because of the difficulty in developing contrast needed to differentiate between the phases. The specimens to be colour etched were polished with particular care using automatic and electrolytic polishing apparatus. Three etchants were used; Le Pera, Klemm and Picral etchants. For the Le Pera etchant, two solutions one consisting of 4% alcoholic picric acid and second one consisting of 1 gram of sodium thiosulphate in 100ml of water were mixed in the ratio of 1:1 shortly before use. For Klemm, 2 grams of potassium pyro-sulphite was mixed with 100ml solution of cold saturated sodium thiosulphate. For picral reagent, 25 grams of sodium hydroxide was mixed with 75ml of water and 2 grams of picric acid was added to 100ml of this solution before etching see Table 4.2. After various tests, specimens were again prepared and the microstructures were again observed, analysed and characterized. The different phases which constitute these steels were qualitatively identified and related to various processing conditions. Quantitative analysis of the phases was carried out using available software. However, the quantification of ε-martensite and α'-martensite was not successful due to difficulty in separation of the phases with increased levels of deformation.

Table 4.2 Etchants used in Optical microscopy.

Etchant	Chemical Composition	Use
Le Pera	Solution I - 4% alcoholic picric acid Solution II - 1 g sodium thiosulphate 100 ml of water	Solution I and II are mixed shortly before use in the ratio of 1:1. The sample is immersed for about 20 s.
Klemm	100 ml cold saturated sodium thiosulphate 2 g potassium pyro-sulphite	The sample is immersed for about 20 s.
Picral	25 g sodium hydroxide 2 g picric acid 75 ml water	Take 100 ml solution of sodium hydroxide and water and add 2 g of picric acid. The sample is immersed for about 20 s at 50°C for best results.

4.2.2 MAGNETIC MEASUREMENTS

After tensile testing, the volume fraction of ferromagnetic α'-martensite was determined using magnetic measurements. Laboratory equipment built in-house at the Institute of Iron- and Steel technology was used. A standard calibrated specimen with a known weight was balanced with each of the specimens in a known magnetic field and the balancing magnetic forces compared. The equation below was used:

$$V_{\alpha'} = \left(\frac{F_{pr}}{F_s} \bullet \frac{M_s}{M_{pr}} \right) \tag{4.1}$$

where $V_{\alpha'}$ is the volume fraction of deformation induced martensite, F_{pr} is the magnetic force on the specimen, F_s is the magnetic force on the standard specimen, M_{pr} is the mass of the specimen, and M_s is the mass of the standard specimen. The standard calibrated specimen was made of ferritic steel X5CrNi13.4. Since during the measurements only current is measured, it was necessary at first to construct a standard curve using the standard specimen.

4.2.3 TEM STUDY

Transmission electron microscopy (TEM) was carried out with a Philips CM30 (300 kV) at the Institute of Physical metallurgy. Thin foils from the specimens were prepared by mechanical thinning and finally by an electrolytic twin-jet polishing. Perchloric acid and ethanol was used as electrolyte in case of AISI 304. The optimum electropolish for Mn-Si-Al steel was achieved at -40°C and 30 V.

4.2.4 MICROHARDNESS MEASUREMENTS

Micro-hardness testing of the specimens was done using a universal hardness tester, FISCHERSCOPE H 100. The measurements were done to distinguish small quantities of martensite and retained austenite. A small load of 20 mN was chosen to increase the accuracy during the indentation. The machine was computer controlled and equipped with software that increases the accuracy and evaluation of measured hardness profiles.

4.2.5 X-RAY DIFFRACTION ANALYSES

X-ray diffraction analysis was carried out to determine the amount of retained austenite and ε-martensite. The X-rays are generated by accelerating a beam of electrons on the target, which was placed in a vacuum tube. The high-energy electrons eject ground-state electrons from the atoms of the target specimen, creating holes, and X-rays are emitted during the filling of these ground states. The equipment used was of the type URD 6 from the company SEIFERT-FPM with a secondary graphite monochromator. The equipment uses a CoKα radiation with an accelerating voltage of 40 kV and a current of 30mA. The measurement parameters were as follows: angle $45° \leq 2\theta \leq 115°$, step size or increment $\Delta\theta = 0.05°$ and counting time of $20\ s \leq t_\theta \leq 60\ s$. These parameters enabled sufficient information to be collected that could be used to identify the crystalline phases present unambiguously. The data was obtained with the aid of a computer attached to the diffractometer and evaluated using a pre-installed APX 63 Software. The primary data collected was fitted using Profile functions (Pseudo-Voigt function). The measured peaks were compared with standard peaks to help in identification of the various phases. To enable quantitative analysis of the various phases, regression analysis techniques were used with the help of theoretical intensities factors from crystallographic data [Vil85].

4.2.6 DILATOMETER TESTS

Continuous cooling was simulated using a computer controlled deformation dilatometer, type Theta 2 from the company Clüsener for the Mn-Si-Al steel. The specimen was enclosed in a vacuum chamber during testing. Heating was done inductively and the temperature of the specimen was measured at the surface using a thermocouple. Nitrogen was used as the cooling medium. For every test, the temperature, time, and length change was recorded (300 data points per second) and evaluated with a computer software.

4.3 HEAT TREATMENT

Heat treatment was carried out in an electric furnace under protecting atmosphere (argon) to prevent oxidation for the Mn-Si-Al steel. The heat treatment cycle is depicted in Figure 4.1. Heat treatment was performed at the Institute of Iron and Steel using the continuous cooling diagram (CCT) constructed from the dilatometer tests. For the steel AISI 304 (German grade X5CrNi18.10), the specimens were austenitised at 1050°C for 30 minutes and then quenched in water.

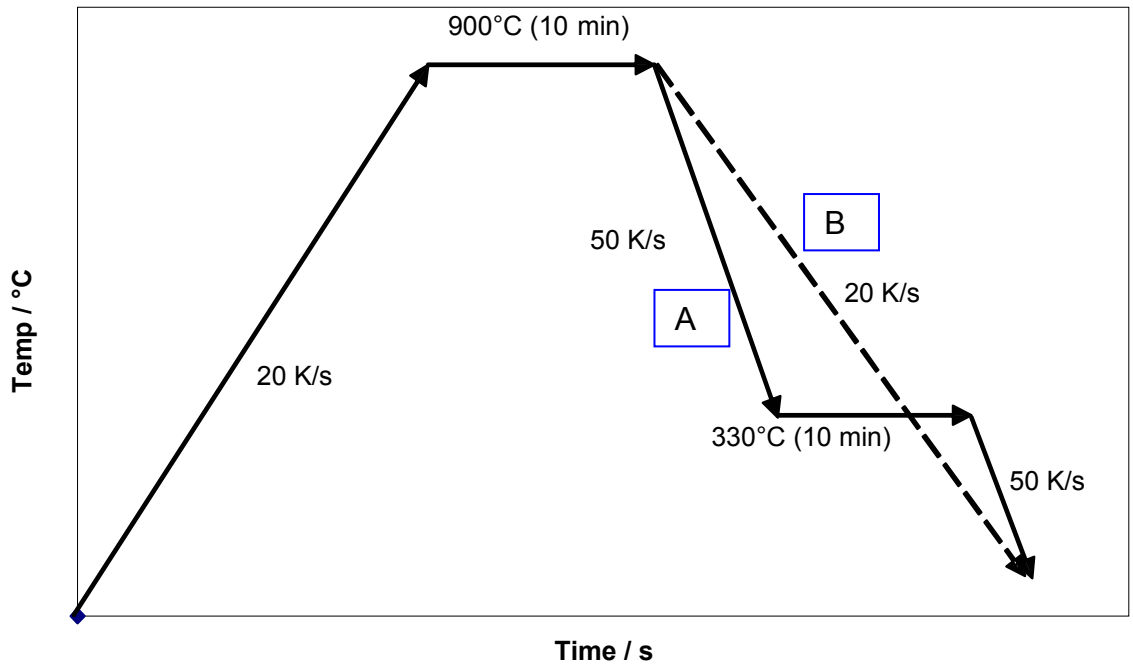

Figure 4.1 Heat treatment processes, A (austempered) and B (continuously cooled) for the Mn-Si-Al steel.

AISI 304 (German Grade X5CrNi18.10)

The tensile test specimens were prepared from the as-received steel, the tensile specimens were austenitised at temperature 1050°C for 30 minutes and then quenched in water. The specimens were then tested in uniaxial tension at different test conditions.

4.4 UNIAXIAL TENSILE TESTING

Uniaxial tensile testing was carried out on a universal testing machine, ZWICK type1476-70. Tests were done using a cross-head speed of 1 mm/min ($5\times10^{-4}/s$) and available load of 100 kN. The machine was equipped with temperature controlled cabin which enabled testing temperatures to be varied from –80°C to 200°C. A thermocouple attached to specimen surface during testing ensured that the temperature measured was that of the specimen. The temperature variation during testing was kept within $\pm$1 K.

Load and extension was measured using a microprocessor attached to the machine and later evaluated using available computer software. The tests were carried out according to the standards DIN EN 10002.

CHAPTER 5

5 RESULTS AND DISCUSSION

5.1 HEAT TREATMENT

Mn-Si-Al Steel

After cold rolling, this steel was subjected to various heat treatment procedures. A deformation dilatometer was used to simulate controlled heating and cooling in order to obtain adequate retained austenite at room temperature. Continuous cooling rate was varied from 230 K/s to 0.2 K/s while the heating rate was held constant at 20 K/s. Continuous cooling transformation was measured from the dilatometric length change during the continuous cooling process and some selected results are shown in Figures 5.1-5.3. From the same specimens, metallographic samples were prepared and analysed using optical microscopy as shown also in the same figures. From the microstructural observations and dilatometer curves, a continuous cooling transformation diagram (CCT) diagram was constructed for this steel shown in Figure 5.4. A comparable CCT diagram from literature is shown in Figure 5.5. Time temperature transformation diagram (TTT) constructed for the same steel is also shown in Figure 5.6. To construct the TTT-diagram, the specimens were austenitised for sufficient time and rapidly quenched and held at the subcritical transformation temperatures. After an elapse of progressively increasing times, each specimen was subsequently quenched in cold water to prevent any further transformation. In the process, any untransformed austenite transforms to martensite. The specimens were then examined by optical microscopy. This provided the extent of transformation during holding. The diagram is constructed by joining all the ‘start’ points and ‘finish’ transformation points.

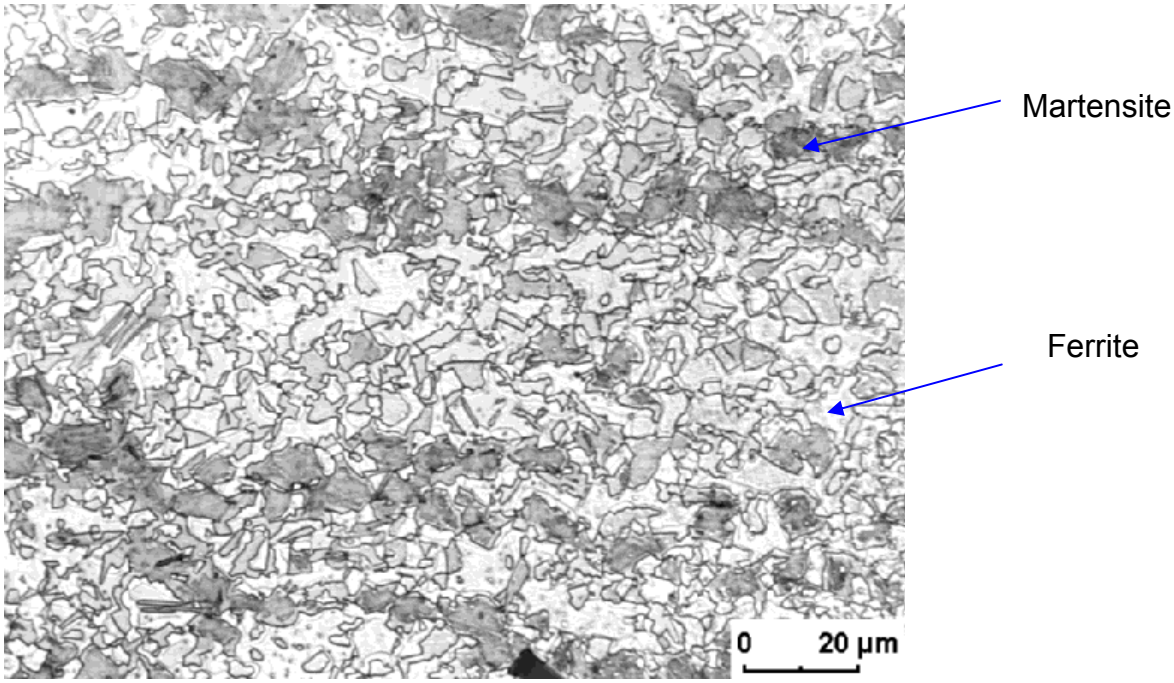

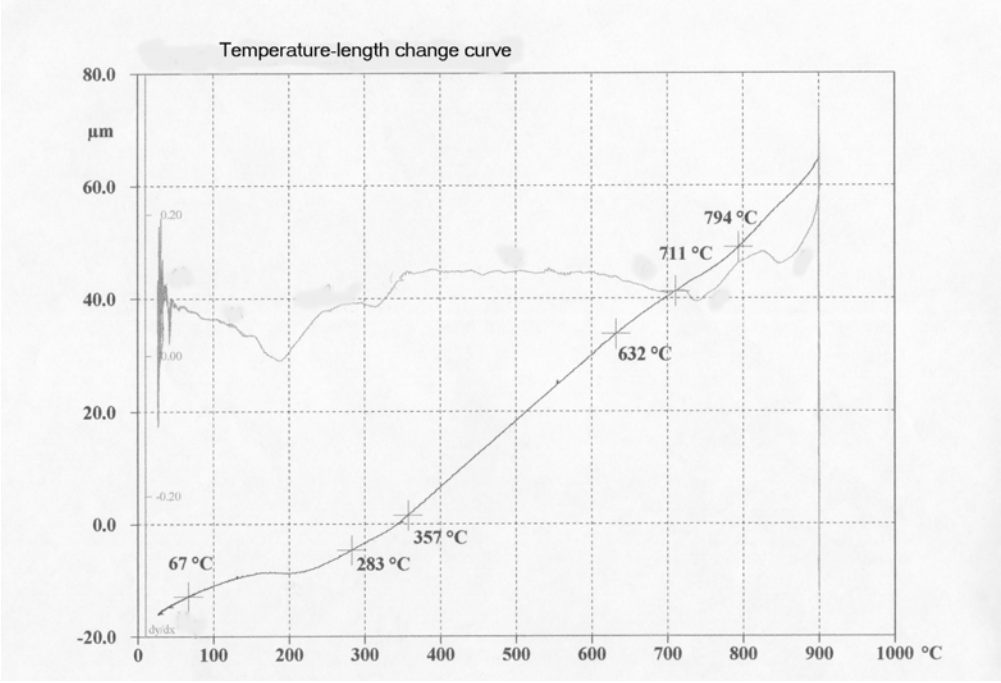

Figure 5.1 Optical micrograph (above) and corresponding dilatometer curve (below) for the Mn-Si-Al steel after continuous cooling at a rate of 50 K/s to room temperature. Bright areas indicate ferrite and dark areas indicate martensite as shown. Because of the small bainite reaction window, it was not possible to unambiguously identify the bainitic phase.

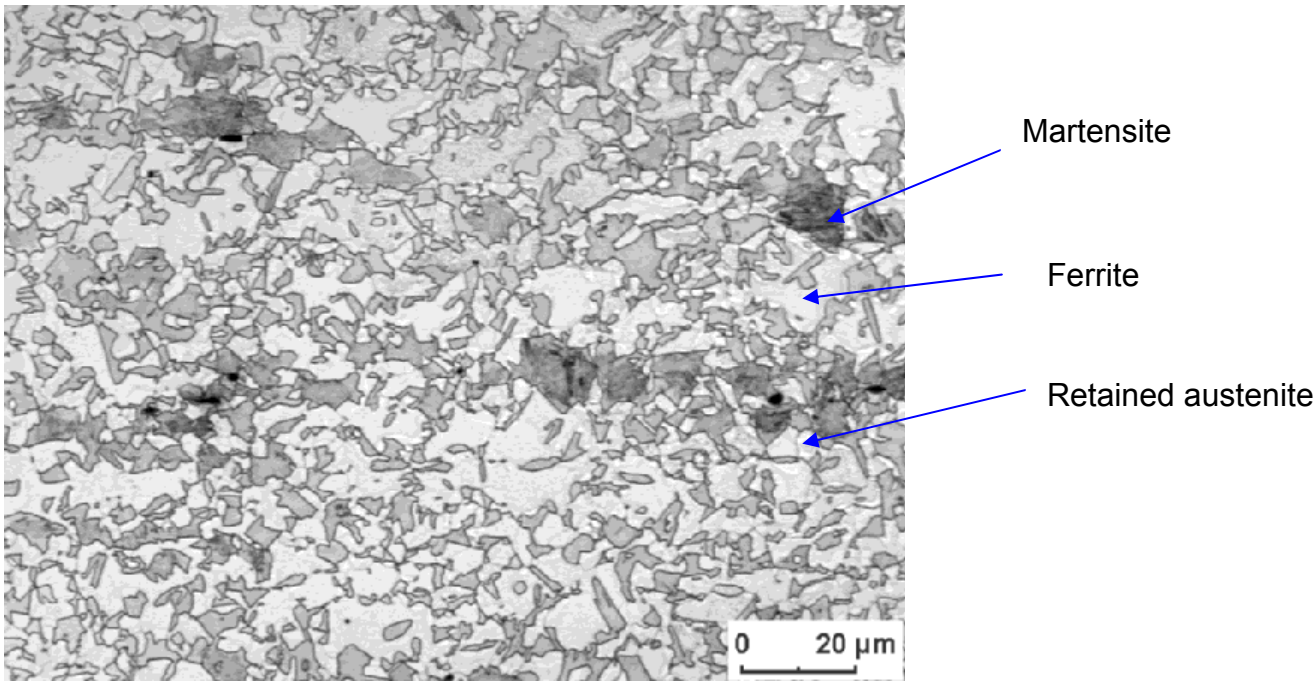

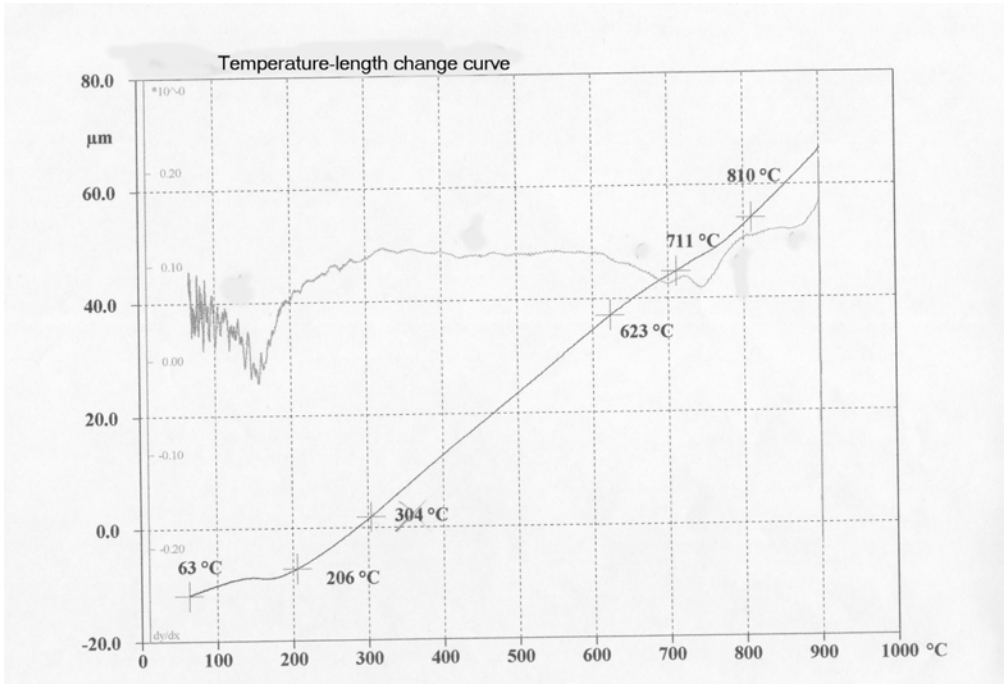

Figure 5.2 Optical micrograph (above) and corresponding dilatometer curve (below) for the Mn-Si-Al steel after continuous cooling at a rate of 20 K/s to room temperature. Grey areas indicate ferrite, small white islands retained austenite and dark areas martensite as shown. Because of the small bainite reaction window, it was not possible to unambiguously identify the bainitic phase.

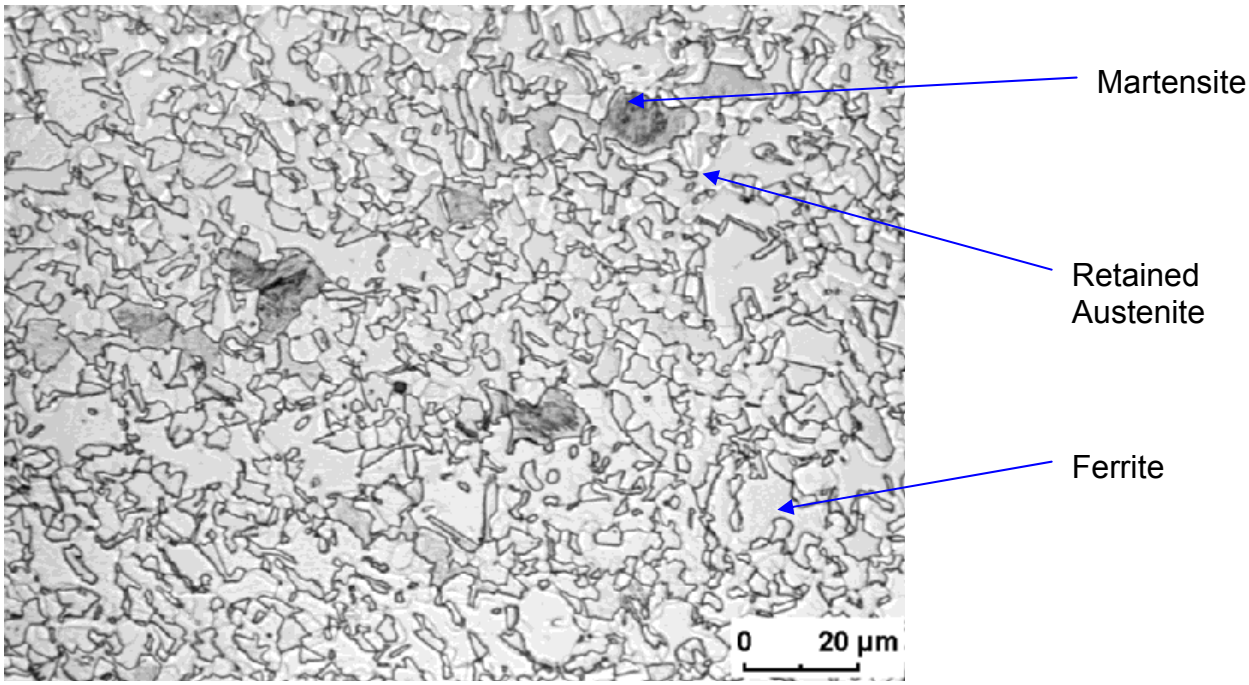

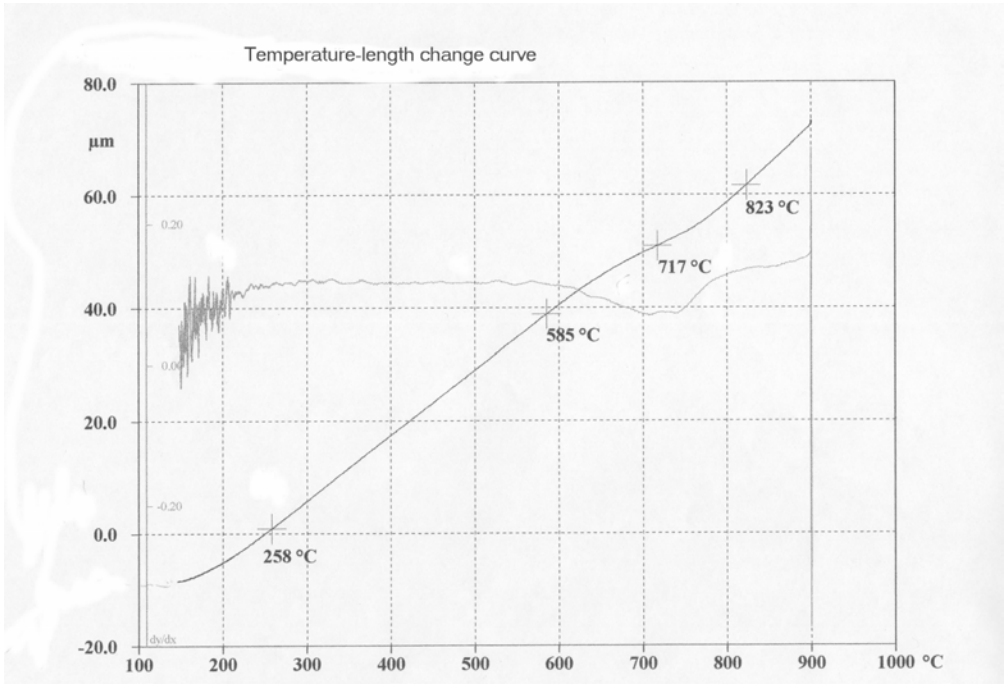

Figure 5.3 Optical micrograph (above) and corresponding dilatometer curve (below) for the Mn-Si-Al steel after continuous cooling at a rate of 10 K/s to room temperature. Grey areas indicate ferrite, small white islands retained austenite and dark areas martensite as shown. Because of the small bainite reaction window, it was not possible to unambiguously identify the bainitic phase.

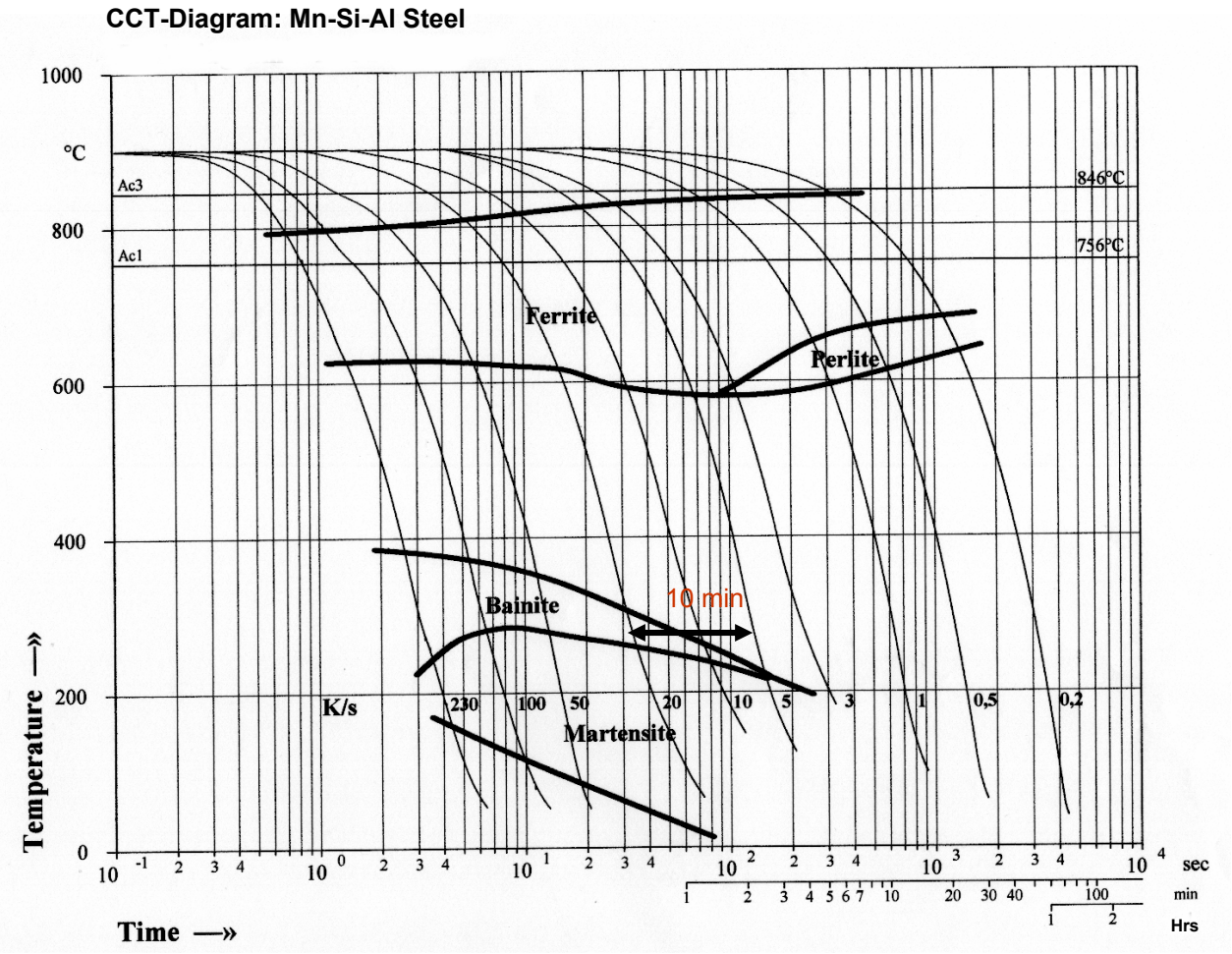

Figure 5.4 Continuous cooling transformation diagram for the Mn-Si-Al steel constructed from the microstructural analysis and the dilatometer curves. 10 min indicates the holding time during austempering. CCT-Diagrams like this were difficult to locate in published literature for comparison for this particular steel but a similar one is shown in Figure 5.5 for comparison. The approximated M_S-Temperature using an expression from literature [Ehr99] is 440°C.

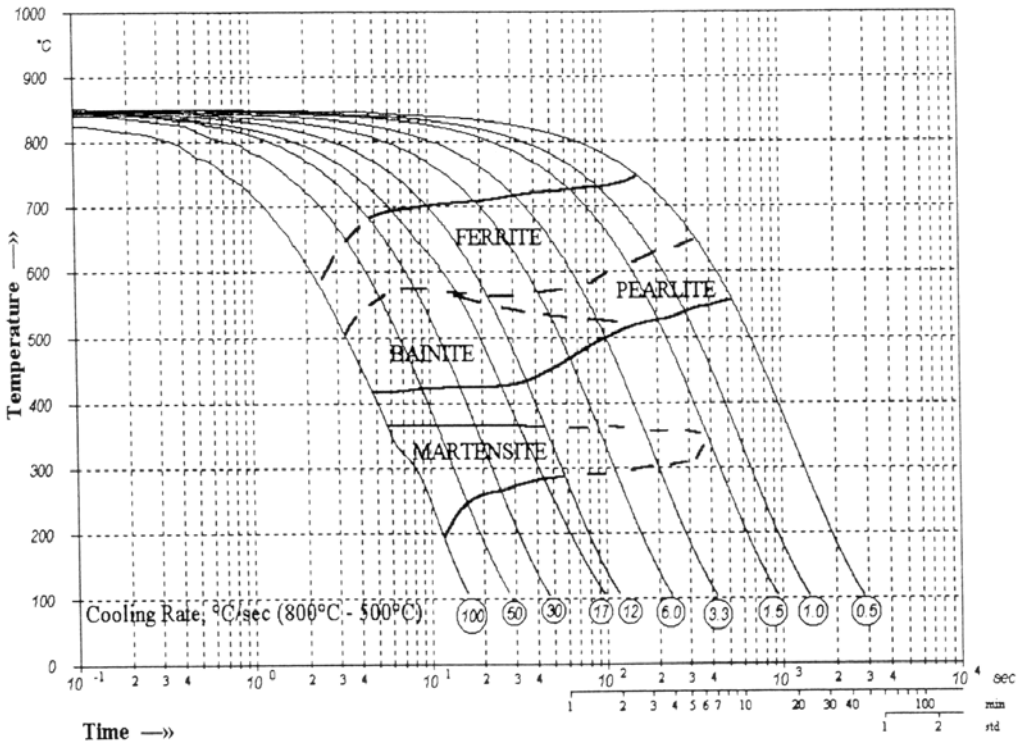

Figure 5.5 CCT diagram Multiphase steels (S6) [Kuj02].

Table 5.1 Chemical composition of the specimens used [Kuj02] (in wt. %).

Steel	C	Si	Mn	P	S	Cr	Al	N
S6	0.21	0.93	1.68	0.011	0.005	0.01	0.031	0.0046

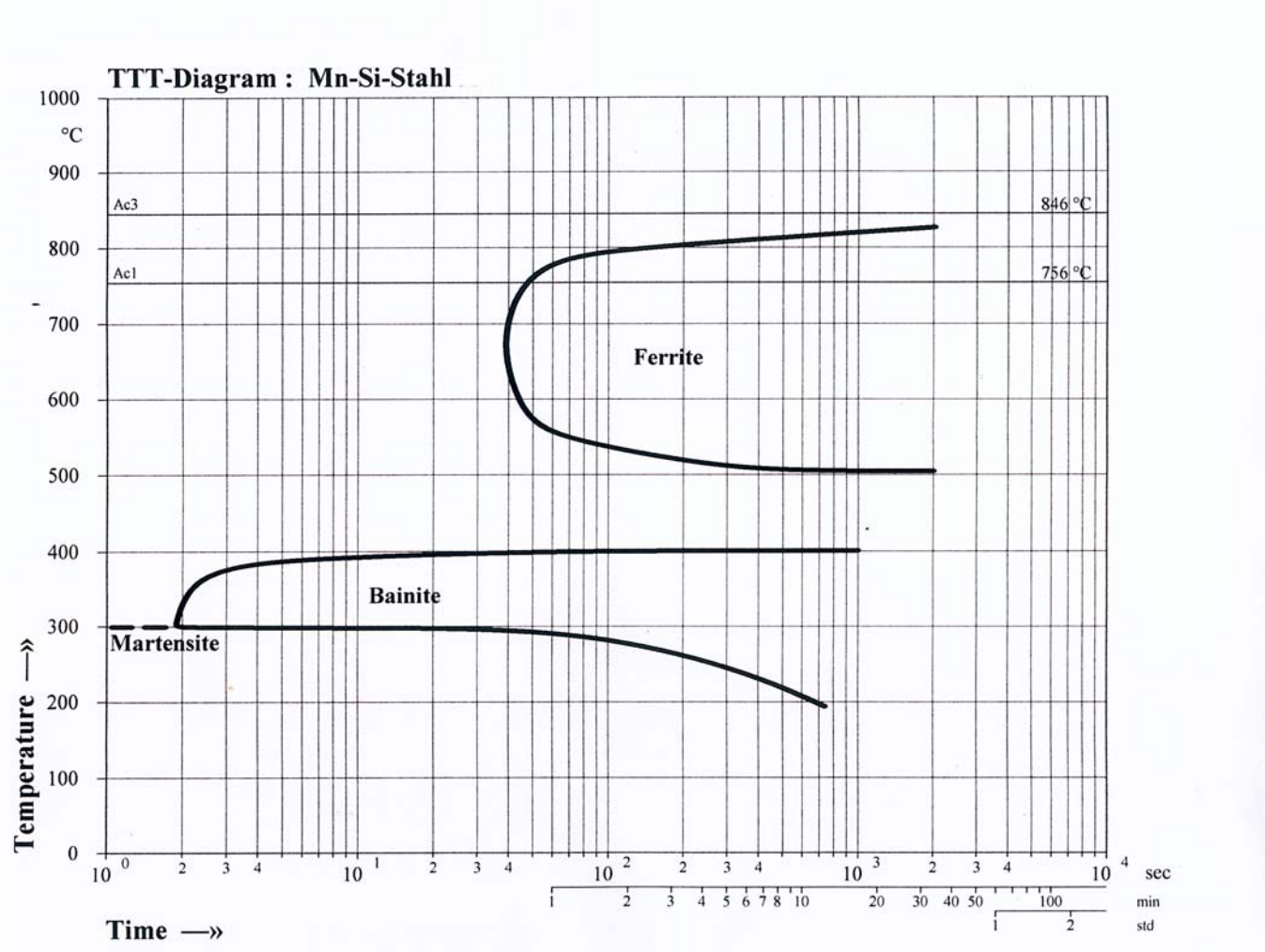

Figure 5.6 Time Temperature Transformation diagram for the Mn-Si-Al steel.

The aim of dilatometer simulations was to establish an appropriate cooling rate from which a large amount of ferrite and subsequent carbon enrichment in the untransformed austenite would be obtained after a longer holding time at the bainitic region. This was necessary to obtain carbon enriched retained austenite which is stable at low temperatures but which upon deformation transforms to martensite. From the observation of the microstructures, it was noted that pearlite forms at continuous cooling rate of 5 K/s and below. It has been suggested that formation of pearlite should be restricted in manufacture of TRIP steels because pearlite consumes large amount of carbon and this hinders carbon enrichment in austenite [Par98]. As the rate of continuous cooling was increased, the microstructure was mainly observed to be composed of ferrite, bainite and martensite. Doubling the cooling rate from 100 K/s to 230 K/s did not change the microstructure significantly. The amounts of retained austenite after continuous cooling rate of 20 K/s, 10 K/s, 5 K/s and 3 K/s were determined by X-ray diffraction method and the results are shown in Table 5.2.

Table 5.2 Continuous cooling rates and volume fraction of retained austenite

Continuous cooling rate (K/s)	Volume fraction of Retained austenite (%)
20	8
10	5
5	6
3	6

Based on the overall transformation behaviour represented in the CCT diagram Figure 5.4, a second heat treatment procedure was designed with varying holding times at the bainite region. The amount of retained austenite obtained was measured by X-ray diffraction and is shown in Table 5.3. It should be noted that at a continuous cooling rate of 20 K/s, varying the holding time from 1 minute to 10 minutes did not have a great effect on the amount of retained austenite. Two heat treatment routes A (austempered) and B (continuously) shown in Figure 4.1 were finally selected for our tensile specimens before uniaxial tensile testing. The uniaxial tensile results and microstructural observations obtained are discussed later in this chapter.

Table 5.3 Volume fraction of retained austenite after a second heat treatment

	Holding time (min) in the bainite region	Volume fraction of Retained austenite
Cooling rate 50 K/s	10	10
	5	8
	1	5
Cooling rate 20 K/s	10	8
	5	7
	1	7
Cooling rate 10 K/s	10	6
	5	4
	1	3

5.2 MICROSTUCTURAL CHARACTERIZATION

5.2.1 INITIAL MICROSTRUCTURE

AISI 304 (German Grade X5CrNi18.10) STEEL

The optical micrograph of this steel after heat treatment but before uniaxial tensile testing is shown in Figure 5.7. Nital solution was used as the etching reagent. Figure 5.8 show the transmission electron micrographs of the same steel. Stacking faults, dislocations, and deformation twins characteristic of metastable austenitic steel can be identified.

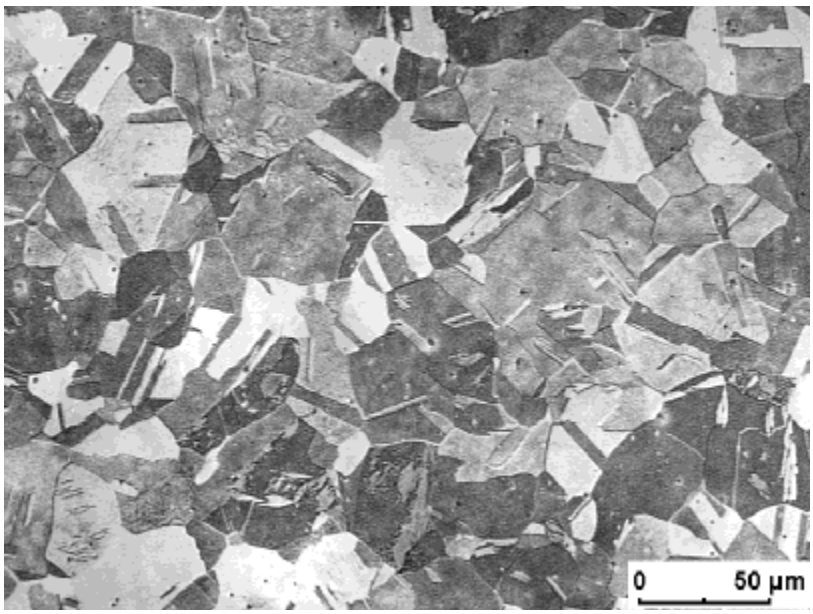

Figure 5.7 Initial optical micrographs of the steel AISI 304 (X5CrNi18.10) after heat treatment. Austenite grains with twins are visible.

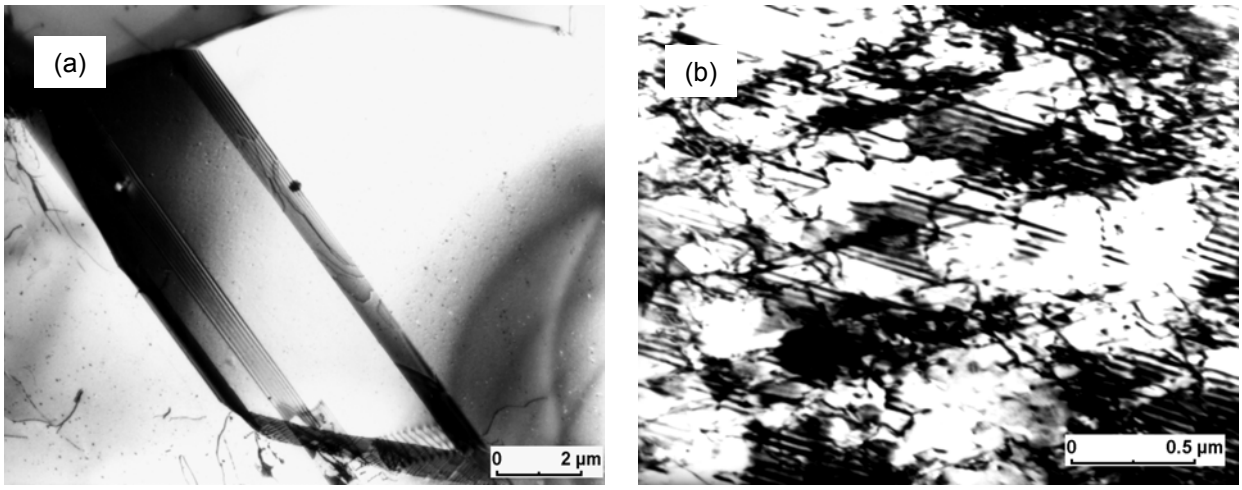

Figure 5.8 TEM initial micrographs of the steel AISI 304 (X5CrNi18.10) after heat treatment. (a) Shows dislocations and stacking faults. (b) Shows deformation twins.

Mn-Si-Al Steel

The optical micrographs of Mn-Si-Al steel after applying the selected heat treatment procedures explained above are shown in Figures 5.9-5.10. Different etchants were used to help in the identification of the position of retained austenite in relation to other phases. To locate exactly the position of retained austenite, transmission electron microscopy was used and the results are shown in Figures 5.11 and 5.12.

Quantification of retained austenite was done using X-ray diffraction analysis. Austenite peaks were measured and the volume fraction of retained austenite was calculated using the theoretical relative line intensities. The amount of retained austenite in both the austempered (A) and continuously (B) cooled was 8% and 12% volume percent respectively. For the specimens which showed enhanced ductility, cooling Route A (Figure 5.9), microstructure consists of a matrix of ferrite grains, blocky bainite with dispersions of island grains of retained austenite located at grain boundaries between ferrite and bainite grains, between ferrite and ferrite grains and inside the ferrite matrix. The amount of ferrite and bainite was approximated using point method analysis and found to be approximately 46% and 42% respectively. Figure 5.9 also shows the microstructure after picral etching, information on carbon enrichment in bainitic areas and in retained austenite can roughly be obtained in the austempered specimen. The results of the TEM examination of the specimens before uniaxial testing are shown in Figures 5.11 and 5.12.

The existence of dislocations was observed both in the austempered and continuously cooled specimens. The position and shape of the retained austenite in relation to other phases could be identified. Retained austenite appears as thin films or in lamellar form inside the bainite areas and also as globules or islands at the grain boundaries. No martensite phase was identified for austempered specimens. It was found that generally retained austenite forms preferentially at the grain boundaries as islands and as lamellar inside the bainitic areas. Retained austenite and martensite appears as brown or yellow and bainite as grey in optical micrographs after colour etching.

For the specimens which were continuously cooled (B) Figure 5.10, the microstructure consists of ferrite matrix with dispersions of retained austenite, bainite and martensite. The retained austenite islands are located along martensite or bainite lath boundary. Some are also located inside these hard second phases. They appear as globules and as thin film or lamellar inside the bainitic areas. It can conclude that retained austenite formed preferentially as globules or lamellas inside the bainitic areas, and as islands at grain boundaries between martensite and bainite grains, and between martensite and ferrite grains. The amount of ferrite and bainite was found to be 50% and 34% volume percent respectively using point method analysis (see Table 5.4).

It should be noted that holding for 1 min, 5 min or 10 min at the bainite transformation region (300°C) after a cooling rate of 20 K/s from the austenite region did not have much effect in the amount of retained austenite as shown in Table 5.3. The austempering treatment for different times did not have much effect on the volume of retained austenite as may be expected. For longer holding time, the bainite transformation goes nearly to completion and only bainite and not martensite is found in the microstructure. For the specimens that were cooled at 50 K/s from the austenite and holding for 10 min at the bainite region, there was a reduction in carbon enrichment in the bainitic areas. For continuous cooling (20 K/s), there was partial martensitic transformation (see Figure 5.2). Carbide precipitation was more pronounced in continuously cooled samples than austempered samples. Generally, bainite transformation leads to a carbon enrichment of austenite [Mat02, Jac98], while carbide precipitation leads to or gives rise to a carbon weakening of austenite.

The microstructure for the continuously cooled specimens consists of ferritic matrix, bainite with a dispersion of martensite and retained austenite as second phases. During cooling of a hypoeutectoid steel, austenite-to-preeutectoid ferrite reaction normally occurs as the first phase transformation. The growth of ferrite takes place by rejection of carbon into the untransformed austenite [Han97a, Han97b]. The carbon enrichment of austenite affects the state of retained austenite in final microstructure in terms of morphology, stability and composition [Han97a, Han97b]. It has generally been reported that volume fraction of retained austenite increases with ferrite quantity [Han97a]. This increase is affected by the prior austenite grain size. The austenite gets trapped by an impingement mechanism during growth of polygonal ferrite. Thus, an increase in retained austenite would be expected with increasing ferrite quantity. As has been reported [Han97a], increasing the holding time or ferrite volume fraction at a given temperature has the effect of increasing the volume fraction of retained austenite. This explains the different amount of retained austenite obtained by the two heat treatment methods.

Table 5.4 Volume fraction of phases before uniaxial testing.

	Point method analysis			X-Ray Diffraction Method
	Ferrite(%)	Bainite(%)	Martensite(%)	Retained austenite(%)
Mn-Si-Al Steel (Route B)	50 ± 4	34 ± 4	8 ± 4	8 ± 2
Mn-Si-Al Steel (Route A)	46 ± 4	42 ± 4	0	12 ± 2

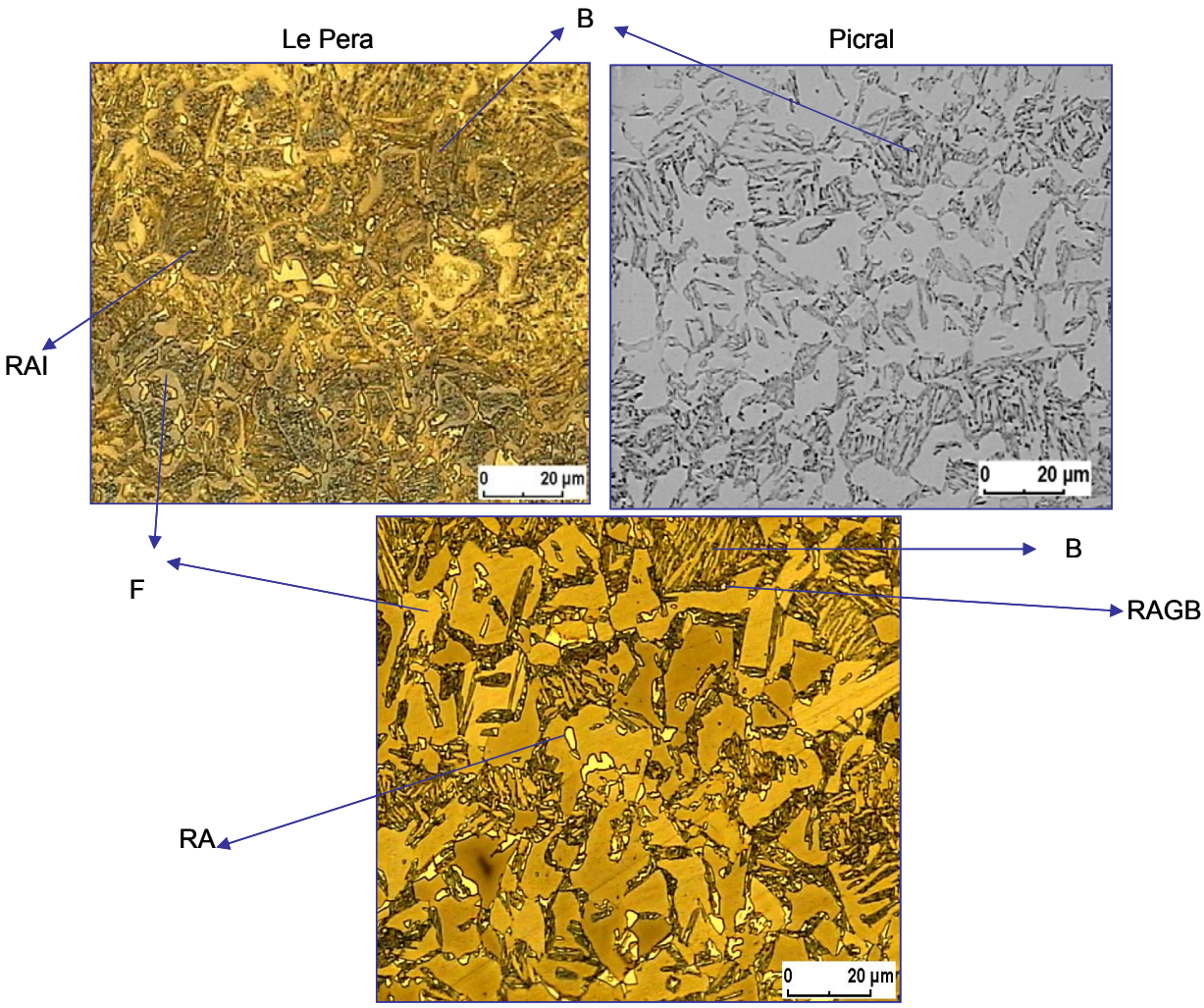

Figure 5.9 Initial microstructures of Mn-Si-Al steel with different etchants before tensile testing. Retained austenite islands (RAI), retained austenite at the grain boundary (RAGB), bainite (B), ferrite (F) and retained austenite in ferrite (RA) were identified as shown above. This specimen was austempered (Route A).

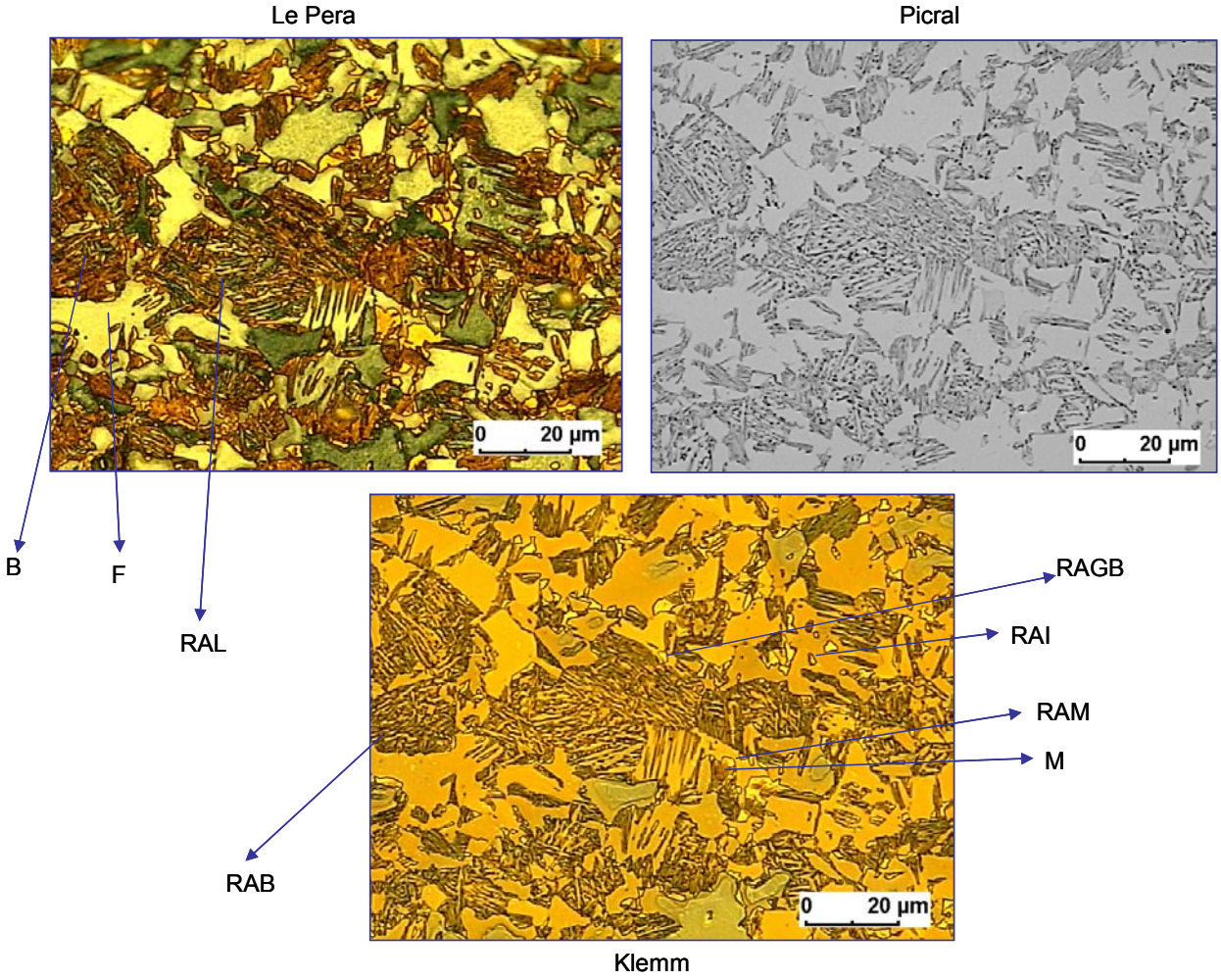

Figure 5.10 Initial microstructure of Mn-Si-Al steel with different etchants before tensile testing. Retained austenite lamellar (RAL), retained austenite island (RAI), retained austenite next to martensite (RAM), bainite (B), ferrite (F), martensite (M) and retained austenite at the grain boundary (RAGB) were identified as shown. Picral etchant gave additional information over carbon enrichment. This specimen was continuously cooled at 20 K/s to room temperature (Route B).

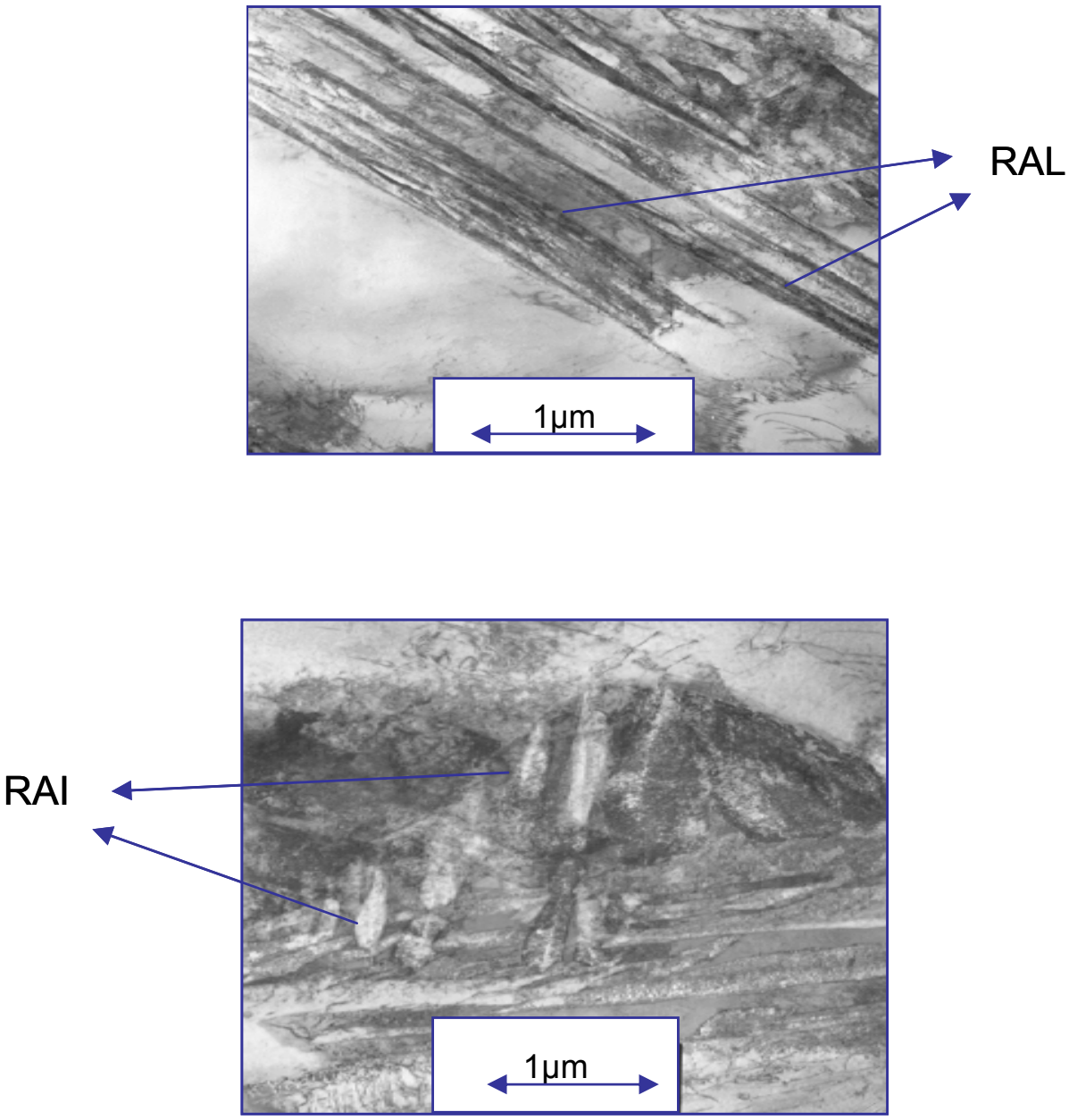

Figure 5.11 Transmission electron micrographs of Mn-Si-Al steel after austempering for 10 minutes showing retained austenite lamellar (RAL) above and retained austenite islands (RAI) below.

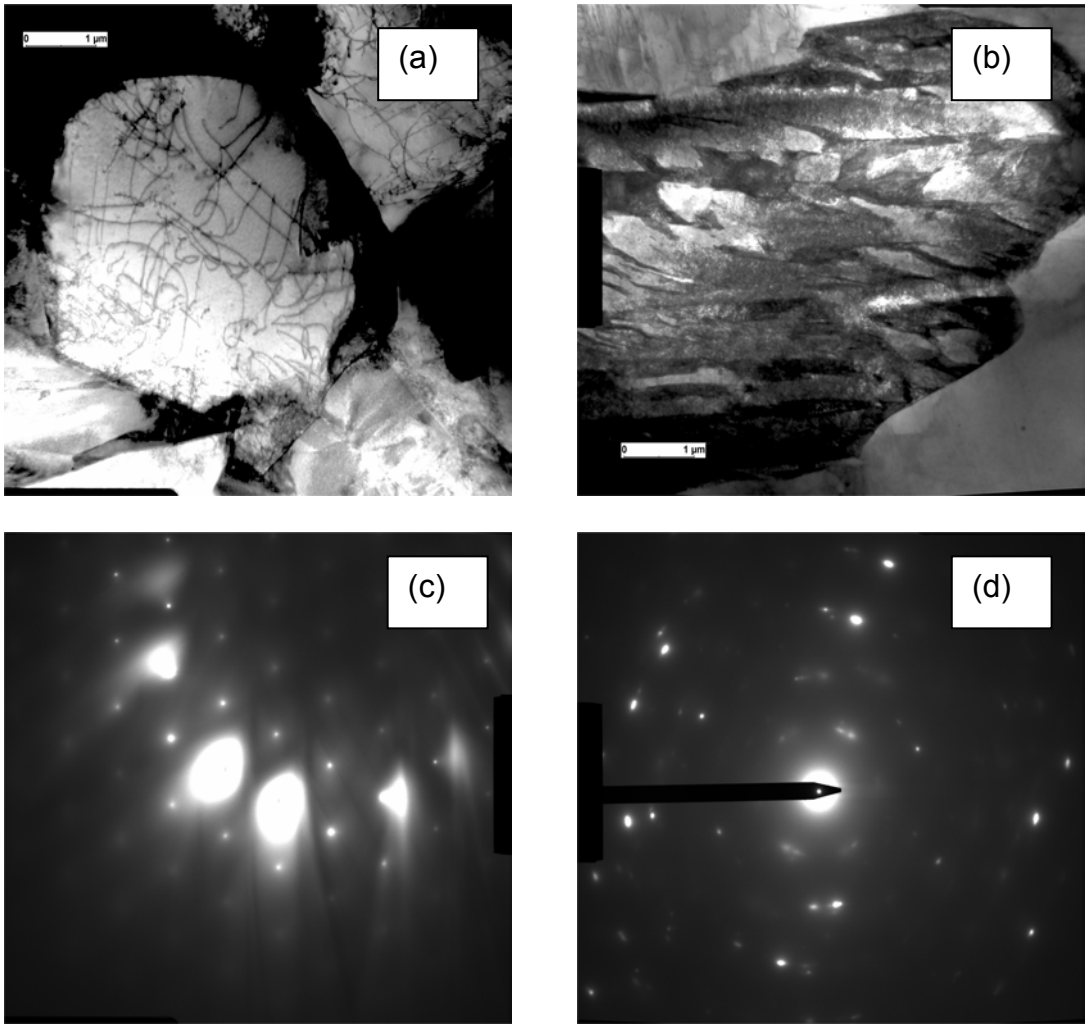

Figure 5.12 TEM micrographs and selected area diffraction (Mn-Si-Al steel) pattern (Route B) showing:

(a) Dislocations in ferrite.

(b) Retained austenite lamellar in bainite.

(c) Zone axis <111>α′-martensite

Diffraction vector g $\{110\}_{\alpha'\text{-martensite}}$

(d) Diffraction vector g $\{200\}_{\gamma\text{-retained austenite}}$

$(011)_{\gamma}$ || $(111)_{\alpha'\text{-martensite}}$

$[1\,\bar{1}\,1]_{\gamma}$ || $[0\,\bar{1}\,1]_{\alpha'\text{-martensite}}$

5.2.2 MICROSTRUCTURE AFTER UNIAXIAL TENSILE TESTING

AISI 304 (German Grade X5CrNi18.10) STEEL

The optical micrographs after uniaxial tensile tests are shown in Figures 5.13-5.18. Figure 5.13 shows the micrographs at 20°C after loading to maximum uniform elongation, 30%, 25%, 20%, 15% and 10% total strain respectively. The amount of α'-martensite in the microstructure was quantified using magnetic measurements. The results are shown in Figures 5.27 and 5.28. ε-martensite was identified at all levels of deformation except at maximum uniform elongation (using optical microscopy Figure 5.13). α'-martensite though could not be unambiguously identified microscopically was assumed present at all levels of deformation. Attempts to determine the quantity of ε-martensite using X-ray diffraction method were unsuccessful. Figure 5.14, shows the micrographs at a temperature of 40°C after the same loading pattern as at 20°C. Here again ε-martensite could be identified at all levels of deformation except at maximum uniform elongation. The amount of α'-martensite obtained is also shown in Figures 5.27-5.28. Figure 5.15 shows the micrographs at 80°C after loading to maximum uniform elongation, 30%, 25% and 20% total strain respectively. At 80°C, ε-martensite could be identified at all levels of deformation. For 150°C and 200°C, no ε-martensite or α'-martensite was identified. For 150°C and 200°C, loading was only done to maximum uniform elongation and the micrographs are depicted in Figure 5.16. At -40°C and -60°C, only micrographs showing deformation levels of 20% and 15% are shown in Figures 5.17 and 5.18. At higher levels of deformation, it was hardly possible to distinguish any features in the microstructure. The appearance of different types of martensite variants and possible transformation paths during deformation is a result of interplay between stress, strain, and temperature. Further discussion on this follows in later sections.

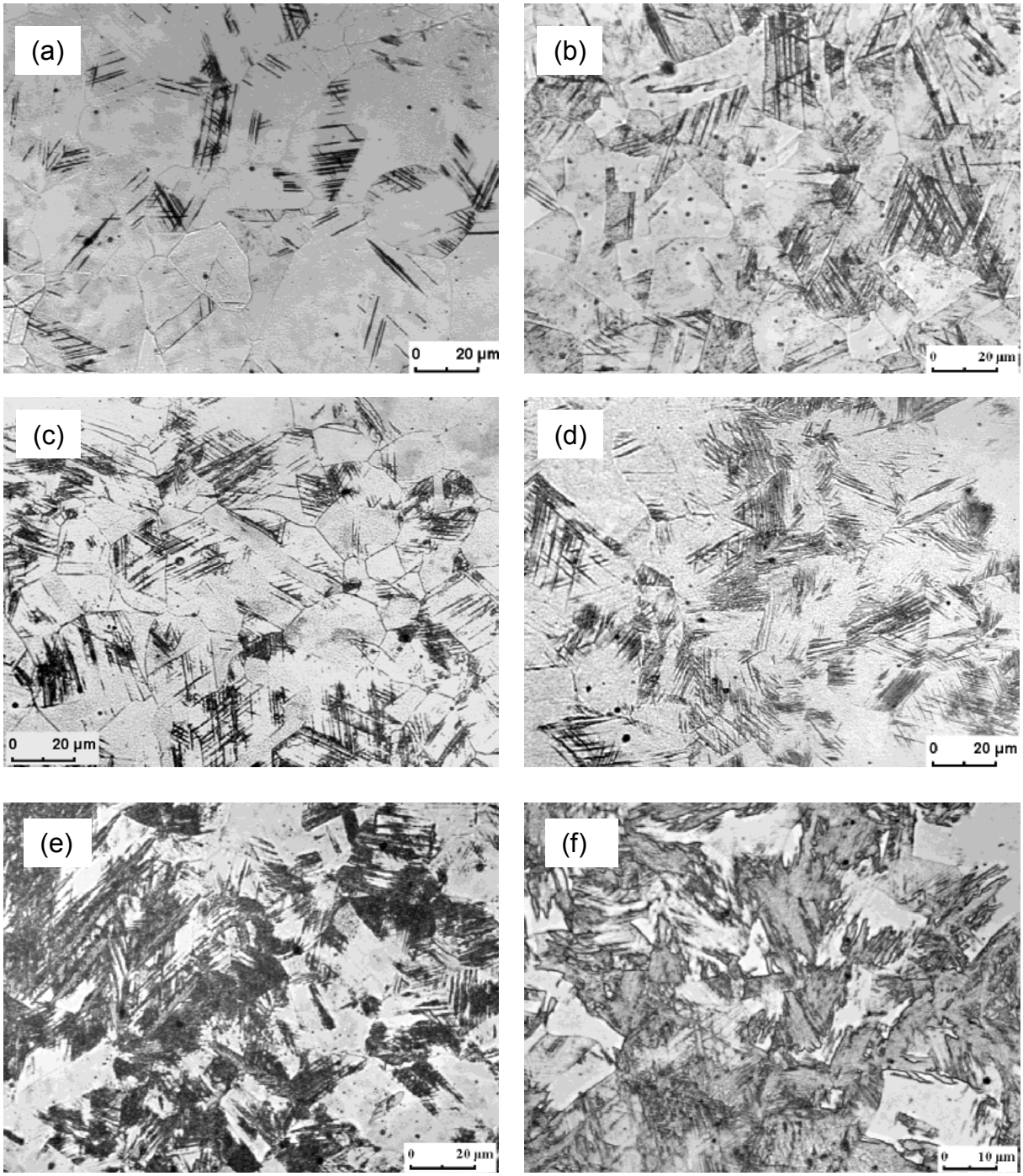

Figure 5.13 Optical micrographs of the steel AISI 304 (X5CrNi18.10) at 20°C; (a) loading to 10% plastic strain, (b) loading to 15% plastic strain, (c) loading to 20% plastic strain, (d) loading to 25% plastic strain (e) loading to 30% plastic strain and (f) loading to maximum uniform elongation. Thin parallel plates in the microstructure indicate ε-martensite.

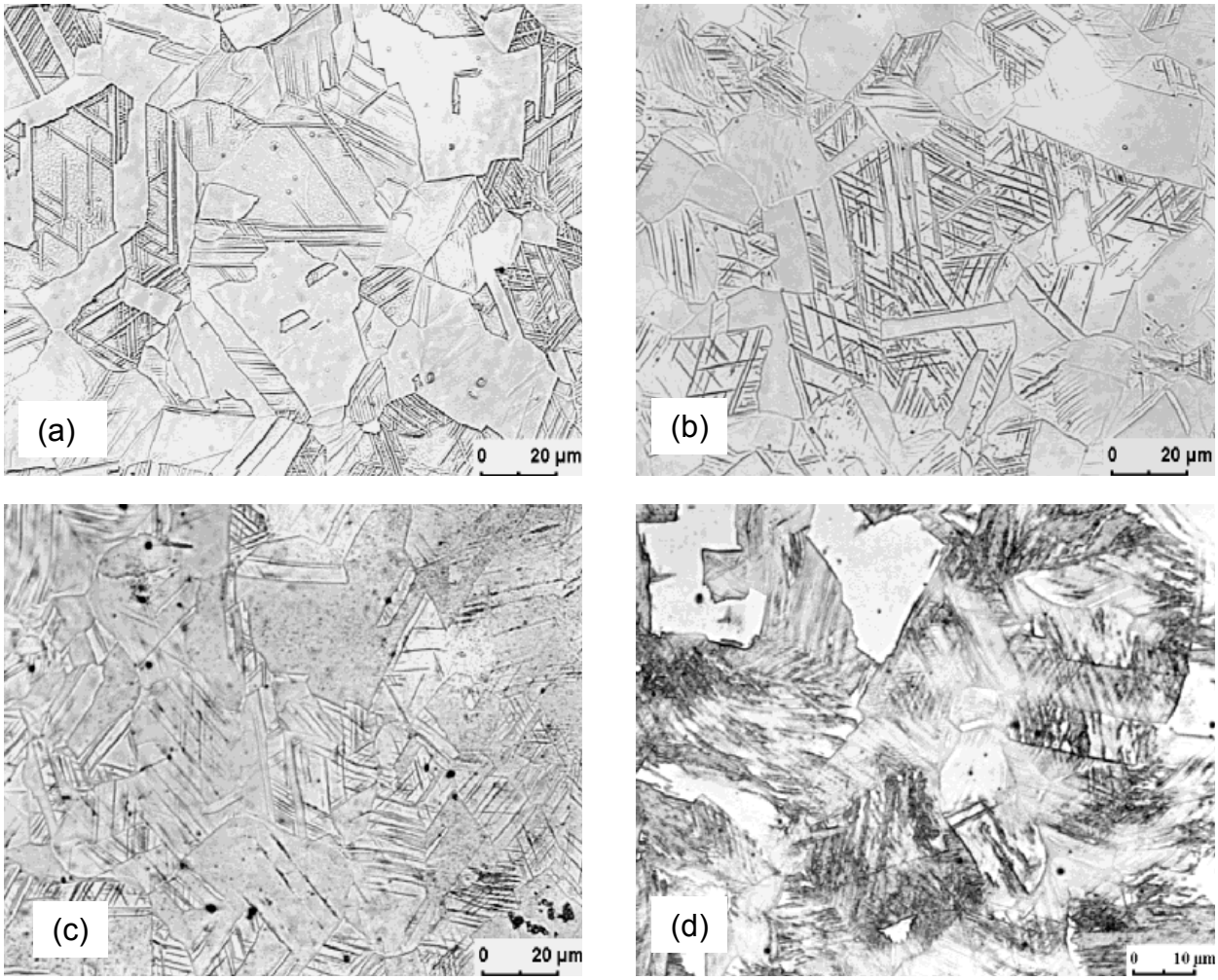

Figure 5.14 Optical micrographs of the steel AISI 304 (X5CrNi18.10) at 40°C; (a) loading to 20% plastic strain, (b) loading to 25% plastic strain, (c) loading to 30% plastic strain, and (d) loading to maximum uniform elongation. Thin plates running across the grains indicate ε-martensite.

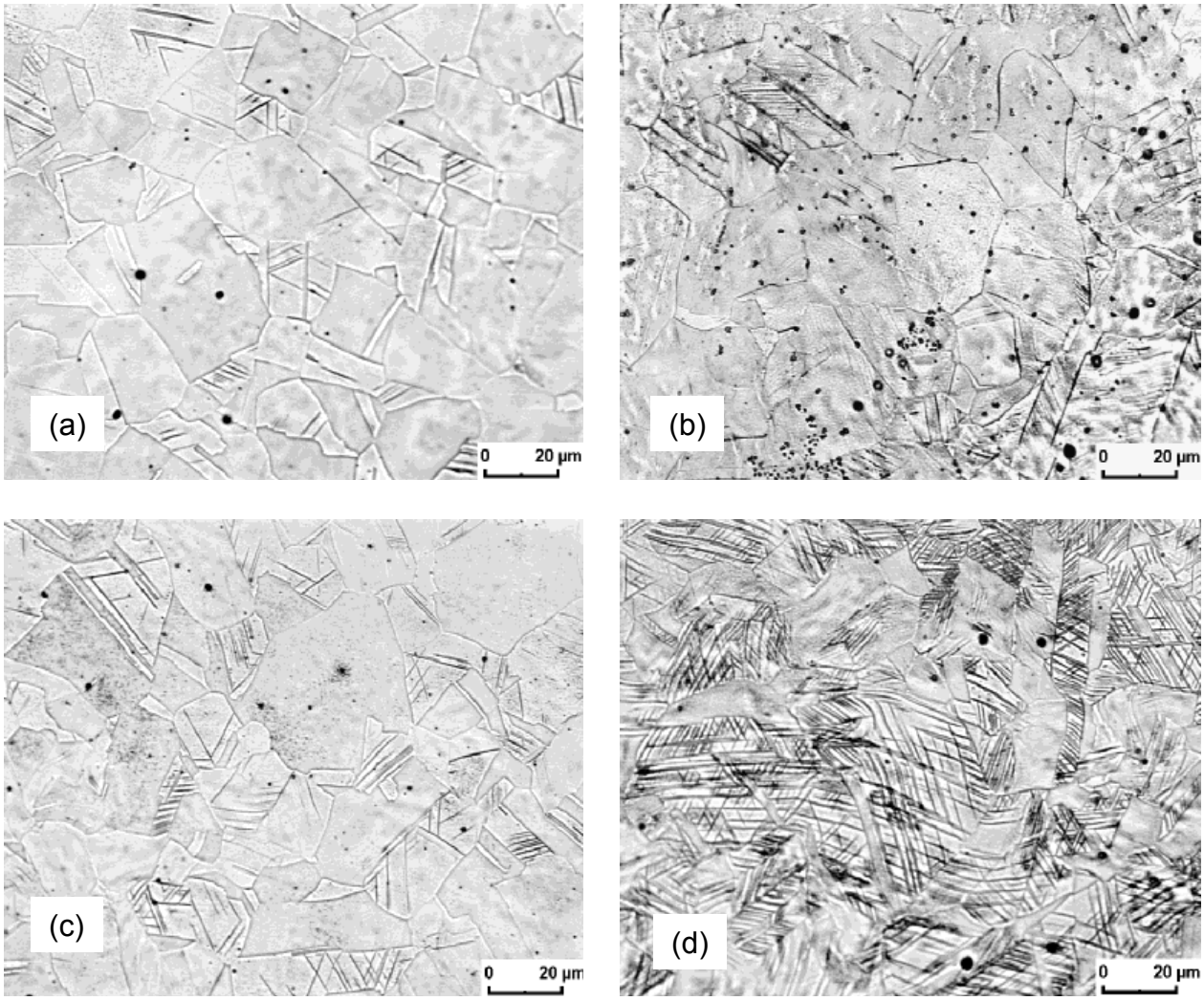

Figure 5.15 Optical micrographs of the steel AISI 304 (X5CrNi18.10) at 80°C; (a) loading to 20% plastic strain, (b) loading to 25% plastic strain, (c) loading to 30% plastic strain, and (d) loading to maximum uniform elongation. Thin parallel plates indicate ε-martensite

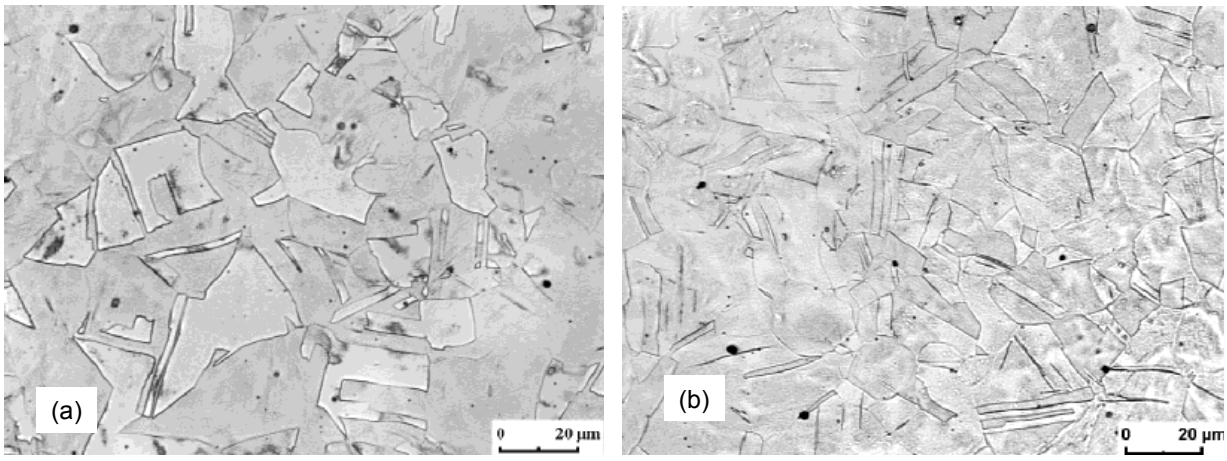

Figure 5.16 Optical micrographs of the steel AISI 304 (X5CrNi18.10) after loading to maximum uniform elongation showing austenite structure after strain hardening; (a) 150°C, (b) 200°C.

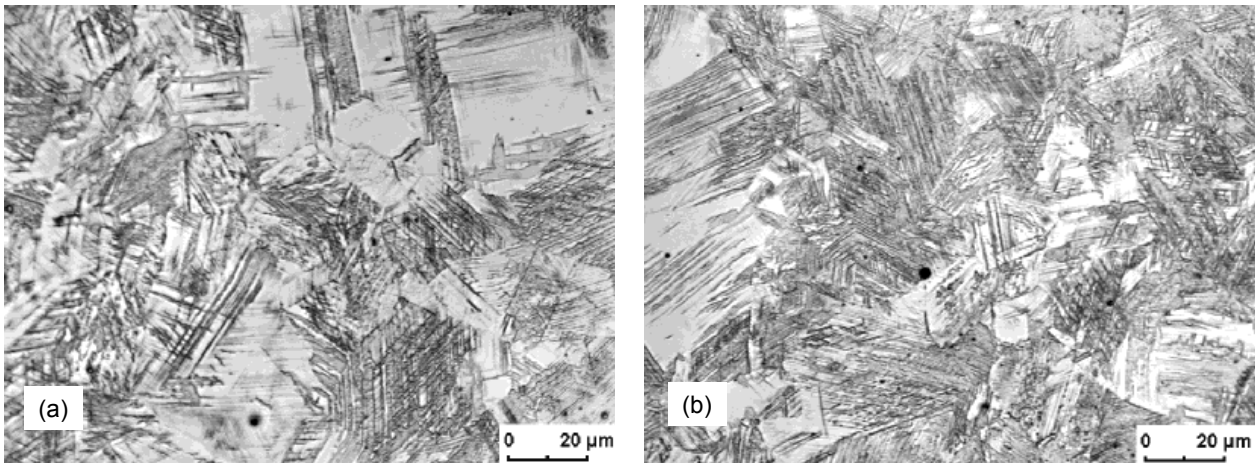

Figure 5.17 Optical micrographs of the steel AISI 304 (X5CrNi18.10) at -40°C when loaded to; (a) 15% plastic strain, (b) 20% plastic strain. ε- and α'-martensite could be clearly distinguished.

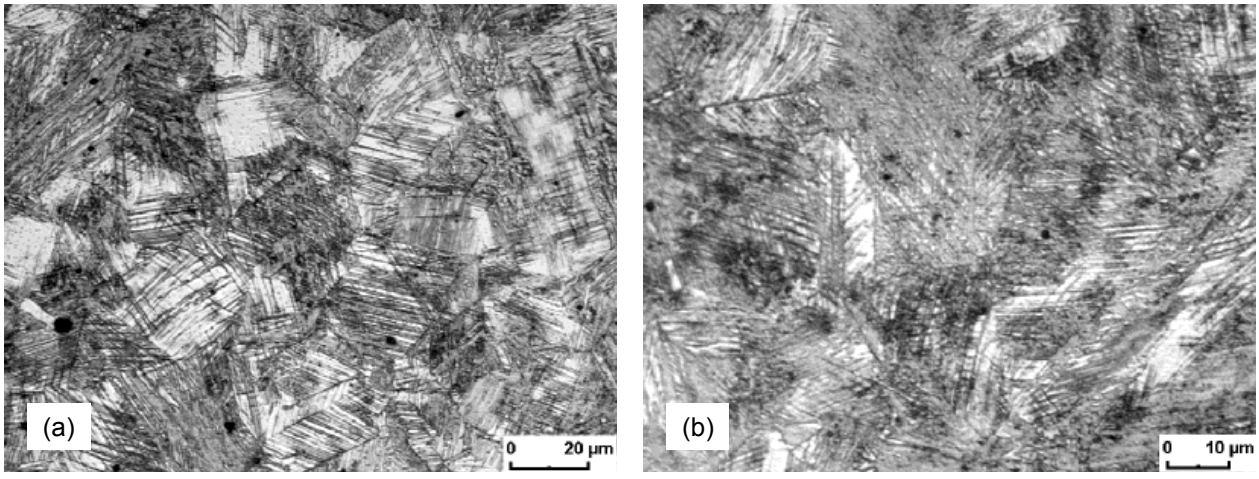

Figure 5.18 Optical micrographs of the steel AISI 304 (X5CrNi18.10) at -60°C when loaded to; (a) 15% plastic strain, (b) 20% plastic strain.

Mn-Si-Al STEEL

After uniaxial tension testing at different temperatures to maximum uniform elongation, metallographic specimens were prepared and analysed. The micrographs after testing, for example, at 40°C and 60°C are shown in Figures 5.19-5.23. A comparison of these micrographs with the ones before uniaxial testing shows that the retained austenite has partially or wholly transformed to martensite due to tensile loading.

The critical driving force for transformation was reached as a result of additional mechanical driving force. Martensite appears brown in colour in the microstructures. Microhardness measurements in the brown areas showed increased hardness due to martensite formation and hardening as shown in Figure 5.20. The microhardness range of 4500-5500 N/mm^2 was obtained in the ferritic areas. For the bright yellow areas the microhardness values of about 5000 or 10000 N/mm^2 were obtained. This indicated that the retained austenite had partially transformed to martensite. Examination of Figure 5.20 reveals that for the austempered specimens (Route A), some retained austenite remained after transformation and could be detected using optical microscopy, while for the continuously cooled specimens (Route B), no trace of retained austenite could be detected (Figure 5.22). This was confirmed by X-ray diffraction measurement of the retained austenite (Table 5.5) and also by micro-hardness measurements. The presence of fine matrix structure of ferrite and bainite for specimens that showed improved ductility was visible from colour etching. Strain hardening effects characterised by browning of ferrite areas were made visible due to colour etching.

Table 5.5 Volume fraction of retained austenite after uniaxial testing.

Mn-Si-Al steel	Temp(°C)	Retained austenite (%)
Austempered (Route A)	-60	2
	-40	2
	40	4
	60	4
Continuously Cooled (Route B)	-60	0
	-20	0
	20	1
	60	1

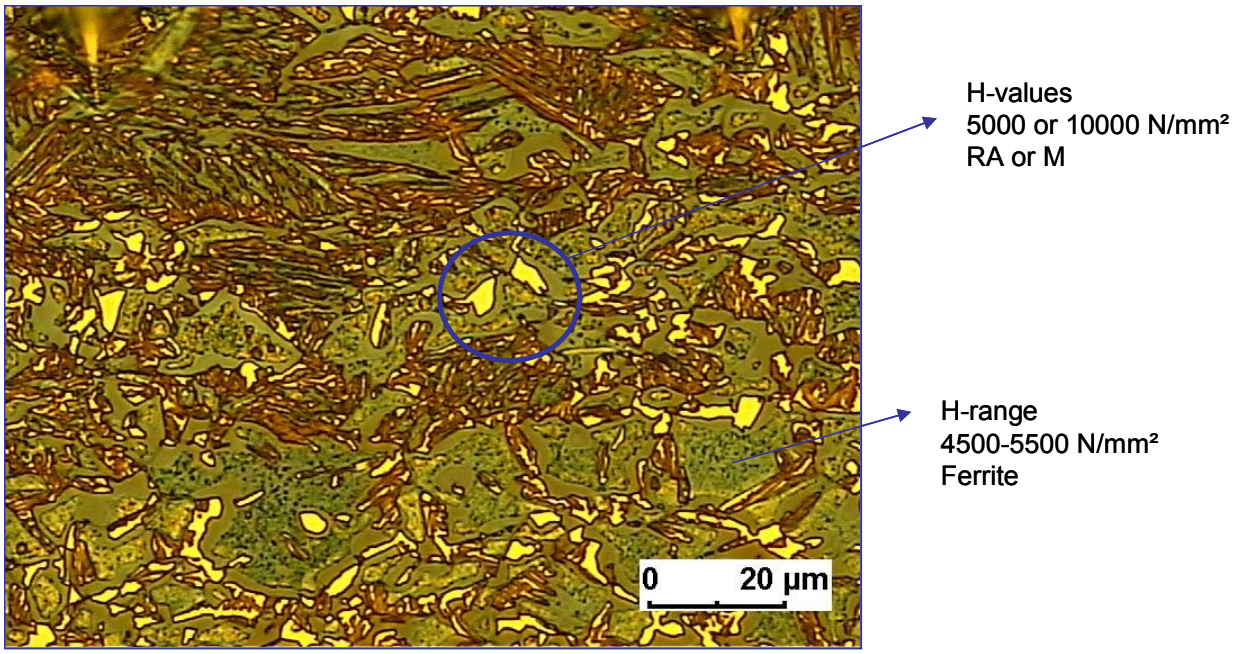

Figure 5.19 Optical micrograph of the Mn-Si-Al steel after loading to maximum uniform elongation using Le Pera etchant. Micro-hardness measurements were carried out to help in identification of the phases. Bright yellow areas are martensite (M) or retained austenite (RA). Orange-green is ferrite (Route A).

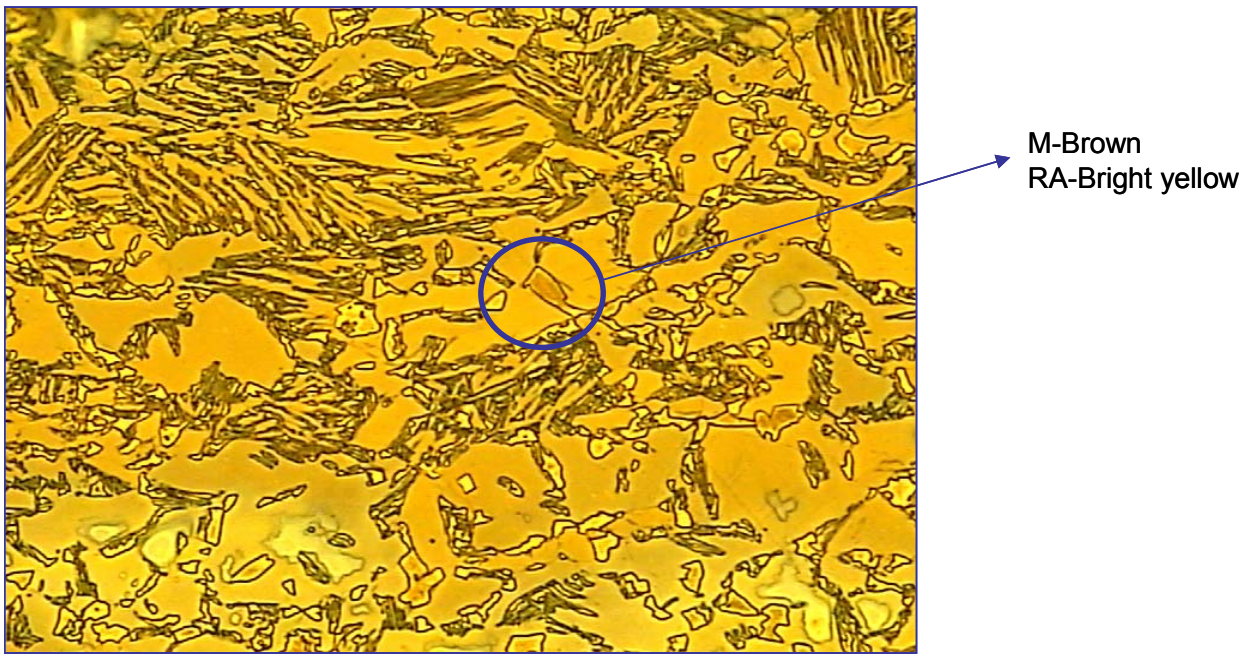

Figure 5.20 Optical micrograph of the steel Mn-Si-Al steel at 40°C after loading to maximum uniform elongation using Klemm reagent. Retained austenite (RA) volume percent was determined to be 4% using X-ray diffraction. The use of colour etchants enabled different phases to be identified as shown. Martensite (M) brown in colour, ferrite (F) appearing as bright orange, and retained austenite (RA) appearing as bright yellow (Route A).

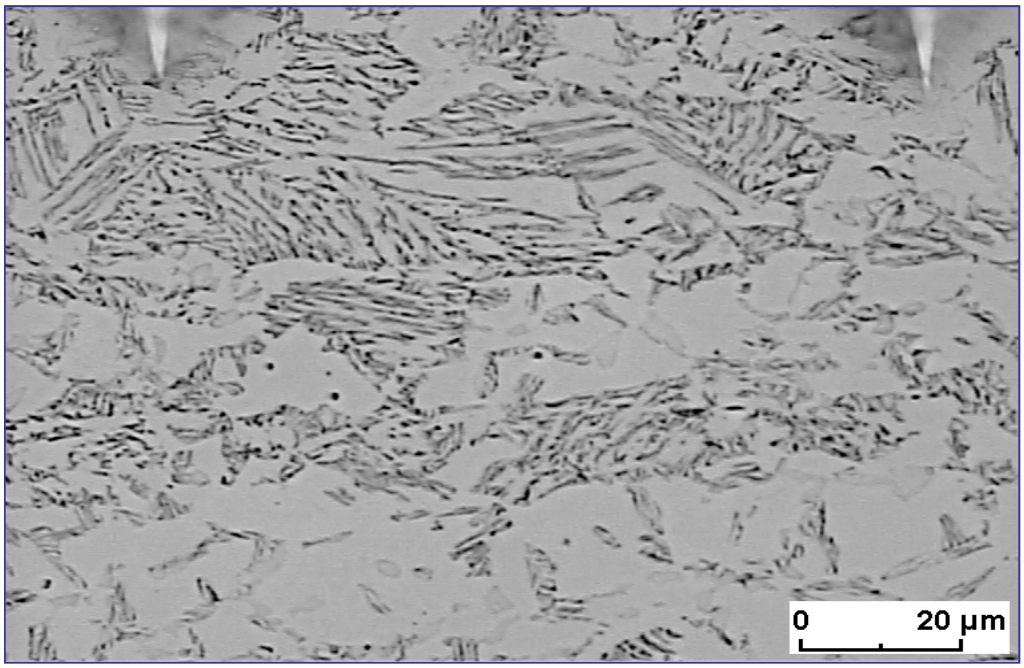

Figure 5.21 Optical micrograph of the Mn-Si-Al steel after loading to maximum uniform elongation using Picral reagent. Information on carbon enrichment on different phases can roughly be obtained (Route A).

At a temperature of 60°C for the specimens that did not exhibit any improved ductility, no retained austenite could be identified in the micrographs as shown in Figure 5.22. Etching using Picral reagent showed a completely different microstructure as compared to Figure 5.21. No information on carbon enrichment on different phases could be obtained.

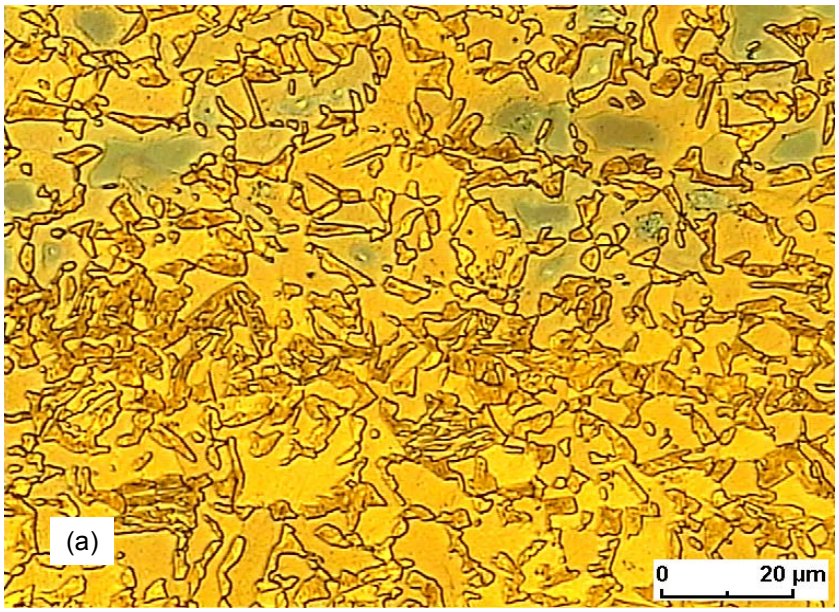

Figure 5.22 Optical micrographs for the Mn-Si-Al steel after loading to maximum uniform elongation for continuously cooled specimen at 60°C (Klemm's reagent) (Route B).

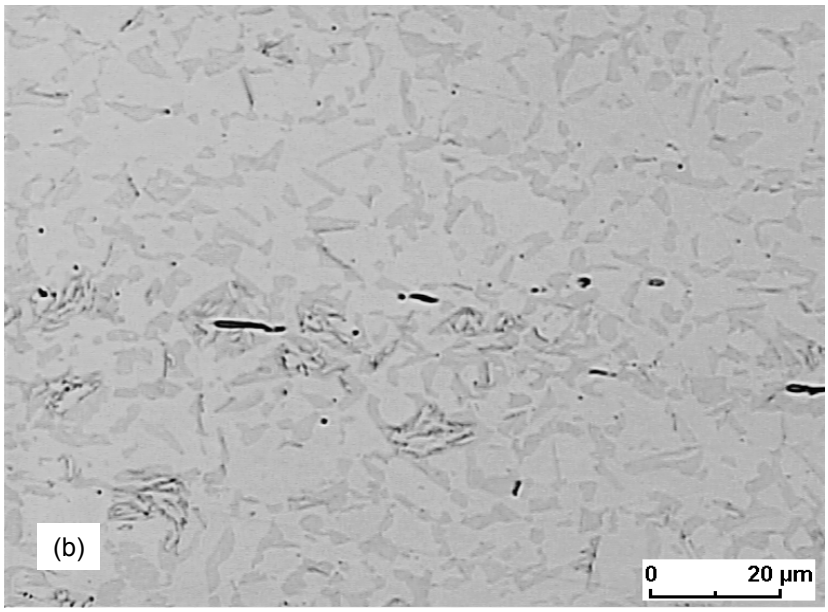

Figure 5.23 Optical micrographs for the Mn-Si-Al steel after loading to maximum uniform elongation for continuously cooled specimen at 60°C (Picral reagent) (Route B).

5.3 PLASTIC DEFORMATION AND PHASE TRANSFORMATION OF STEEL AISI 304

5.3.1 RESULTS OF UNIAXIAL TENSILE TESTING

The results of uniaxial tensile testing for this steel are shown in Figure 5.24. It can be observed that strength increases with decreasing temperature. A maximum uniform elongation was obtained at about 40°C which amounts to about 170% of the lowest uniform elongation obtained at 200°C.

Figure 5.25 shows the work-hardening rate as a function of true strain. For temperatures -40°C and -60°C, there is an increased hardening in the early stages of deformation and an accompanying very high rate of decay of work-hardening rate for true strains up to 0.1. Between 0.1 and 0.2 true strain, there is sharp increase in work-hardening rate followed by a high rate of decay. For temperatures 20°C, 40°C, 80°C, 150°C and 200°C, there is an increased hardening in the early stages of deformation but a slower rate of decay of work-hardening rate as the deformation progressed. At a temperature of 20°C, the slowest rate of decay of work-hardening rate was recorded followed by that at 40°C, 80°C, 150°C and 200°C in that order.

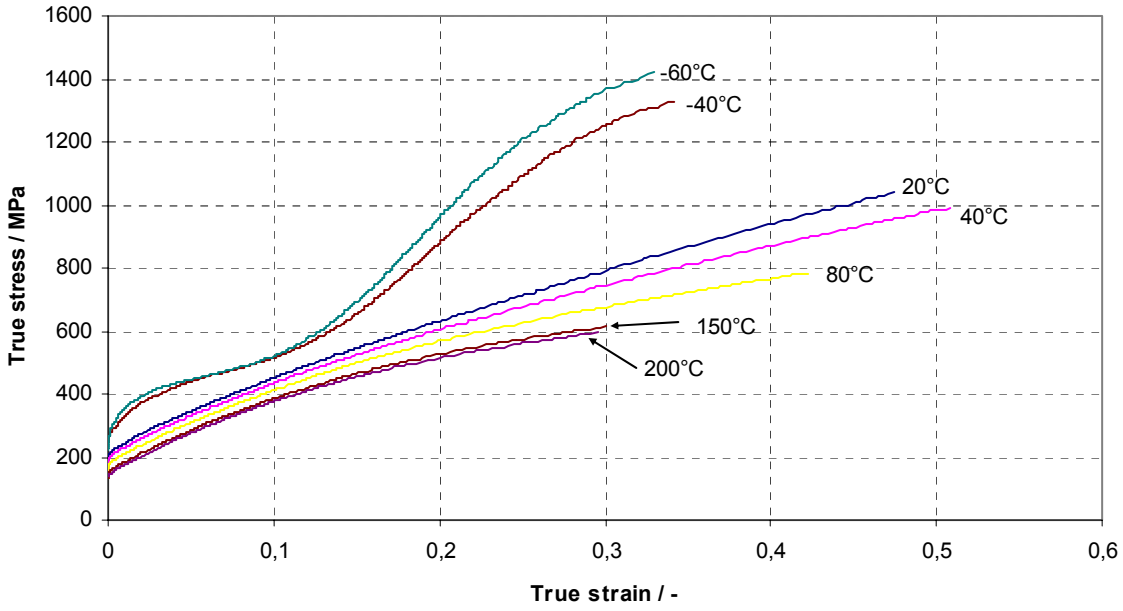

Figure 5.24 True stress-true strain curves at different temperatures and loading up to maximum uniform strain at all the temperatures.

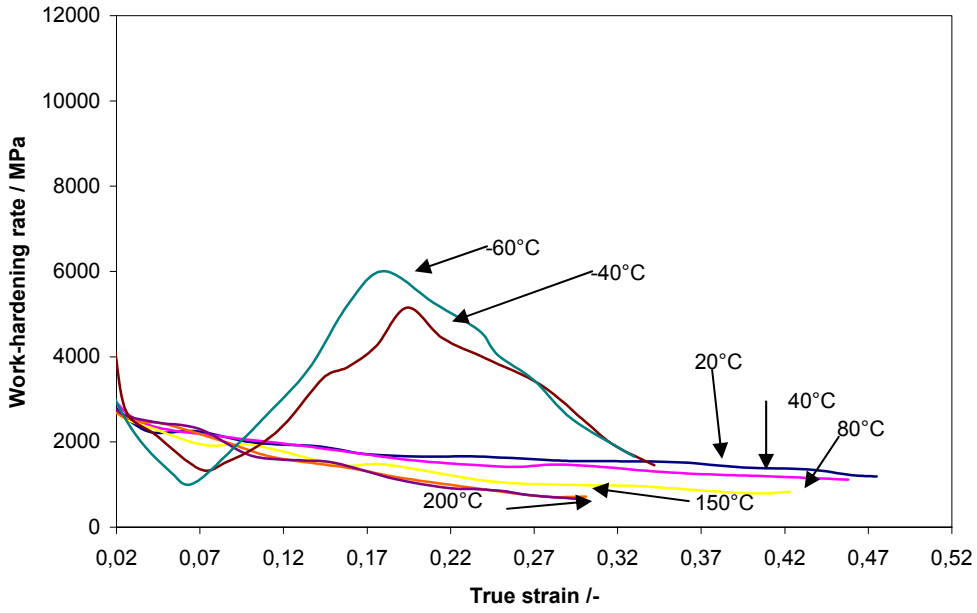

Figure 5.25 Work-hardening rates as a function of true strain at different temperatures.

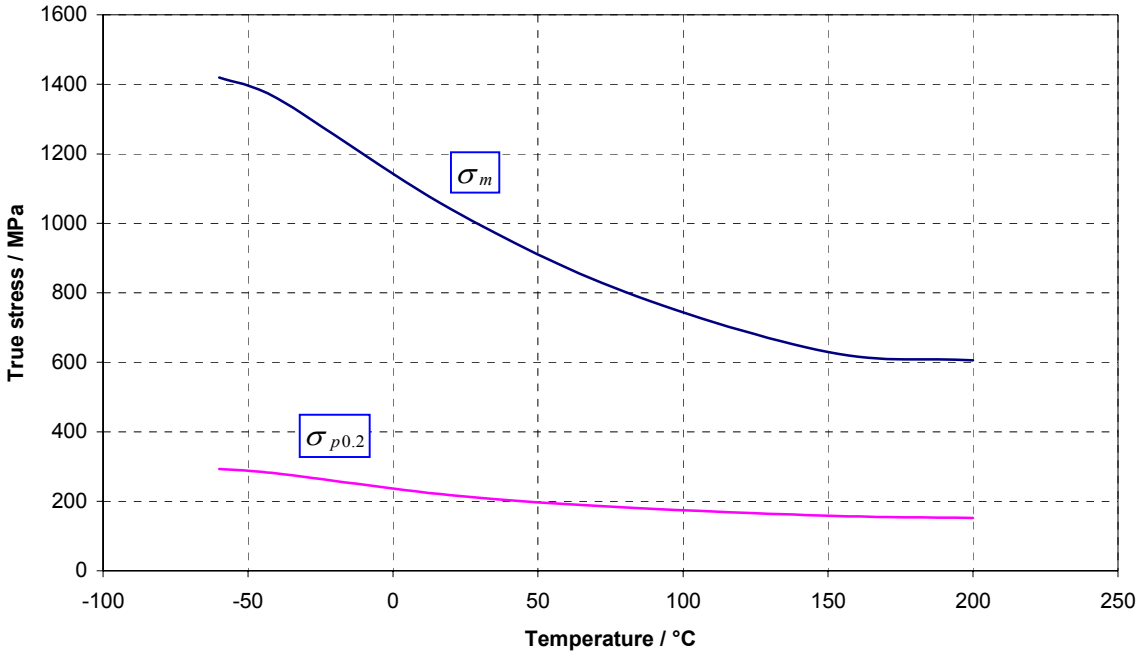

Figure 5.26 Maximum true stresses (σ_m) and yield stresses ($\sigma_{p0.2}$) as a function of temperature (X5CrNi18.10).

The variation of tensile strength (σ_m) and yield stress ($\sigma_{p0.2}$) as a function of temperature is shown in Figure 5.26. As can the seen both increases with decreasing temperature. This is due to increased formation α'-martensite as temperature decreases.

5.3.2 PHASE TRANSFORMATION

Phase transformation is concerned with how one or more phases in an alloy change into a new phase or new phases. Transformation normally occurs because one state is unstable relative another. The relative stability of a phase at constant temperature and pressure is determined by its Gibbs free energy. In our case, the phase transformation was studied by identifying and quantifying the initial and final phases after deformation to various stages at given constant temperatures.

The kinetics of deformation-induced martensitic transformations as previously mentioned is traditionally treated as a function of strain. In this work, Ludwigson and Berger [Lud69] expression for kinetics of martensitic transformation has been adopted and modified to take temperature into consideration. Volume fraction of deformation induced α'-martensite as a function of true strain and true stress at different temperatures for the steel X5CrNi18.10 is shown in Figures 5.27 and 5.28. As can be clearly seen in Figure 5.27, there is a gradual α'-martensite formation during the entire deformation process at temperatures 20°C and 40°C. For temperatures -40°C and -60°C, the rate of formation of α'-martensite is very high resulting in high strength due to the high strength of martensite phase [Ang54]. This dramatic increase in strength at -40°C and -60°C can be attributed to a high rate and direct $\gamma \rightarrow \alpha'$-martensite transformation [Wei95].

Weiss and his co-workers [Wei95, Wei01, Wei02b] hypothesised that the first inflection point on the flow curve and the minimum of the work hardening rate, respectively, characterises the stress for initiating the direct $\gamma \rightarrow \alpha'$-martensite transformation. At this point, α'-martensite has formed but mainly from ε-martensite [Wei02b]. This direct transformation is recognised by the sharp increase in work hardening rate as depicted in Figure 5.32. For temperatures where a high direct $\gamma \rightarrow \alpha'$-martensite transformation does not take place (20°C, 40°C, and 80°C), the rate of decay of work hardening continue decreasing until the point of maximum uniform elongation.

Ludwigson and Berger's expression (Equation (2.1)) was used to fit our experimental data. The results are shown in Figure 5.29. Table 5.6 shows the constants that were used to fit our data and the accompanying correlation coefficients. As can be seen the transformation kinetics proposed by Ludwigson and Berger generally gives a good agreement with our experimental data irrespective of whether true strain or engineering strain is used and was thus adopted for our subsequent analysis.

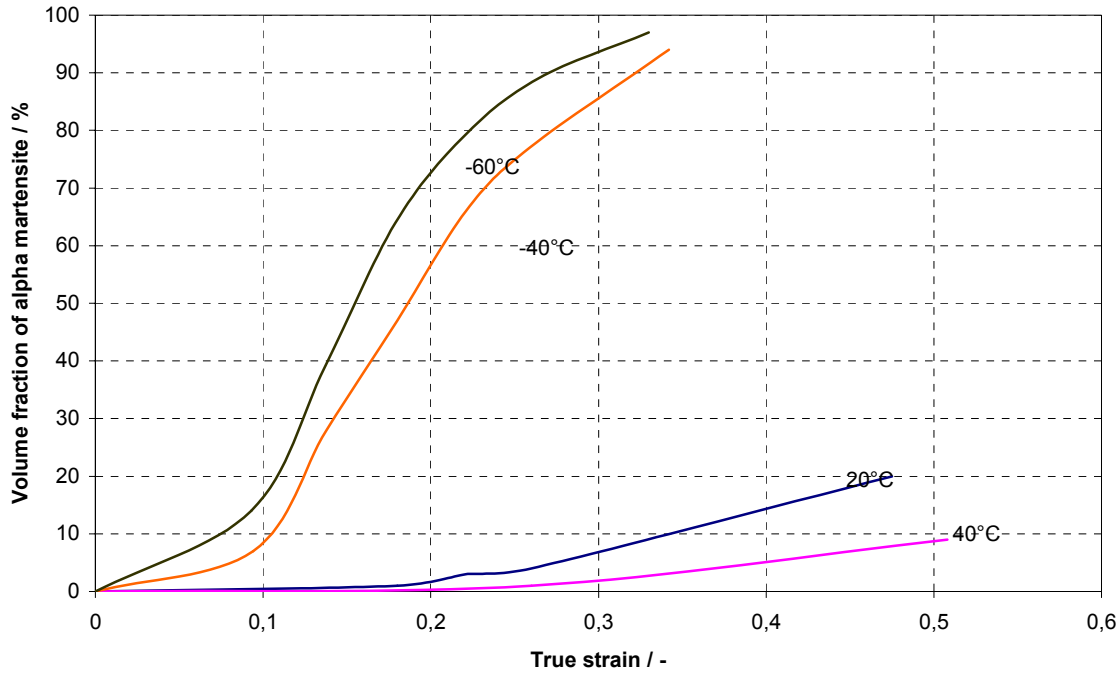

Figure 5.27 Volume fraction of deformation induced α'-martensite as a function of true strain at different temperatures for the steel X5CrNi18.10.

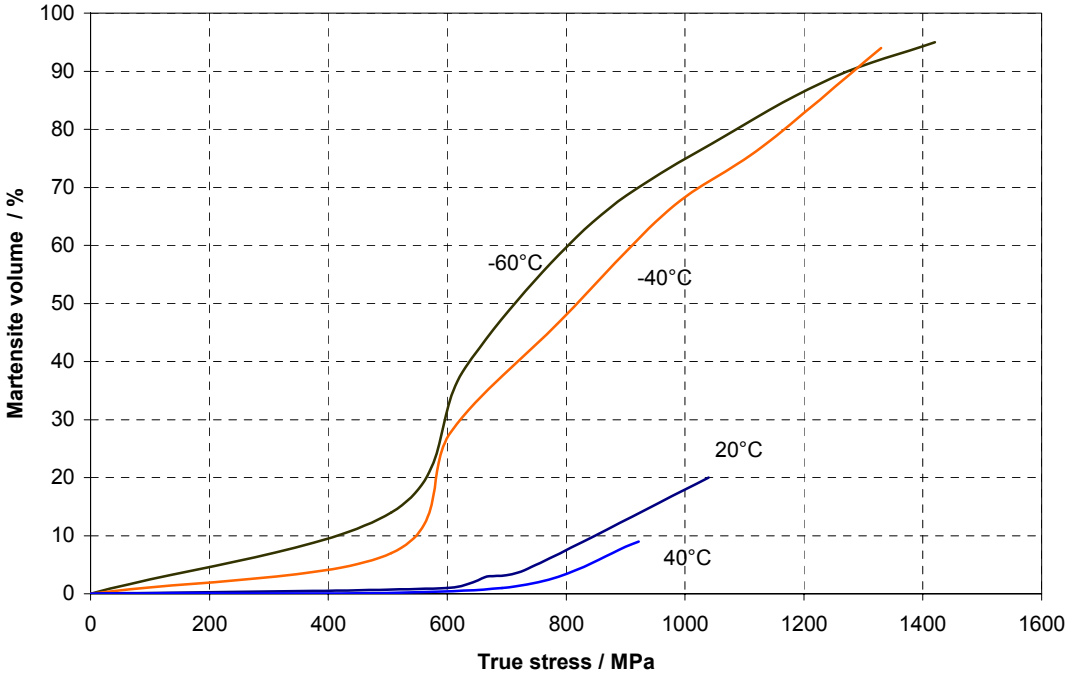

Figure 5.28 Volume fraction of deformation induced α'-martensite as a function of true stress at different temperatures for the steel X5CrNi18.10.

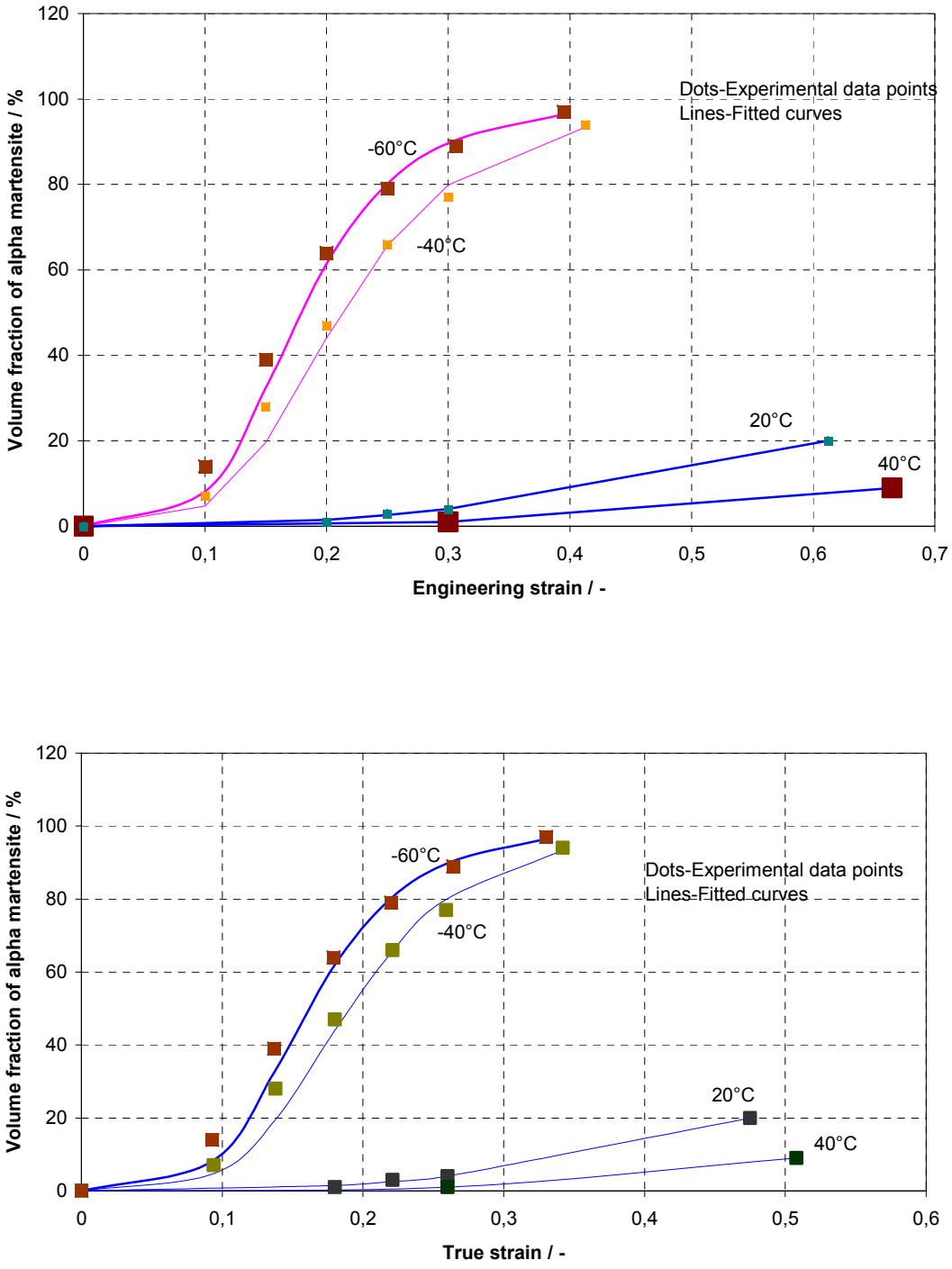

Figure 5.29 Volume fraction of alpha martensite as a function of (a) engineering strain above and (b) true strain below.

Table 5.6 Constants from Ludwigson and Berger's expression used to fit own experimental data.

Temp (°C)	Constants (equation 2.1)	
	A	B
-60	1310.58	4.17
-40	484.54	3.99
20	0.85	2.5
40	0.32	2.86

TEMPERATURE MODIFICATION OF LUDWIGSON AND BERGER'S EQUATION

The expression from Ludwigson and Berger does not explicitly mention how the temperature dependence of transformation kinetics during isothermal loading can be taken into consideration. The constant B was meant to take into consideration the autocatalytic transformation behaviour of martensite. The constant A was found to linearly vary with composition and was defined as the propensity factor. The assumption made in this work is that temperature dependence is implicitly implied in constants A and B. A plot of natural logarithm of A and B (see Table 5.6) versus temperature is shown in Figure 5.30 together with fitting functions. As can be seen, A is strongly temperature dependent unlike B. Assuming that the gradient is approximately zero in B-line, the value of B is approximately 3 which confirms the prediction of Lugdwigson and Berger [Lud69].

Starting from Equation (2.1), temperature dependence can be derived as follows:

$$V_{\alpha'} = A\, e_C^B V_{\gamma R}$$

As a function of temperature and strain, the equation can be written as:

$$V_{\alpha'}(T,e) = A(T)\, e^B V_{\gamma R} \tag{5.1}$$

But from the fitting function

$$\ln A = 2.1233 - 0.0892T \tag{5.2}$$

where T is the test temperature.

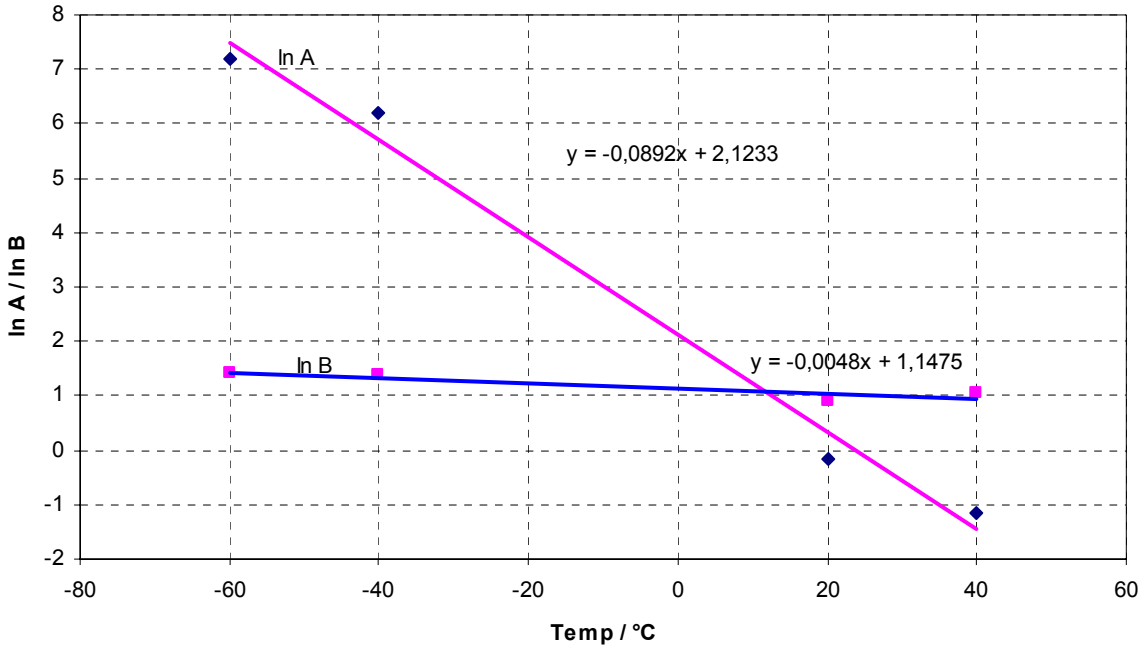

Figure 5.30 Natural logarithm of constant A and B from Ludwigson and Berger's expression (see Table 5.6) versus temperature.

Rearranging Equation (2.1) one gets

$$\frac{V_{\alpha'}}{1-V_{\alpha'}} = A e^{B} \tag{5.3}$$

Taking natural logarithms one gets

$$\ln \frac{V_{\alpha'}}{1-V_{\alpha'}} = B \ln e + \ln A \tag{5.4}$$

Substituting Equation (5.2) in Equation (5.4) and rearranging one gets

$$\frac{V_{\alpha'}}{1-V_{\alpha'}} = \exp\left(B \ln e + \left[2.1233 - 0.0892T\right]\right) \tag{5.5}$$

In general form this expression can be expressed as,

$$\frac{V_{\alpha'}}{1-V_{\alpha'}} = \exp\left\{f(\sigma,\varepsilon) + f(M_d, T)\right\} \tag{5.6}$$

where M_d is the temperature above which no deformation induced martensite is formed, T is the test temperature, σ is the true stress and ε is the true strain.

The expression for the transformation kinetic taking into consideration temperature dependence is given as,

$$\frac{V_{\alpha'}}{1-V_{\alpha'}} = \exp\left(B\ln e + C\left[M_d^{\gamma\to\alpha'} - T\right]\right) \tag{5.6}$$

where e is engineering strain and B, C are constants. The above expression gives the volume of deformation induced martensite as a function of strain and isothermal test temperature for the steel X5CrNi18.10. Empirical equations for the calculation of martensite transformation temperatures $M_d^{\gamma\to\varepsilon}$, $M_d^{\gamma\to\alpha'}$, and $M_d^{\varepsilon\to\alpha'}$ from chemical compositions are hardly available in literature [Wei90]. However, empirical equations relating $M_{d30}^{\alpha'}$-Temperature and chemical composition are available [Wei90]. $M_{d30}^{\alpha'}$-Temperature is the temperature where 50% α'-martensite has formed after 30% plastic deformation.

As shown in Figures 5.27 and 5.28 the volume fraction of α'-martensite formed increase with decrease in temperature and an increase in both true strain and true stress. The effects of temperature on martensite phase transformation are depicted in temperature-true stress transformation diagram, Figure 5.31, and temperature-true strain transformation diagram, Figure 5.32. These diagrams were constructed following the work of Weiss, Peisker and Tranta [Wei01, Wei02a, Wei02b] who investigated several types of metastable austenitic steels including the one investigated in this work. Comparisons of chemical compositions of the two similar steels are shown in Table 5.7. The two steels differed slightly in chemical composition and so the behaviour is expected not to totally agree one to one. The transformation diagrams from the work of Weiss and co-workers [Wei01] are shown in Figure 5.33.

Table 5.7 Comparisons of the chemical compositions of the investigated steels in wt-%.

Steel	C	Si	Mn	P	S	Cr	Ni	Ti	N	Mo	V
X5CrNi18.10 (investigated)	0.043	0.38	1.15	-	-	19.19	9.03		0.096	0.23	0.18
X5CrNi18.10 (H2) [Wei02a]	0.047	0.47	1.79	0.034	0.026	17.13	8.77	0.02	0.017	-	-
X6CrNiTi18.10(H3) [Wei02a]	0.051	0.58	0.76	0.042	0.007	17.06	9.46	0.41	0.018	-	-

To construct the temperature-true stress transformation diagram, the graph of volume fraction of α'-martensite versus true stress (Figure 5.28) was used to obtain various values of temperatures and true stresses for a specific amount of α'-martensite. Using the same method, the graph of volume fraction of α'-martensite versus true strain (Figure 5.27) was used to construct the temperature-true strain transformation diagram. To help obtain the M_d-Temperatures, ultimate tensile strength values and true strain values at maximum uniform elongation were superimposed on the diagrams and appropriately extrapolated as proposed by Weiss and his co-workers [Wei01, Wei02a]. Weiss and his co-workers [Wei01] managed to quantify the amount of ε-martensite in their investigated steels and this enabled them to approximate the $M_s^{\sigma}\gamma \rightarrow \varepsilon$ temperature for the above steel which has used in the present construction of our diagrams. Given a general lack of published literature and agreement on the definition of $M_d^{\gamma\rightarrow\varepsilon}$, $M_d^{\gamma\rightarrow\alpha'}$ and $M_d^{\varepsilon\rightarrow\alpha'}$, the theory proposed by Weiss and his co-workers [Wei01, Wei02a] has been used in estimating these temperatures for our diagrams. The temperature-true stress and temperature-true strain transformation diagrams from Weiss and his co-workers [Wei01] are shown in Figure 5.33 for comparison.

At 80°C and above, no α'-martensite was detected even after loading to maximum uniform elongation. At 40°C, only 9% α'-martensite was detected at maximum uniform elongation. This is because the critical stress required to initiate martensite formation increases linearly with increase in temperature as been pointed previously by several research workers [Tam82, Pat53, Wei01]. As hypothesised by Weiss, Peisker and Tranta [Wei01, Wei02a, Wei02b] the three possible transformation paths require different critical initiating stresses as shown in Figure 5.31 (a). $R_c^{\gamma\rightarrow\varepsilon}$, the critical stress required to initiate $\gamma \rightarrow \varepsilon$-martensite transformation is less than $R_c^{\varepsilon\rightarrow\alpha'}$ and $R_c^{\gamma\rightarrow\alpha'}$. $R_c^{\gamma\rightarrow\varepsilon}$-Critical stress line is equivalent to the 1% volume fraction of ε-martensite line (adapted from the work Weiss [Wei01]). The $R_c^{\varepsilon\rightarrow\alpha'}$-Critical stress line is equivalent to 1% volume fraction of α'-martensite line extrapolated to ultimate tensile strength line. The $R_c^{\gamma\rightarrow\alpha'}$-Critical stress line is equivalent to 20% volume fraction of α'-martensite line extrapolated to ultimate tensile strength line. The critical stress required to initiate $\varepsilon \rightarrow \alpha'$-martensite transformation ($R_c^{\varepsilon\rightarrow\alpha'}$) is less than the critical stress required to initiate $\gamma \rightarrow \alpha'$-martensite transformation ($R_c^{\gamma\rightarrow\alpha'}$). As can be the seen from Figure 5.31, with increasing temperature, ε-martensite becomes stable and does not transform to α'-martensite.

This was confirmed by metallographical analysis as shown in Figures 5.13 to 5.18. Since ε-martensite could not be identified at 150°C, but at 80°C, $M_d^{\gamma\to\varepsilon}$ for this steel was approximated to be 150°C. Weiss and his co-workers [Wei01] estimated $M_d^{\gamma\to\varepsilon}$ for this steel to be 140°C. At 80°C and above, no deformation induced α'-martensite can be formed. This is because the critical stresses to initiate martensitic transformation from metastable austenite and ε-martensite could not be attained i.e. austenite phase and ε-martensite phase becomes more stable. The presence of ε-martensite for example at 20°C and 10% plastic deformation but no α'-martensite confirms the hypothesis by Weiss and his co-workers [Wei01] that the critical chemical driving force for ε-martensite formation is smaller than that of α'-martensite and that the first 20% α'-martensite formed probably comes mainly from ε-martensite. As the plastic deformation increases, α'-martensite starts to form in the microstructure. For example at 20°C and at maximum uniform elongation, no ε-martensite could be identified. This implies that the ε-martensite that was present has transformed to α'-martensite. It can be concluded that when metastable austenitic steels are deformed at room temperature, austenite transforms firstly to ε-martensite and then $\varepsilon \to \alpha'$ transformation takes place. It is also possible that ε-martensite transforms to α'-martensite during the entire deformation period [Kra99, Wei01, Wei90]. At low strains, ε-martensite plate's form uniformly through the grain as can be seen in the micrographs Figures 5.13-5.15. As transformation progresses, some thin plates nucleate and grow close to the ones formed earlier and this leads to a band structure of the thin ε-martensite plates [Berg97].

Following the proposal of Weiss and co-workers [Wei01, Wei02a], $M_d^{\gamma\to\alpha'}$ defined as the temperature at which maximum uniform true strain is recorded, was estimated to be 40°C. $M_d^{\varepsilon\to\alpha'}$, defined as the temperature at which 1% α'-martensite has formed was estimated to be about 70°C. Figure 5.31 (b) shows the temperature-true stress transformation diagram showing curves where different volume fractions of α'-martensite has formed. With decrease in temperature and increase in stress the amount of martensite formed increases. Figure 5.32 shows the temperature-true strain transformation diagram showing different volume fractions of α'-martensite that has formed. It is important to note that for both diagrams no curve cuts the temperature axis. This implies that the M_s for this steel lies below -196°C.

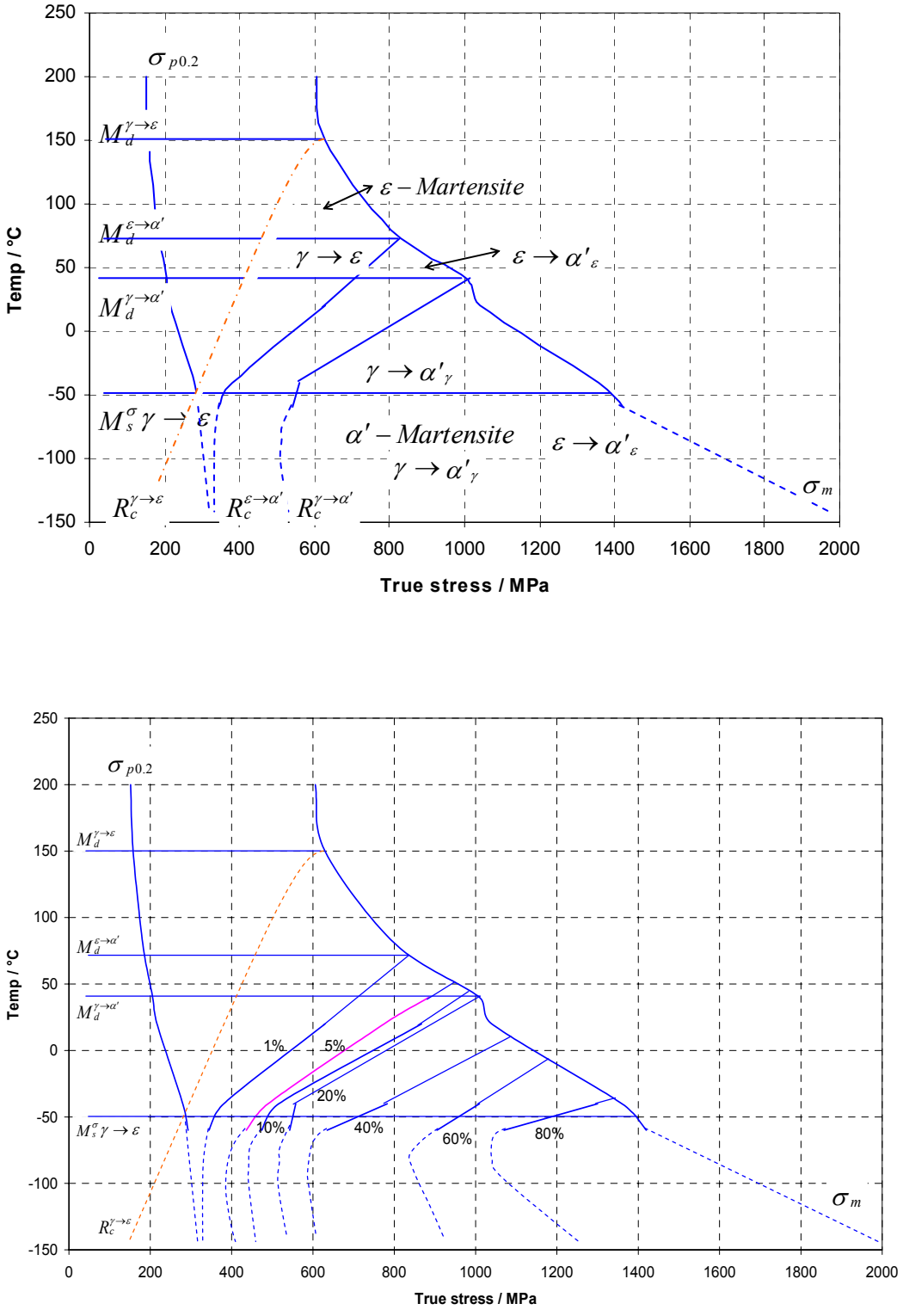

Figure 5.31 Temperature-true stress transformation diagrams for the steel X5CrNi18.10 showing (a) critical initiating stresses and possible transformation regions and (b) volume fraction of α'-martensite formed as a function of temperature and stress.

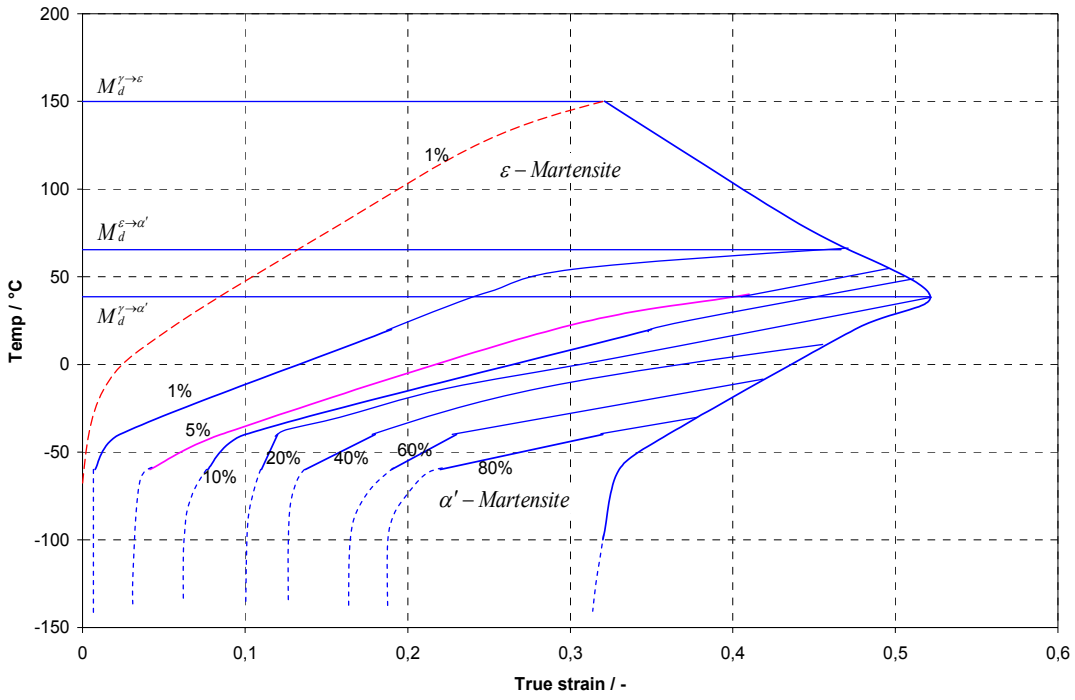

Figure 5.32 Temperature-true strain transformation diagrams for the steel X5CrNi18.10.

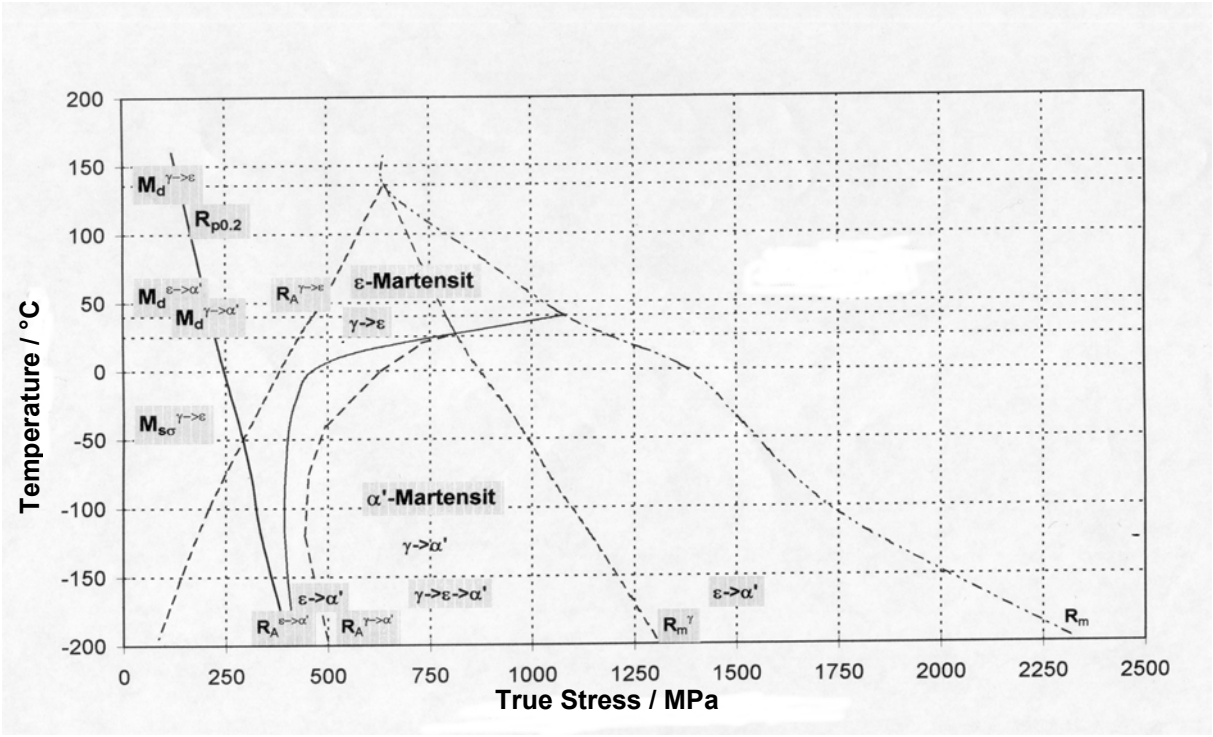

Figure 5.33 (a) Temperature-true stress phase transformation diagram for the steel X5CrNi18.10 (H2) showing critical transformation stress [Wei01].

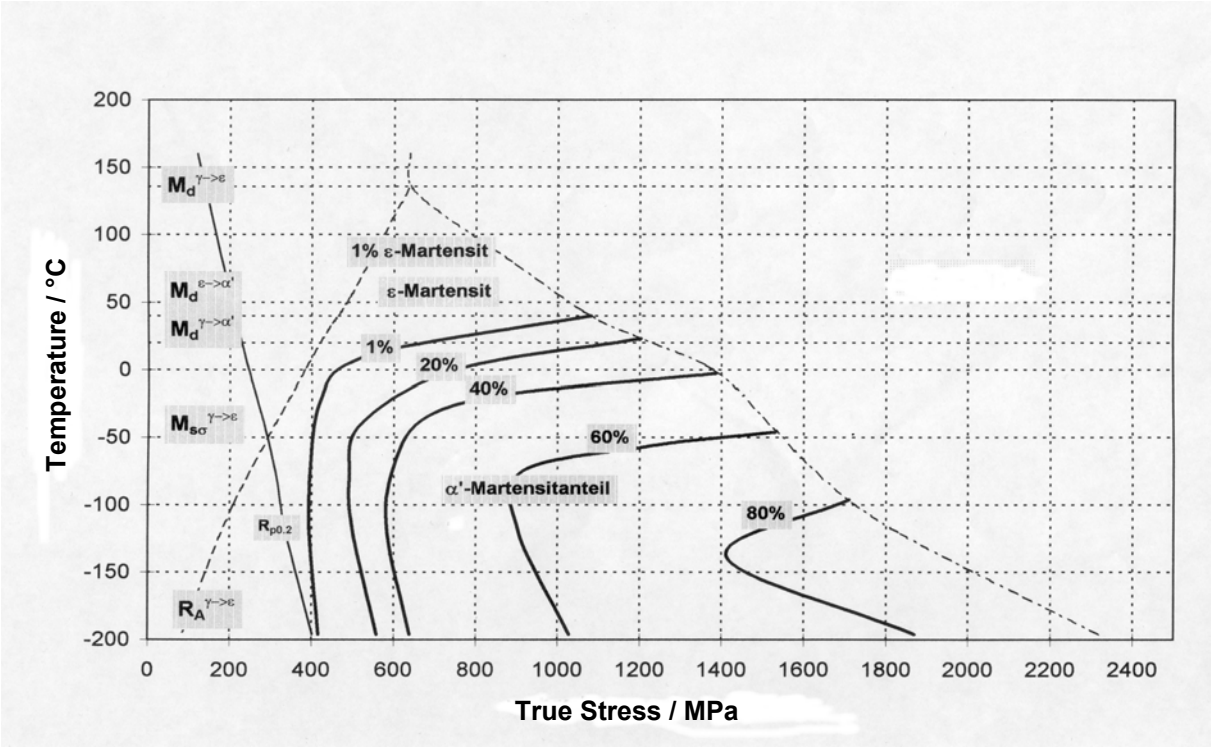

Figure 5.33 (b) Temperature-true stress phase transformation diagram for the steel X5CrNi18.10 (H2) showing volume fraction of α'-martensite formed [Wei01].

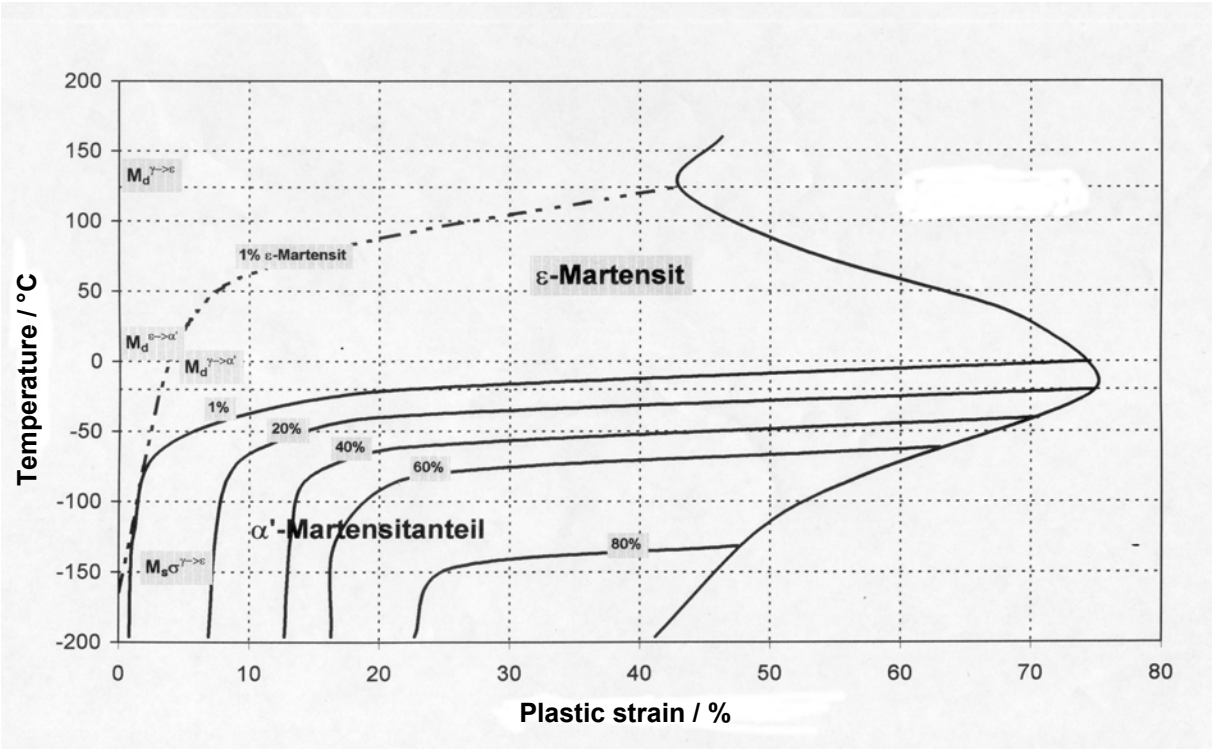

Figure 5.33 (c) Temperature-true strain phase transformation diagram for the steel X5CrNi18.10 (H2) showing volume fraction of α'-martensite formed [Wei01].

5.3.3 DISCUSSION OF MAXIMUM UNIFORM ELONGATION

Figure 5.34 shows the volume of deformation induced martensite as a function of temperature only at an engineering strain of 0.3. Figure 5.35 shows the relationship between maximum true strain obtained at maximum uniform elongation and temperature with the maximum volume fraction of α'-martensite superimposed.

From the temperature-true strain transformation diagram, the 20% volume fraction α'-martensite curve extrapolated to meet the maximum uniform true strain versus temperature curve, should give the $M_d^{\gamma\to\alpha'}$-Temperature. As hypothesised by Weiss and his co-workers [Wei01], at this temperature one should have the maximum uniform true strain. This was confirmed by our experiments as shown in Figure 5.35. The maximum true strain was obtained at 40°C. This temperature was taken to be our $M_d^{\gamma\to\alpha'}$-Temperature. Above this temperature, no direct $\gamma\to\alpha'$-martensite transformation is supposed to take place. The ε-martensite theory first mentioned by Schumann [Sch69] and applied by Weiss and co-workers [Wei01, Wei02a, Wei02b, Wei90, Wei95, Wei92] was confirmed by our metallographical analysis as depicted in the optical micrographs shown in Figures 5.13-5.14. At 20°C and 40°C, ε-martensite was optically identified at all levels of straining except at maximum uniform elongation. From this theory, one can conclude that the enhanced ductility observed at 20°C and 40°C was due to the delayed rate of transformation of $\gamma\to\alpha'$ due to the formation of metastable ε-martensite variants which later transforms to α'-martensite. It is interesting to note that at 40°C, a maximum of only about 10% volume fraction of α'-martensite was detected from our experiments even though the highest maximum uniform true strain was recorded at this temperature. It is not the amount of α'-martensite that forms that determines the enhanced ductility but the phase transformations $\gamma\to\alpha'$, $\gamma\to\varepsilon$, $\varepsilon\to\alpha'$ which result in enhanced ductility. At -40°C and -60°C, the presence of ε-martensite could not be confirmed by optical microscopy. Because of the low temperatures considered here ($T < M_{d\alpha'}$), the formation of α'-martensite begins already at low deformations. ε-martensite formation is also expected to take place. According to the theory of Weiss and his co-workers [Wei01, Wei02a, Wei02b], when 1% volume fraction α'-martensite curve is extrapolated to meet the maximum true tensile strength curve versus temperature in the stress-temperature transformation diagram, $M_d^{\varepsilon\to\alpha'}$-Temperature should be read directly from the diagram.

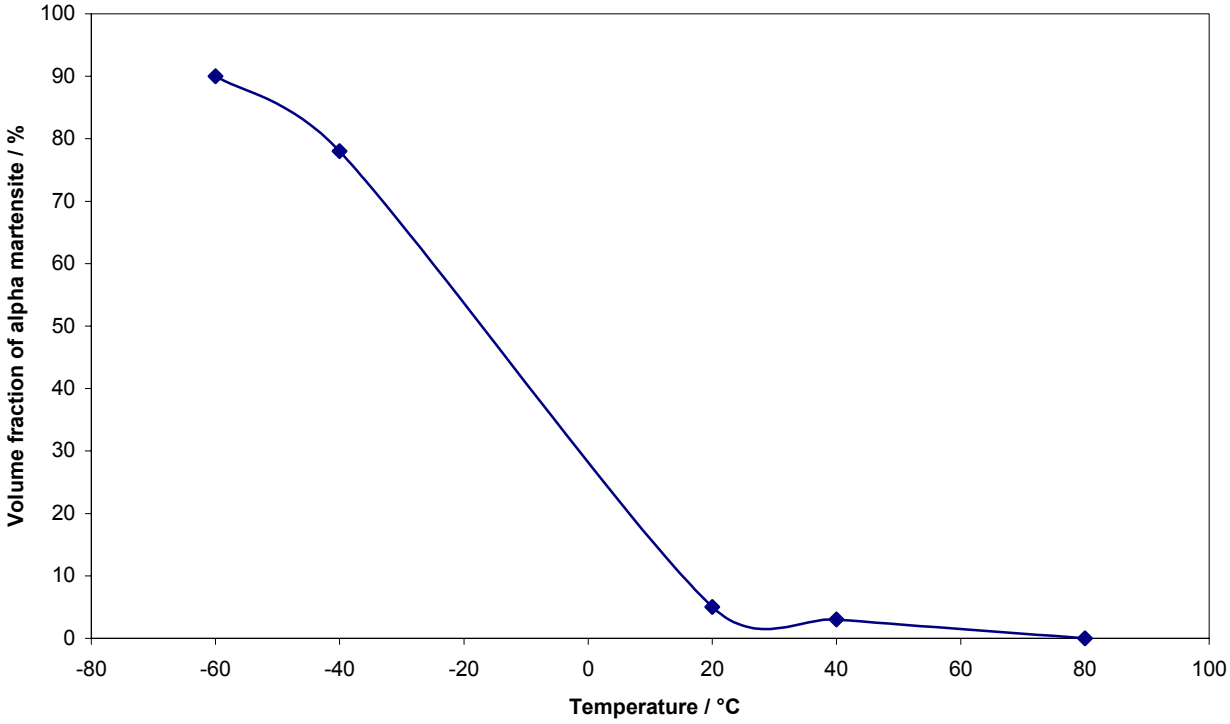

Figure 5.34 Volume fraction of deformation induced α'-martensite as a function of temperature when the engineering strain is 0.3.

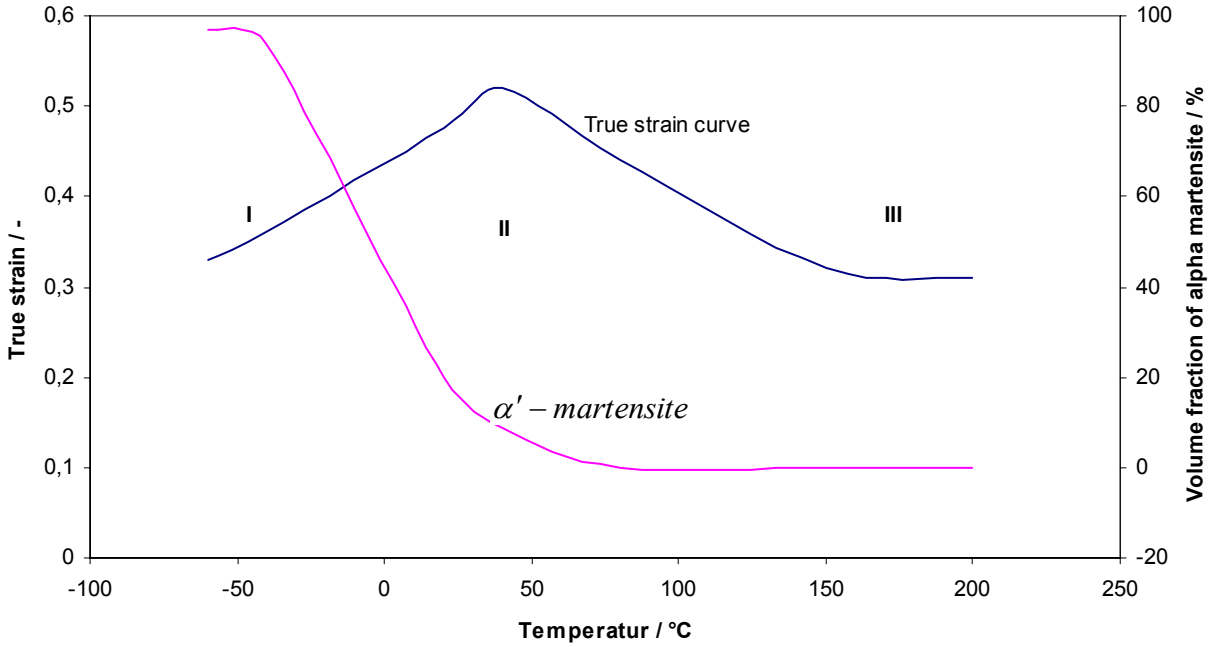

Figure 5.35 Maximum true strains and maximum volume fraction of α'-martensite at maximum uniform elongation as a function of temperature.

Above the $M_d^{\varepsilon\rightarrow\alpha'}$-Temperature, no $\varepsilon\rightarrow\alpha'$-martensite transformation is expected. From Figure 5.31, $M_d^{\varepsilon\rightarrow\alpha'}$-Temperature was estimated to be about 70°C. At 80°C, ε-martensite could be identified at all levels of deformation as shown in Figure 5.15. However, no α'-martensite was detected even at maximum uniform true strain. It can be concluded that the $M_d^{\varepsilon\rightarrow\alpha'}$-Temperature estimated by this method is fairly accurate.

The transformation $\gamma\rightarrow\varepsilon$-martensite resulted in increased hardening and hence better enhancement of ductility as observed at 80°C. At 150°C, no ε-martensite or α'-martensite was detected by optical micrography and magnetic measurements. Therefore, the $M_d^{\gamma\rightarrow\varepsilon}$-Temperature for this steel was approximated to be between 80°-150°C. At this temperature the maximum true strain is limited by hardening of austenite only.

Kranz [Kra99] investigated the fracture properties of the same type of steel investigated in this work (X5CrNi18.10: Fe-0.033C-0.41Si-1.49Mn-20.12Cr-9.36Ni-0.37Mo-0.038P-<0.004N-<0.003S wt%). He found out that a relationship exists between the maximum uniform true strain values obtained in uniaxial testing and fracture toughness. The J-integral values were found to have a maximum at the temperature where 10-15% α'_ε-martensite has formed. The measured α'-martensite volume fraction before the crack tip was found to show a maximum of 25%.

Figure 5.35 can be subdivided into three regions. In the temperature regime III (T>150°C) the maximum uniform true strain are almost constant. No deformation induced phase transformation takes place. 150°C lies above $M_d^{\gamma\rightarrow\alpha'}$, $M_d^{\gamma\rightarrow\varepsilon}$ and $M_d^{\varepsilon\rightarrow\alpha'}$ temperatures. In the temperature regime II (0°C<T<150°C), phase transformations detected by X-ray diffraction and microscopy takes place. The phase transformations $\gamma\rightarrow\varepsilon$-, $\varepsilon\rightarrow\alpha'$-, $\gamma\rightarrow\alpha'$ occurs resulting in enhanced maximum uniform true strain and increased strength. The maximum true uniform strain and ultimate tensile strength achieved depends on the rate of phase transformations and the variant conversion already mentioned. At temperatures below 0°C (region I) the maximum true uniform strain decreases with decreasing temperature in spite of the phase transformation. The phase transformation rate increases with decreasing temperature (see also Figure 5.31).

As a consequence, the phase transformation is completed in an early stage of deformation characterised by less maximum true uniform strain attained and increased ultimate tensile strength. The question of how fast a transformation proceeds cannot be got by calculating the driving force for a transformation using thermodynamics relations but by considering the activation free energy barrier. The discussion of how fast a metastable austenite transforms to martensite in this work is discussed with reference to known martensite variants as possible energy barriers controlling the speed of transformation.

An energy hypothesis has been proposed here as an alternative to the ε-martensite theory of Schumann and Weiss [Sch69, Wei01] to account for how fast instability is reached and hence maximum uniform elongation attained. The hypothesis simply states that the plastic work that can be sustained by a material before instability remains constant. However, if phase transformation takes place, the amount of plastic work will depend on how the different types of transformations affect the fracture kinetics (see Figure 5.36). A material normally undergoes distortion in such a way as to cause a maximum dissipation of energy. The plastic work values give an indication of critical resistance before instability. This critical resistance gives an indication of fracture kinetics processes taking place in the material. Figure 5.36 can be divided into three regions as shown depending on the type of phase transformation taking place. In region I, the phase transformations $\gamma \rightarrow \varepsilon$, $\varepsilon \rightarrow \alpha'$, and $\gamma \rightarrow \alpha'$ are taking place. The plastic work remains constant irrespective of the quantities of α'- or ε-martensite formed. In region III, no phase transformation takes place and the plastic work remains constant. Region II; only ε-martensite is formed and it is expected that the plastic work will remain constant as in the other two regions. The ultimate tensile strength and true strain at maximum uniform elongation attained is as a result of the hardening behaviour of the various phases in the microstructure and not necessarily due to variants conversions as suggested by Schumann and Weiss [Sch69, Wei01]. The condition of instability, under which necking starts, was tested using Considere Criterion ($\frac{\partial \sigma}{\partial \varepsilon} = \sigma$ at instability). The results together with the values of calculated plastic work (per unit volume) are shown in Table 5.8 at the point of maximum uniform elongation. As can be seen, the condition of instability is approximately fulfilled.

It is well known that the formation of a tensile neck is accompanied by a concentration of stress and an increase in triaxiality at the centre of the neck. As a result of the increased triaxiality, the probability of martensite nucleation and formation is increased [Str92]. A local phase transformation at points having high stress concentrations leads to blunting of crack tip irrespective of the type of transformation ($\gamma \rightarrow \varepsilon$, $\varepsilon \rightarrow \alpha'$, $\gamma \rightarrow \alpha'$). For a crack to advance, progressive breaking of inter-atomic bonds and formation of free surfaces must take place. Therefore the enhanced uniform elongation is achieved because of retardation of local necking [From98]. If local necking occurred, phase transformation in the matrix will preferentially take place in this area. This leads to intensive local strain hardening. Further deformation will take place in other local areas which possess lower flow stresses. This multiple deformation mechanism which accompanies phase transformations will result in enhanced uniform elongation and hence delayed necking.

Phase transformation is always accompanied by temporal decrease in stress concentration. However, α'-martensite is less ductile than ε-martensite and its formation increase cleavage initiation because it restricts plastic flow. With increased α'-martensite volume fraction, strength increases due to increased rate of strain hardening leading to increased plastic work but also to increased cleavage activity. This ultimately leads to instability being reached earlier because of critical sizes of voids being reached (i.e. less elongation). The rate of strain hardening of ε-martensite is lower than α'-martensite so high volume fraction of ε-martensite is required to achieve the same elongation as low volume fraction of α'-martensite, though the plastic work will be less as shown in Figure 5.36. A comparison of true strain values at 80°C with the values at 20°C and 40°C confirms the above alternative hypothesis that seeks to combine phase transformation, plastic work and fracture kinetics. At 80°C, only ε-martensite could be identified at all levels of deformation and according to our temperature-true stress transformation diagram; a greater amount of ε-martensite volume fraction is expected to form. At low temperatures, -40°C and -60°C, the dramatic increase in strength is due to α'-martensite formation and the low ductility is due to effect of α'-martensite on fracture kinetics. The volume fraction of α'-martensite that can effectively blunt the cracks is about 10-20%.

Table 5.8 True stress, true strain, volume fraction of α'-martensite, and energy values at the point of maximum uniform elongation.

Temp (°C)	$\frac{\partial\sigma}{\partial\varepsilon}$ (MPa)	σ (MPa)	W_p (MJ/m^3)	α'-martensite (%)	True strain	ε-martensite
-60	1610	1420	352	97	0.33	+
-40	1450	1330	360	94	0.36	+
20	1150	1030	335	20	0.48	+
40	986	987	346	9	0.52	+
80	782	778	246	0	0.44	+
150	676	615	153	0	0.32	-
200	649	606	143	0	0.31	-

(+)--present

(-)--absent

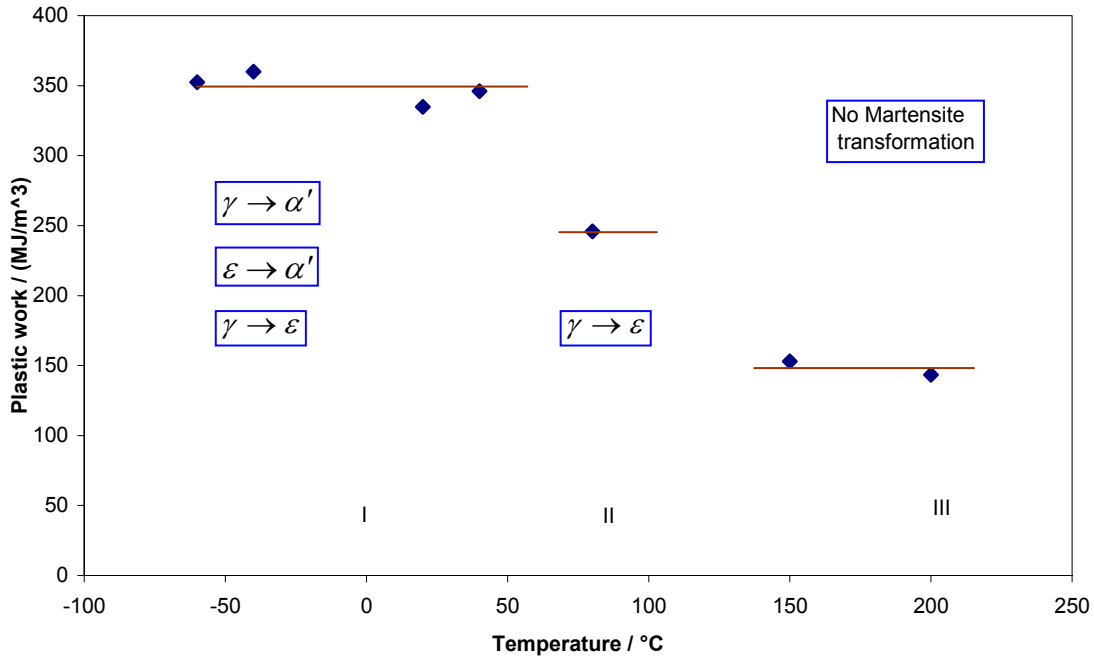

Figure 5.36 Diagram showing plastic energy and types of transformations as a function of temperature.

5.4 DEFORMATION BEHAVIOUR OF Mn-Si-Al STEEL

The results of uniaxial tensile testing of Mn-Si-Al steel at some selected different temperatures and corresponding work-hardening rate versus true strain are shown in Figures 5.37-5.39. Figure 5.40 shows the plot of maximum true uniform strain as a function of temperature for the two heat treatment routes (A and B). For the austempered specimens (Route A), the maximum true uniform strain attained was found to be higher than that for continuously cooled specimens (Route B) at all the test temperatures as shown in Figure 5.40. The corresponding work-hardening rate versus true strain curves shows that for continuously cooled specimens (Route B), the decay of work-hardening rate is faster than for the austempered specimens.

An improvement of strain of about 4-8% over the entire temperature range was obtained. This performance is quite remarkable and the increase in ductility was attributed to the effect of phase transformations on fracture kinetics as well as the composite deformation behaviour of the phases which constitute these high strength low alloy multiphase steels. A microstructure mix of ferrite matrix, bainite and retained austenite at the boundaries and as lamellar inside the bainite areas contribute more to enhanced ductility than when martensite is present in the initial microstructure.

The heat treatment cycles for the two series of samples produced retained austenite amounts that did not differ appreciably from one another. After uniaxial testing at different temperatures for both samples, the amount of retained austenite was determined again using X-ray diffraction (see Table 5.5). Retained austenite could be detected in all the samples that exhibited enhanced ductility, while virtually no retained austenite was detected on samples that showed higher strength but poor ductility. Also by colour etching for example at 40°C, retained austenite could be identified as shown in Figure 5.20. It can be concluded that the retained austenite in the samples that showed poor ductility, transformed very rapidly in the early stage of plastic deformation resulting in higher strain hardening due to the martensite phase. The rate at which a transformation takes place is determined by activation free energy barrier which was attained faster for continuously cooled specimens. This resulted in higher strength but lower ductility.

In the samples that exhibited enhanced ductility, the transformation to martensite must have been gradual due to high free energy barrier, resulting in gradual strengthening. However, since the transformation was gradual, the strain hardening was not as high resulting in lower strength but higher ductility. The presence of martensite prior to deformation also seems to play a crucial part. This resulted in higher yield strength due to the strengthening effect of martensite phase. The faster austenite-martensitic transformation leads to higher strain hardening, high strength but to poor ductility. Phase transformation during deformation leads to extensive strain hardening so that the strain hardening increases with increasing strain. Gradual phase transformation results in continuous gradual increase in strain hardening and a high rate of phase transformation is accompanied by high increase in strain hardening.

A higher rate of phase transformation leads to an early saturation, a decrease in elongation and an increase in the ultimate tensile strength [From98]. More gradual austenite-martensite transformation leads to a better improvement of ductility through a combined effect of phase transformation on fracture kinetics and composite deformation of the phases. The rate of the austenite-martensite transformation depends on the mechanical stability of austenite. Holding at the bainite transformation region increases the carbon enrichment in austenite and thus the stability with respect to mechanical activation of the martensitic transformation. Ductility of low alloy multiphase high-strength steels is mainly controlled by M_s-Temperature and volume fraction of retained austenite [Sug93]. Improvement of ductility is supposed to be attained by suppressing moderately the strain induced transformation by stabilising the retained austenite and increasing the initial volume by adding carbon, manganese, silicon, and aluminium [Sug93, Sug99].

The retained austenite morphology present in the microstructure could be classified as follows;

- For the austempered specimens, the retained austenite appeared as islands on the grain boundary between ferrite matrix grains, between ferrite and bainite grains or inside the bainite as thin films or lamellar (see Figures 5.9 and 5.11).
- For continuously cooled the specimens, the retained austenite appeared as islands on the grain boundary between ferrite matrix grains, between ferrite and bainite grains, between ferrite and martensite grains, and as lamellar in bainite areas (see Figure 5.10).

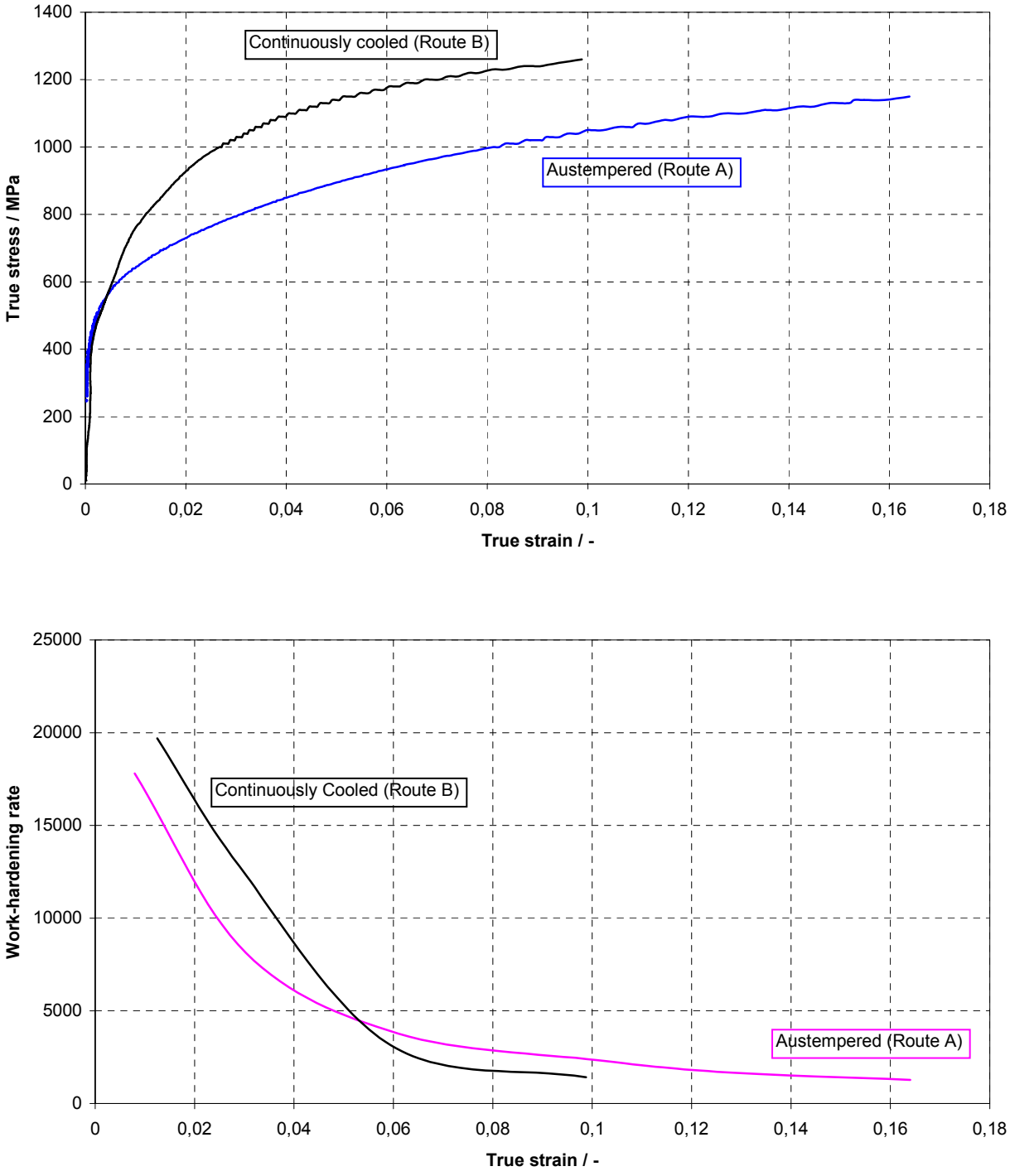

Figure 5.37 True stress-true strain curve when loaded to maximum uniform elongation and the corresponding work-hardening rate curve of the Mn-Si-Al steel at temperature -60°C.

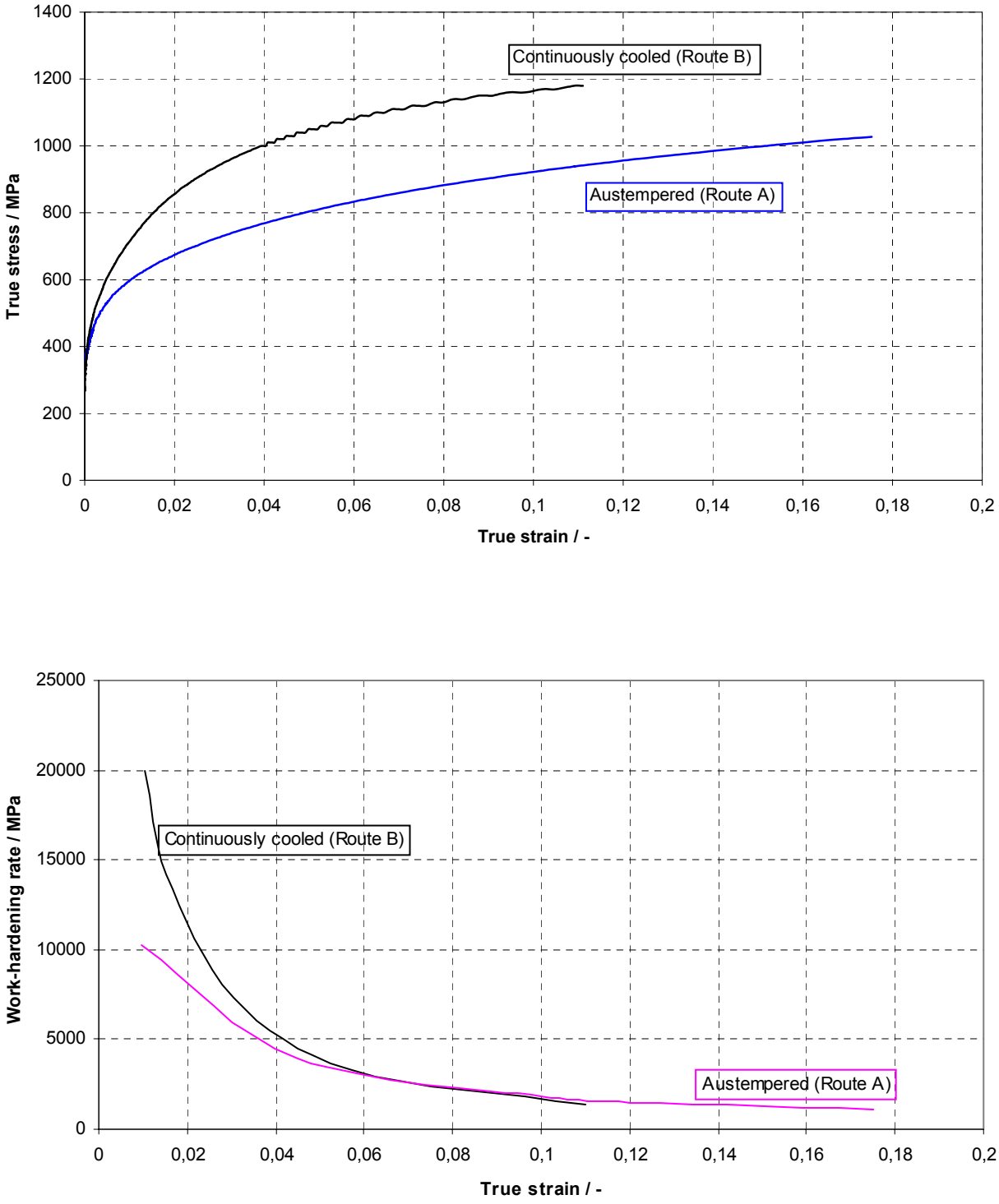

Figure 5.38 True stress-true strain curve when loaded to maximum uniform elongation and the corresponding work-hardening rate curve of the Mn-Si-Al steel at temperature 20°C.

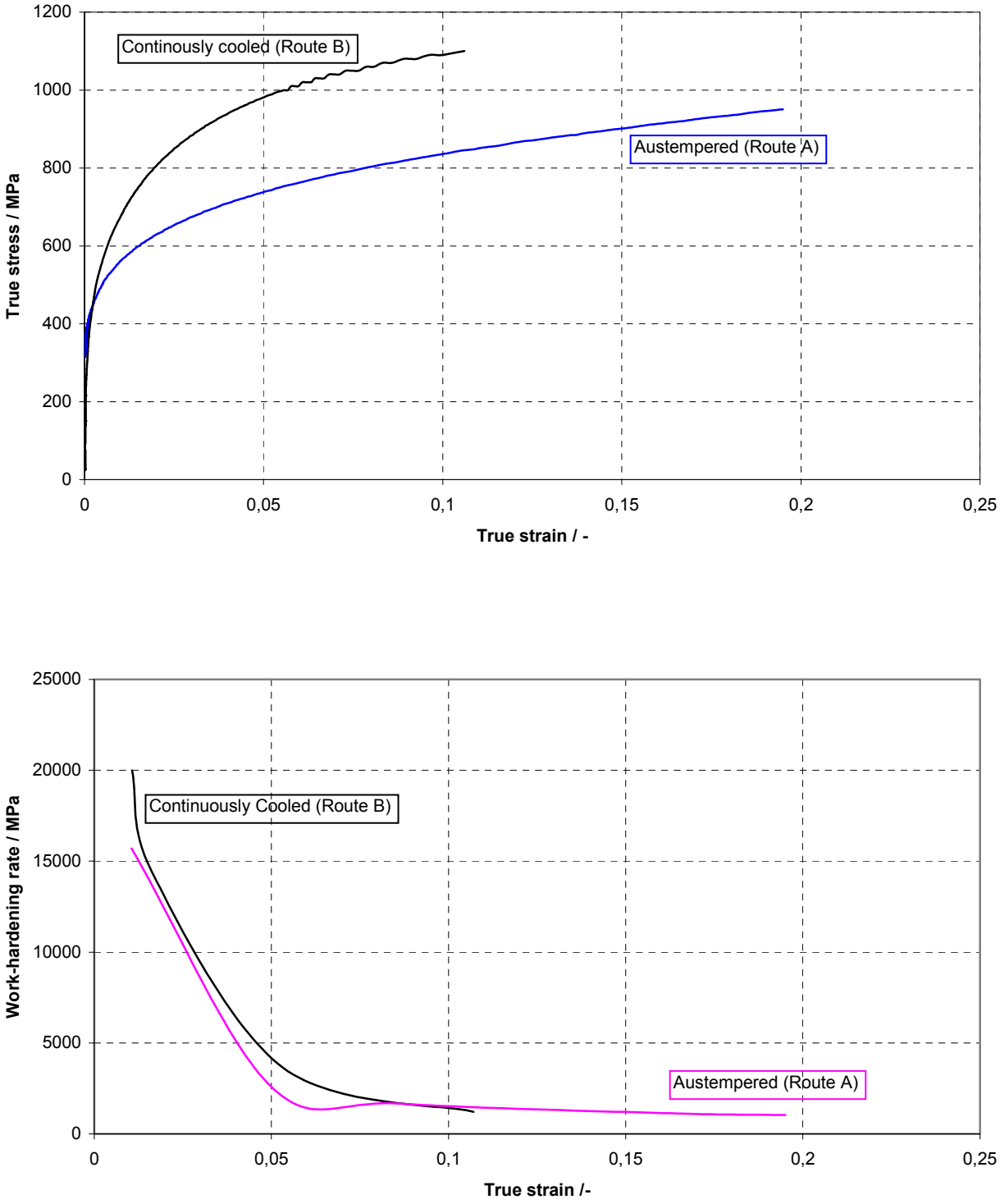

Figure 5.39True stress-true strain curves when loaded to maximum uniform elongation and corresponding work-hardening rate curves of the Mn-Si-Al steel at temperature 80°C.

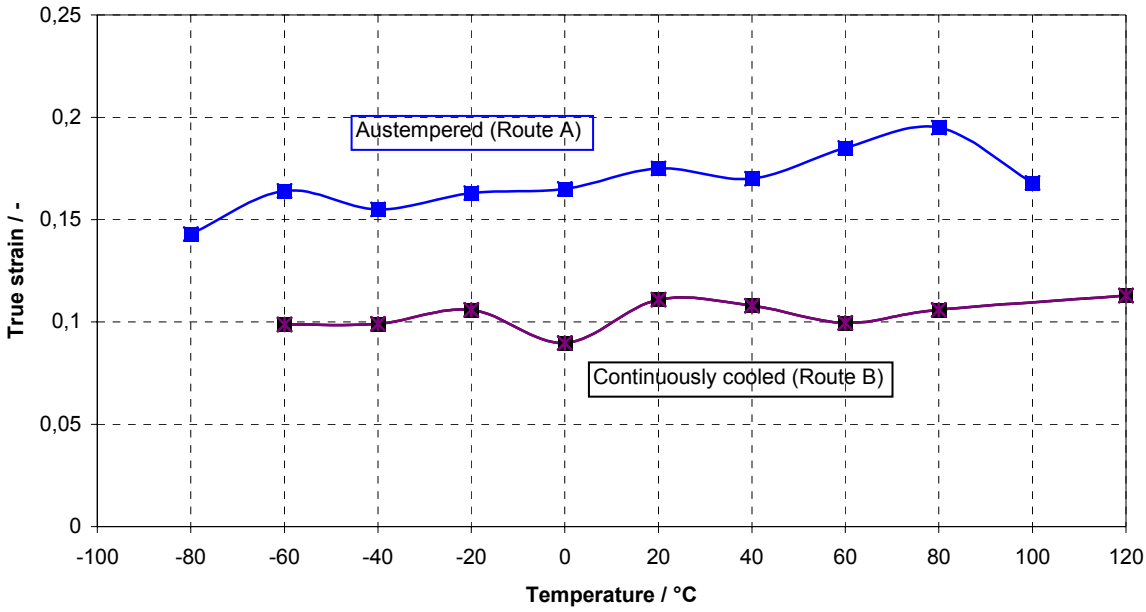

Figure 5.40 Maximum true uniform strains as a function of temperature for the Mn-Si-Al steel.

The type of retained austenite morphology found in the microstructure could influence the M_s-Temperature and accommodation effect by altering the hydrostatic pressure [Sug93]. Generally, hydrostatic pressure constrains volume expansion and the shear deformation that normally accompanies strain induced martensitic transformation. The yield stress and the strain hardening rate of the phases surrounding or next to the retained austenite determines the composite deformation behaviour. The amount of carbon and manganese in the retained austenite was obviously affected by the austempering and the continuous cooling heat treatment procedure [Han97a]. It has been suggested that M_s-Temperature is modified by carbon and manganese content in the retained austenite [Sug93, Min96]. In the continuously cooled specimens, the M_s-Temperature seems to have increased. Factors that were not considered like grain size, carbon concentration in the various phases and the presence of other elements in appreciable amounts could have played important roles in raising the M_s-Temperature [Han97a, Han97b]. This means that the strain induced martensitic transformation was very fast and complete for the continuously cooled specimens. This was confirmed later by X-ray diffraction measurements (see Table 5.5). No trace of retained austenite was detected for continuously cooled specimens while some retained austenite was detected at maximum uniform elongation for austempered specimens.

It is the slow progressive strain induced martensitic transformation over the entire deformation range accompanied by hardening that has beneficial effect on elongation and strength [Wak77, Dav78a, Dav78b]. This led to the conclusion that the enhanced strength and ductility in the multiphase low alloy high-strength steels is not so much dependent on the amount of austenite transformed but also more importantly on the stability of the retained austenite leading to gradual or progressive phase transformation [Sug99]. Highly unstable retained austenite which transforms very fast to martensite leads to increased work hardening rate or extensive strain hardening in the early stages of deformation resulting in higher strength and reduced ductility. Retained austenite of moderate stability results in a slower rate of strain hardening, gradual phase transformation and because both phases harden as deformation progresses, there is a combined enhancement of ductility.

An alternative rival explanation to the idea of rate or speed of transformation of retained austenite also seem evident from the results. The results also point to the fact that maybe the enhancement of ductility in these low alloy-multiphase steels is not due to transformation but the presence of stable retained austenite that does not transform during deformation (see Table 5.5). The focus in the development of high strength low alloy-multiphase steels should be the stabilisation of retained austenite in a matrix of bainite and ferrite that does not transform during deformation. The improvement of strength and ductility is therefore due to combined strain hardening of the phases and composite deformation behaviour. The hard phase (martensite or bainite) in multiphase steel has a large strain hardening coefficient, high strength and low ductility. By contrast, the soft phase (ferrite, stable retained austenite) has a low strength and high ductility. When the composite microstructure is stressed, the plastic strain is at first focussed in the ductile soft phase, which work-hardens. Eventually, the harder phase also deforms plastically. This composite deformation behaviour leads to better combinations of strength and ductility. Many studies concerning microstructure and property relationships of TRIP-assisted steels normally highlight the presence of retained austenite and many imply that the observed high uniform elongation is a consequence of the martensitic transformation of the retained austenite under the influence of an applied stress or strain. From the results of this study, it is possible that the role of TRIP has been exaggerated in explaining the good mechanical properties of these steels.

CHAPTER 6

6 SIMULATION OF DEFORMATION BEHAVIOUR (AISI 304)

6.1 SIMULATION OF DEFORMATION BEHAVIOUR BY FINITE ELEMENT

6.1.1 THE BASIS AND APPLICABILITY OF THE FINITE ELEMENT METHOD

The basic concept underlying the finite element method (FEM) is that a real body can be modelled analytically by it's subdivisions into finite number of elements. The behaviour of a single element can be studied independently from others in the ensemble by a set of assumed functions approximating the stresses or displacements in that region. Implicit with each element is its displacement function which, in terms of parameters to be determined, defines how the displacements of the nodes are interpolated over each element.

The FEM is an approximate numerical method, which has been successfully used to predict solutions of various boundary value problems of stress analysis [Bae00, Tsu93, Iwa01]. The solution of a continuum mechanics problem is approximated by polynomials on simple areas, the finite elements. The parameters of solution, usually the values of solution at the nodes of the finite element mesh, are determined by solving a usually large system of linear algebraic equations assembled as a result of matrix operations and equations which express physical principles specific to the given problem. With the necessary input data, the FEM can be used for the study of the mechanical behaviour of multiphase alloys, provided the stress-strain behaviour of the individual phase are known or can be approximated.

6.1.2 THE PROBLEM

The beneficial effect of the strain induced martensitic transformation on the ductility and strength of metastable austenitic steels and low alloy high strength multiphase steels is due to the impediment to strain localization by the additional local hardening caused by the martensitic transformation or by other internal hardening mechanism [Zac67, Ols78].

For useful technical application, the transformation of the austenite to martensite should be progressive over the entire deformation range. The main problem is whether this interplay between hardening and the various phases during transformation as deformation progresses can be captured by FEM.

Flow stress is characterised by the yield stress of the different phases and the stress-strain relationship in the plastic range [Oll88]. The flow stress σ is affected by numerous variables such as plastic strain (ε), strain rate ($\dot{\varepsilon}$), temperature (T) and structure,

$$\sigma = \sigma(\varepsilon, \dot{\varepsilon}, T, \xi) \tag{6.1}$$

where ξ represents structural parameters (grain size, dislocation density etc).

The experimental stress-strain curve is normally determined by measurement on a standard cylindrical tensile test specimen, in the middle of which the state of idealised macro-stress is one dimensional.

In this work, FEM was mainly employed to,

- To investigate the role of each constituent phase in the stress-strain behaviour.
- To investigate stress and strain distribution.
- To investigate the influence of hardening.

The transformation strain is normally responsible for the irreversible deformation of an iron-based alloy during and after martensitic transformation. The transformation strain has been attributed to orientation of martensitic variants which accounts for about 60-70% of the total transformation strain and accommodation effect which accounts for about 40-30% of the total transformation strain [Fis00, Mar97]. The transformation strain given in literature is in the magnitude of 0.03 or 0.011 for 100% martensite transformation [Mar97,Tsu00] in the temperature range 77-473K. This indicates that the influence of transformation strain especially when considering strain in the range of 0.1-0.6 and stresses much higher than the yield stress of austenite is small and was therefore ignored. It is important to note that in case of transformation strain, the macroscopic material response is a result of microscale mechanisms governed by couplings between stress, strain and the transformation mechanism itself.

If different sources of microstresses apart from transformation itself are involved, the orientation contribution will be quantitatively different from the above mentioned figures [Mar97] and the direct application of the transformation criterion proposed by Fischer and his co-workers may not be possible [Rei97, Mar97, Fis00]. In addition, a 2-D model does not allow a real distribution of the martensitic variants [Fis00]. Several mechanisms normally contribute to the macroscopic response of high strength steels and since our aim was to simulate the flow behaviour in the plastic region, additional sources of microstresses apart from the transformation itself were possible [Mar97]. Because of the complexity of identifying the mechanisms themselves, multiple mechanisms were not considered in this work. It was assumed that coupling of different scales was achieved by applying the boundary conditions of the finite element method on representative volume element (RVE). The discrete units of the representative volume element respond to strain via in-built constitutive equations assuming equilibrium and compatibility conditions [Mar97, Ank82]. Because of the use of volume averaging, it was assumed that the effect of distribution is taken into consideration.

BASIC HYPOTHESES

- The material is macroscopically homogeneous.
- The material is microscopically heterogeneous.
- An even distribution of the microstructure; the microstructure can have different morphologies corresponding to different macroscopic points.

6.1.3 THE MODEL

The physical and geometrical properties of the specimen were given by a Representative Volume Element (RVE). It was assumed that the RVE is large enough to represent the microscopic behaviour of the sample. A two dimensional plane strain model was used. The displacement was prescribed on the boundary. Attempts were made to prescribe a uniformly distributed load σ at the boundary but because of convergence difficulties beyond 800MPa, this method was abandoned. From the theory of elasticity, it is known that there is a similarity in the solutions of two- and three dimensional problems. This resemblance can also be found in the plastic range if one considers the two-dimensional problem in plane strain [Sun73, Kou01].

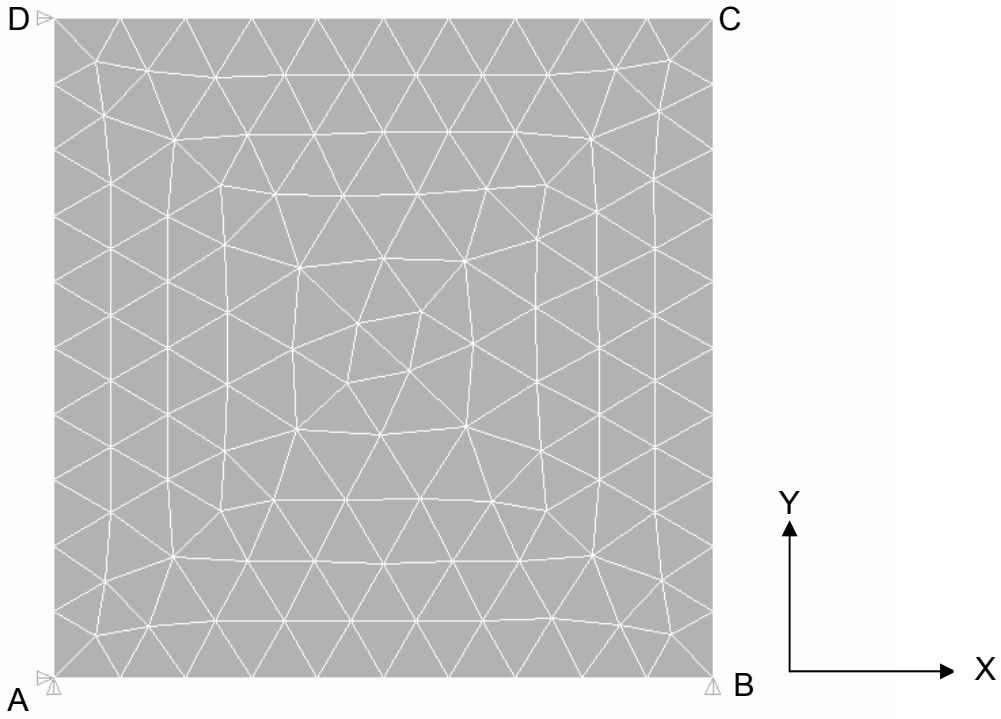

Figure 6.1(a) Example of a 2-D model that was used to calculate the stresses. Length AB=BC=CD=AD=L. Displacement was prescribed in the Y-direction.

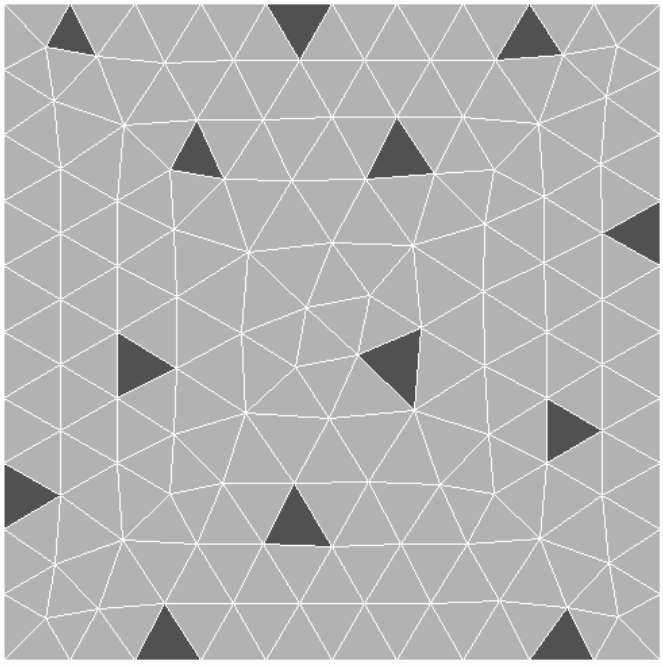

Figure 6.1(b) A mesh showing deformation induced martensite (shaded) in austenitic matrix (6% volume fraction of martensite).

BOUNDARY CONDITIONS

To fulfil displacement continuity and symmetry requirements, the following boundary conditions were imposed;
X=0 face; zero displacement in the x-direction.
Y=0 face; zero displacement in the y-direction.
Y=L face; All nodes have the same prescribed displacement.
The displacements of the vertices were prescribed by applying the local macroscopic deformation gradient tensor to the initial positions of these vertices. This performs the actual transition of the macroscopic deformation field to the micro-level.

MATERIAL CONSTANTS

Input data for the FE calculation used in this work was chosen from literature and our own experimental data as described below.

1. Fem0

The data used here were obtained from [Gan92] however, the hardening rate was modified. This was done to test the effect of the magnitude of the hardening rate on the flow stresses. Several other values of hardening rates were used but the values ones presented here gave the best possible agreement with experimental results. From our experimental results, the hardening rate of pure austenite at 200°C varied from 1740 MPa at 0.1 true strain to 745 at 0.3 true strain. The chosen value of 1200 MPa was therefore deemed reasonable in accordance with our experimental results. Ganghoffer [Gan92] attempted micromechanical simulation of martensitic transformation by finite elements without any reference to any particular steel composition.

Table 6.1 Material parameters used in Fem0

Phase	Young's Modulus (E)	Poisson's ratio (ν)	Yield strength	Hardening rate (Tangent mod.)
Austenite	200000 MPa	0.3	300 MPa	1200 MPa
Martensite	200000 MPa	0.3	1000 MPa	2000 MPa

Here, bilinear isotropic hardening was assumed.

2. Fem1

From the analysis of our experimental data, we assumed a function of the form:

$$\sigma = \sigma_y + k\,\varepsilon^n \tag{6.2}$$

where σ is the true stress, σ_y is the yield stress, ε is the true strain, and k, n are constants. To calculate the input data, the true stress-true strain curve experimental results at 150°C was used as a guide to obtain constants for pure austenite. The variation of the constants with temperature was neglected. The error resulting from such an assumption was assumed negligible considering the fact that the homologous temperature, T/T_m, lies between 0.24 (150°C) and 0.12 (-60°C) for the steel AISI 304. Therefore, because of the low stacking fault energy of this steel (15 mJ/m^2), dynamic recovery is not expected to take place. The flow stresses are expected at any given plastic deformation to approximately change with the temperature in the same order of magnitude as the product of $G \cdot b$ (The increase is expected to be less than 10 % in the temperature range 150°C to -60°C). For martensite, the pure austenite parameters were modified (see Table 6.2). This was done because the amount of carbon in this steel is very low and the toughness of martensite was assumed relatively high. The E-modulus for austenite and martensite were taken to be the same. The differentiation of the E-modulus between the phases was not found necessary given the fact that the texture influence could not be quantified in the loading direction. Therefore, a precise value of E-modulus for each of the phases could not be given.

Table 6.2 Material parameters used in Fem1

Phase	Parameter	Value
Metastable austenite	k	940 MPa
	n	0.61
	E	200000 MPa
	σ_y	200 MPa
Martensite	k	950 MPa
	n	0.7
	E	200000 MPa
	σ_y	1000 MPa

Here, a multilinear kinematic hardening was assumed.

3. Fem2

The second FE data was approximated using simple power law (Equation (3.40)) given in Chapter 3 as:

$$\sigma = k\,\varepsilon^{n}$$

where σ is the true stress, ε is the true strain, and k, n are constants. The stress-strain behaviour of the individual phases was approximated using the above power law.

The values of the constants given in Table 6.3 were taken from the work of Rizk, Bourell, Goel and co-workers for Fe-3Ni-3Mo steel [Bou83, Goe85].

Table 6.3 Material parameters used in Fem2

Phase	Parameter	Value
Metastable austenite	k	689 MPa
	n	0.18
	E	210000 MPa
	ν	0.3
Martensite	k	1496 MPa
	n	0.08
	E	210000 MPa
	ν	0.3

A multilinear kinematic hardening was assumed.

4. Fem3

For the third FE data, the stress-strain curve for each of the phases in the steel microstructure was approximated using the Swift equation (Equation (3.16)) given in Chapter 3 [Tsu00]. The constants shown in Table 6.4 are from the work of Tsuchida and co-workers for a Fe-30Ni-0.2C [Tsu00].

$$\sigma = a\left(b + \varepsilon_0\right)^{N}$$

where σ is the stress, ε_0 is the strain, and a, b, N are constants.

Table 6.4 Material parameters used in Fem3

Phase	Parameter	Value
Metastable Austenite	a	883 MPa
	b	0.02
	N	0.39
	E	200 GPa
	ν	0.3
Martensite	a	2498 MPa
	b	1E-07
	N	0.29
	E	200 GPa
	ν	0.3

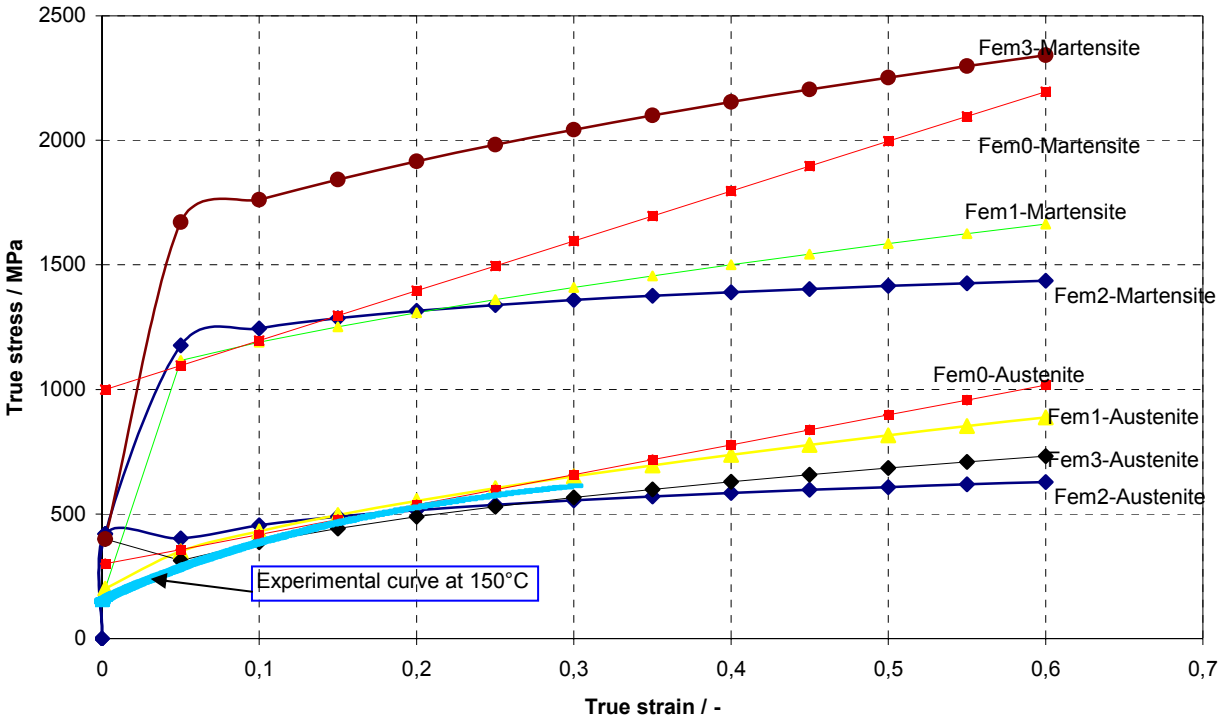

Figure 6.2 True stress-true strain input data for pure austenite and pure martensite from different stress-strain relations.

The true stress-true strain input data for pure austenite and pure martensite from different stress-strain relations are shown in Figure 6.2. Experimental true stress-true strain curve at 150°C is also superimposed as shown. At 150°C, no martensite transformation took place. Therefore, the curve could be used as a guide for pure austenite input data. In the range 0 to 0.3 true strain, all the models used gave reasonable pure austenite input data in comparison to the experimental data at 150°C. Between 0.3 to 0.6 true strains, there is a growing difference in the values of true stresses obtained. The data for pure martensite is hardly available in literature. The ultimate strength of martensite was approximated to be about 1400 MPa at 0.3 true strain from the experimental results at -60°C. This point was used in estimating the martensite data for Fem1. As shown in Figure 6.2, there is a big difference in pure martensite values. Apart from the physical mechanism that could not be considered during the simulation, a major difference in the predicted values lies in input data.

6.1.4 IMPLEMENTATION

The aim of the numerical effort was to predict the flow curves of metastable austenitic steel AISI 304 (German grade X5CrNi18.10) taking into consideration phase transformation and volume fraction of various phases using a commercially available finite element software (ANSYS 5.6/5.7). For the metastable austenitic steel, the initial structure was pure metastable austenite which transformed upon loading at various temperatures above M_s to martensite.

A lot of effort and time was spent in trying to couple the transformation kinetics (structure evolution) to the stress and strain using the available software. This was not successful and was later abandoned. For the transformation kinetics, the work of Ludwigson and Berger [Lud69] was followed and it was assumed that the volume of martensite formed as a result of strain-induced transformation of austenite to martensite was a continuous function of strain and the volume fraction of austenite available for further transformation at each particular temperature. These parameters could easily be accessed through our experiments. Because of the failure to couple the transformation kinetics to the software, an automatic criterion to be implemented in the software could not be defined. Therefore, everything had to done manually.

In order to minimise the effort required for the preparation of element mesh description input data, a mesh of 222 triangular elements was used. Sub-areas of α'-martensite were distributed manually at each strain level. At each strain level, the amount of α'-martensite was known from the experiments and was part of the input data.

The numerical calculation was carried out on a Digital UNIX alpha V4.0 878 Computer by a finite element ANSYS 5.6/5.7 programme developed by Swanson Analysis System, Inc [ANS01]. An Euler backward scheme was used to enforce the consistency condition (see appendix A for details). This ensures that the updated stress, strains and internal variables are on the yield surface.

The displacement was prescribed by applying the local macroscopic deformation to the initial position of the vertices in the microscopic model. This performs the coupling of the macroscopic and microscopic levels [Leg98, Mar97]. The true strain was determined from the displacement of the y = L by,

$$\varepsilon = \ln\left(1 + \frac{U_y}{L}\right) \tag{6.3}$$

where U_y the displacement and L is the original length in the y-direction before deformation. True stress was taken to be averaged stress normal to the displaced face.

$$\overline{\sigma} = \frac{1}{A}\int_A \sigma_y dA \tag{6.4}$$

6.2 FEM RESULTS

The material constants denoted as Fem0, Fem1, Fem2 were used to predict the flow curves for our own tested commercially available metastable austenitic steel, AISI 304 (German Grade X5CrNi18.10) while Fem1, Fem2, and Fem3 was used to predict the flow curves of a metastable austenitic steel data obtained from Dr. Weiß of the Institute of Iron and Steel Technology, Freiberg University of Mining and Technology (X6CrNiTi18.10 (H3)). In the present work, plastic strain is taken as equivalent to true strain.

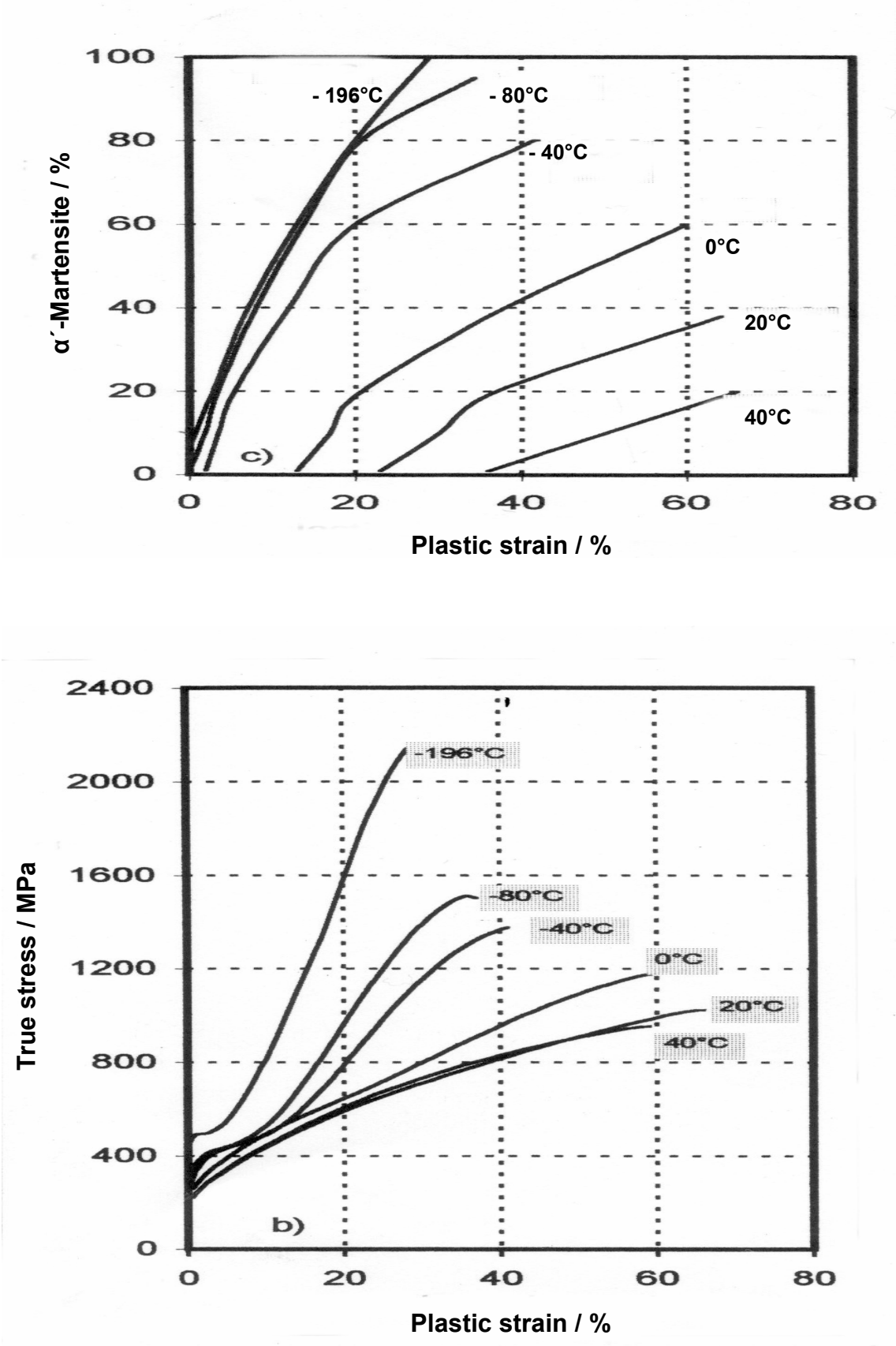

Figure 6.3 Experimental results from [Wei01] used for finite element simulations showing martensite-plastic strain curves above and true stress-plastic strain curves below (Steel X6CrNiTi18.10 (H3)).

6.2.1 COMPOSITE TRUE STRESS-TRUE STRAIN CURVES

The composite true stress-composite true strain curves are depicted in Figures 6.4-6.7 for the steel X5CrNi18.10 and Figures 6.8-6.12 for the steel X6CrNiTi18.10 (H3). It can be seen from Figures 6.4 and 6.5 that the calculated true stress values were slightly lower than the experimental values while for Figures 6.6 and 6.7 the calculated values are slightly higher. This was true for the different material constants and stress-strain relations. The agreement with experimental values depends on the type of stress-strain relations.

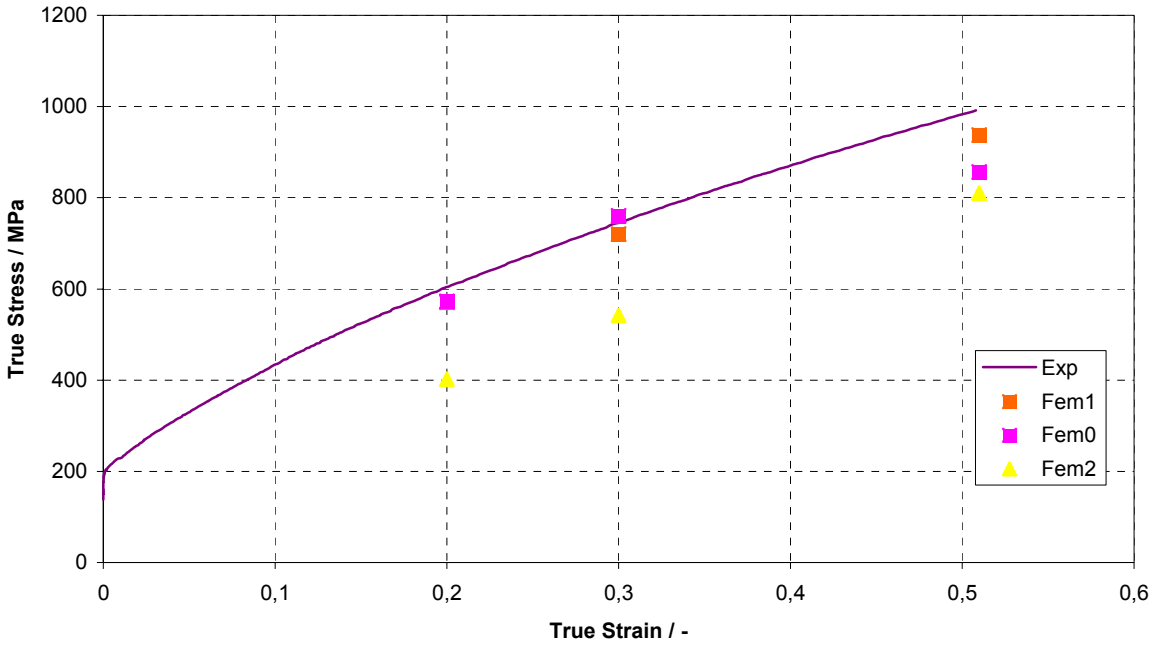

Figure 6.4 True stress-true strain curves of the steel X5CrNi 18.10 at 40°C.

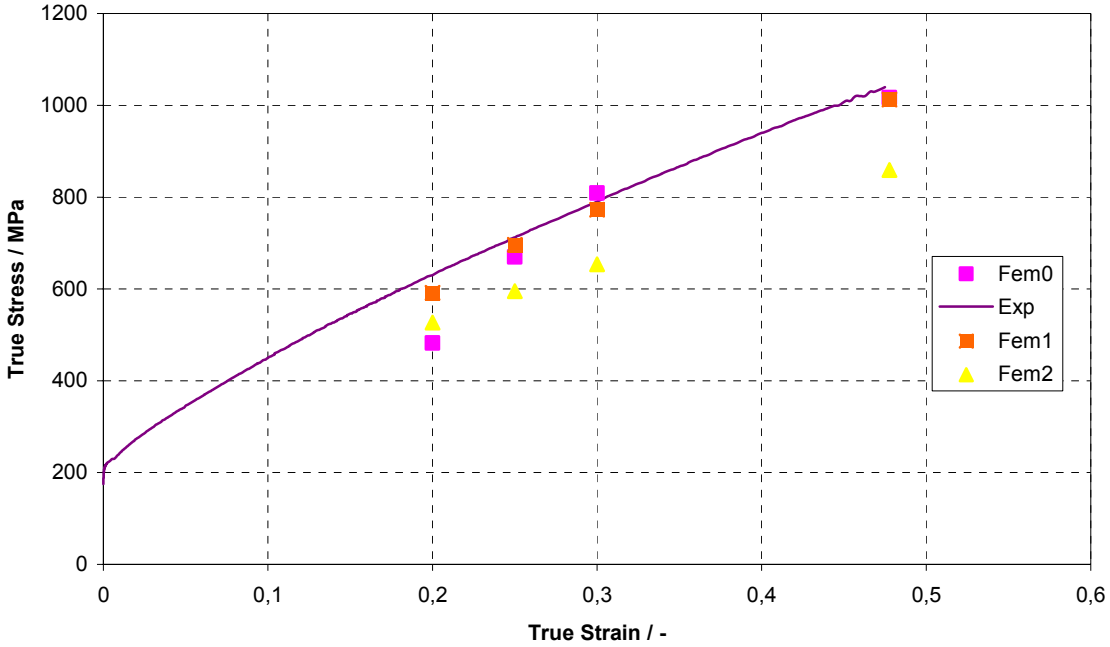

Figure 6.5 True stress-true strain curves for the steel X5CrNi18.10 at 20°C.

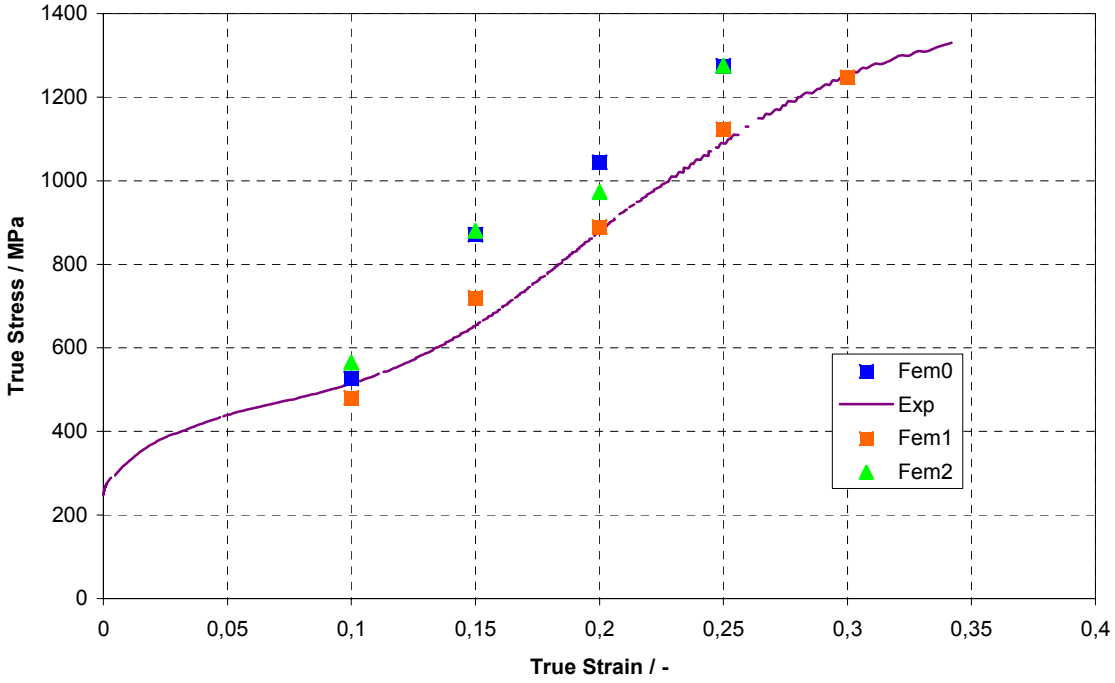

Figure 6.6 True stress-true strain curves for the steel X5CrNi18.10 at -40°C.

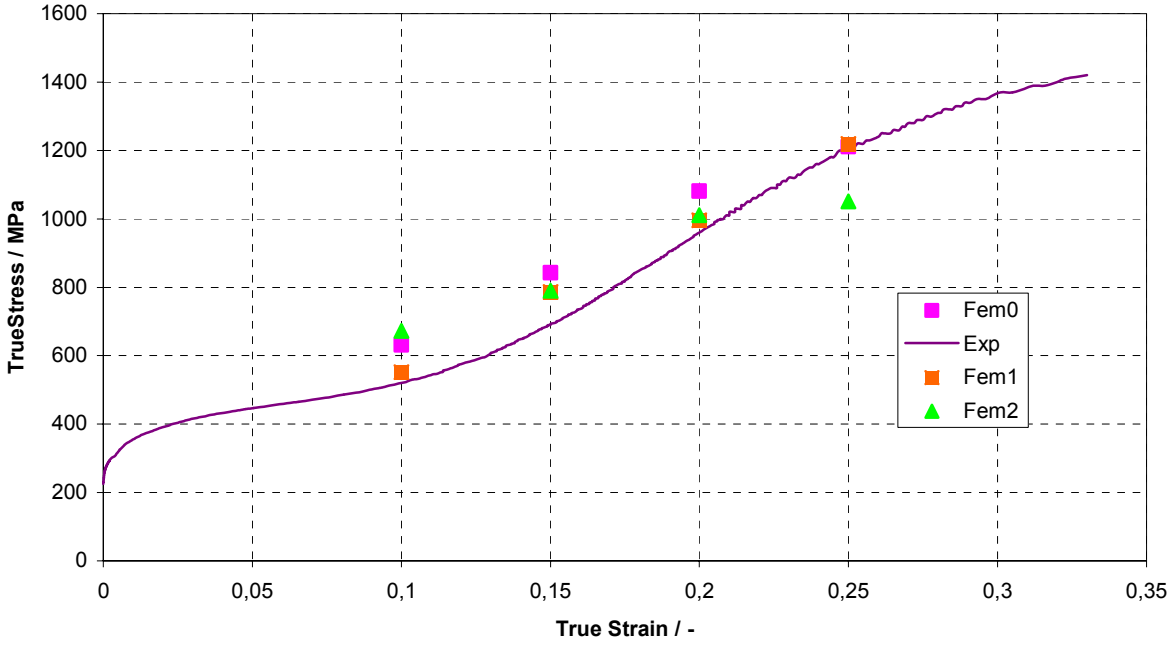

Figure 6.7 True stress-true strain curves for the steel X5CrNi18.10 at -60°C.

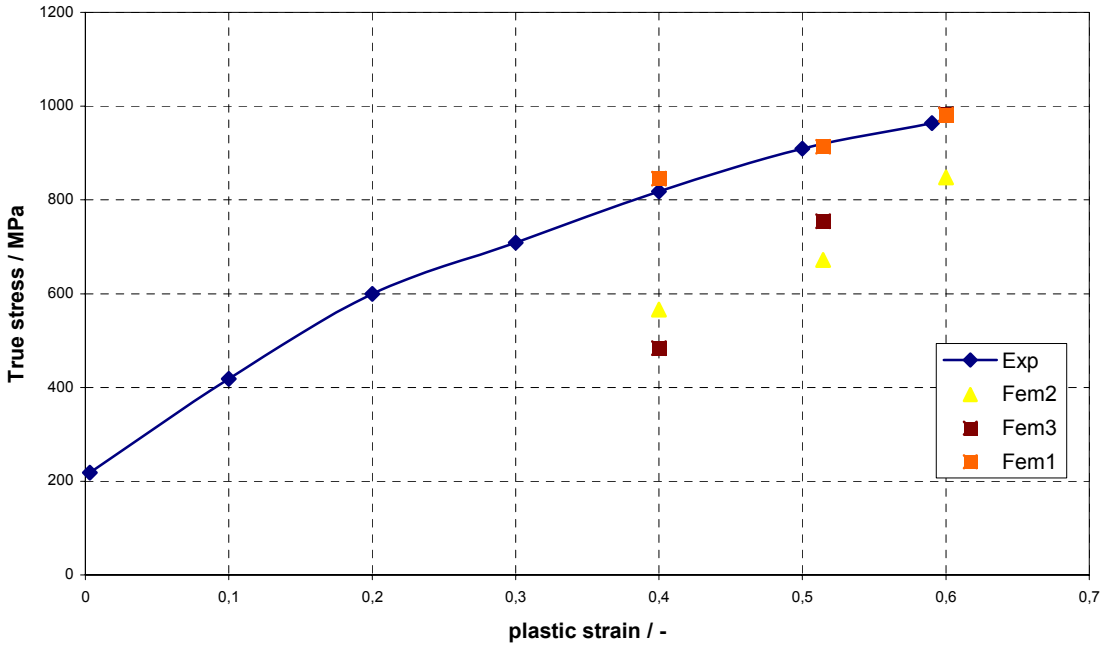

Figure 6.8 True stress-plastic strain curves for the steel X6CrNiTi18.10 (H3) at 40°C, experimental data [Wei01].

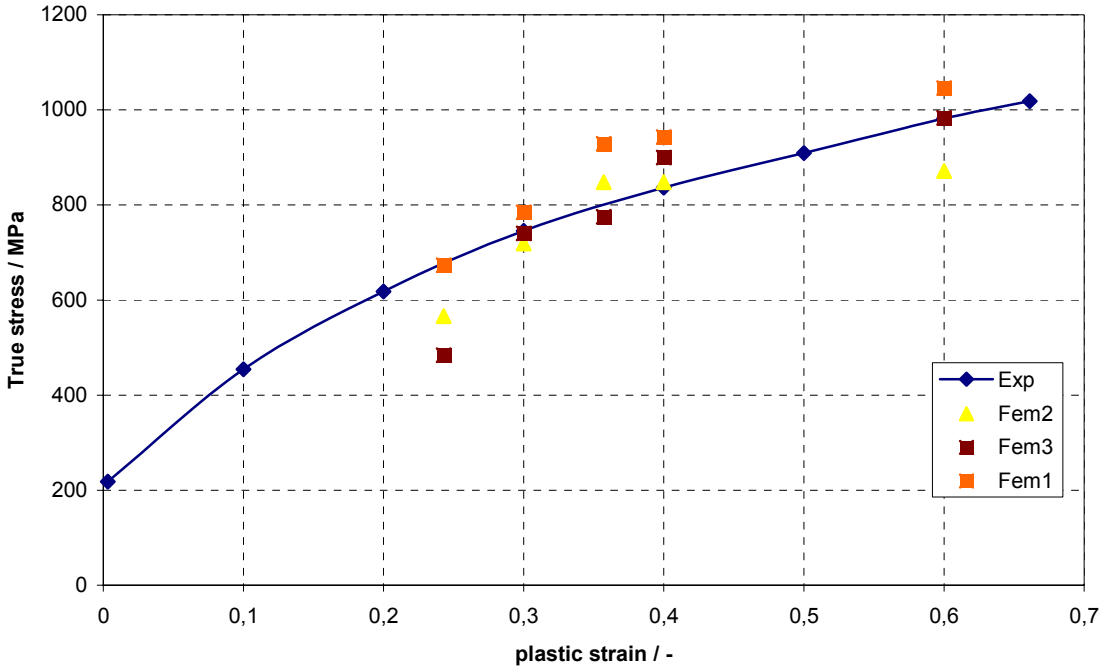

Figure 6.9 True stress-plastic strain curves for the steel X6CrNiTi18.10 (H3) at 20°C, experimental data [Wei01].

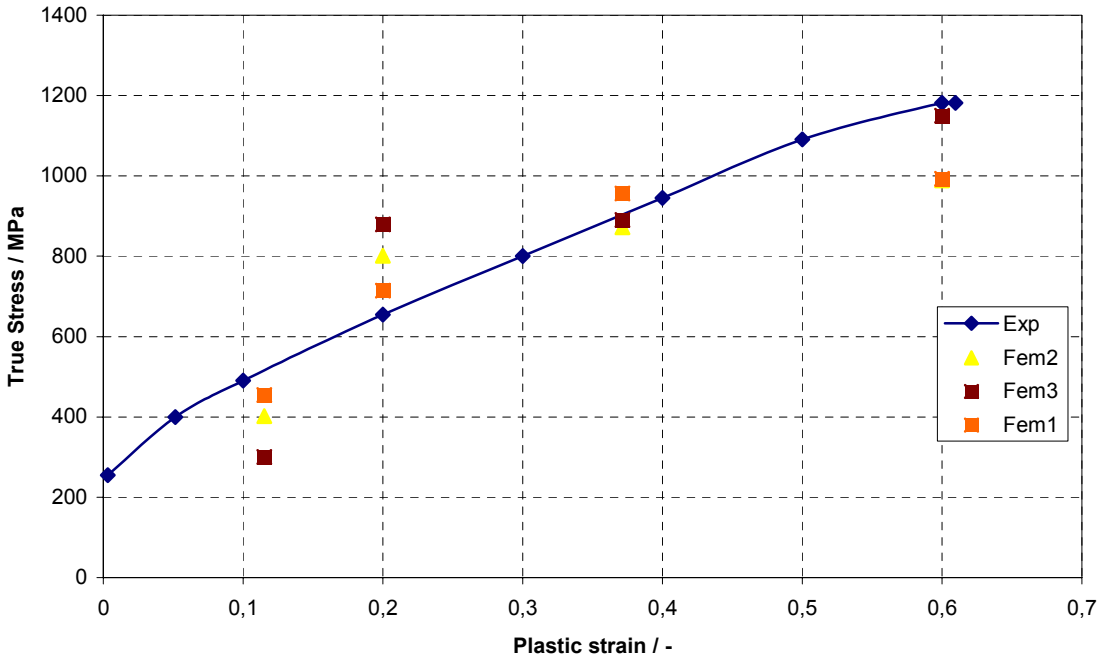

Figure 6.10 True stress-plastic strain curves for the steel X6CrNiTi18.10 (H3) at 0°C, experimental data [Wei01].

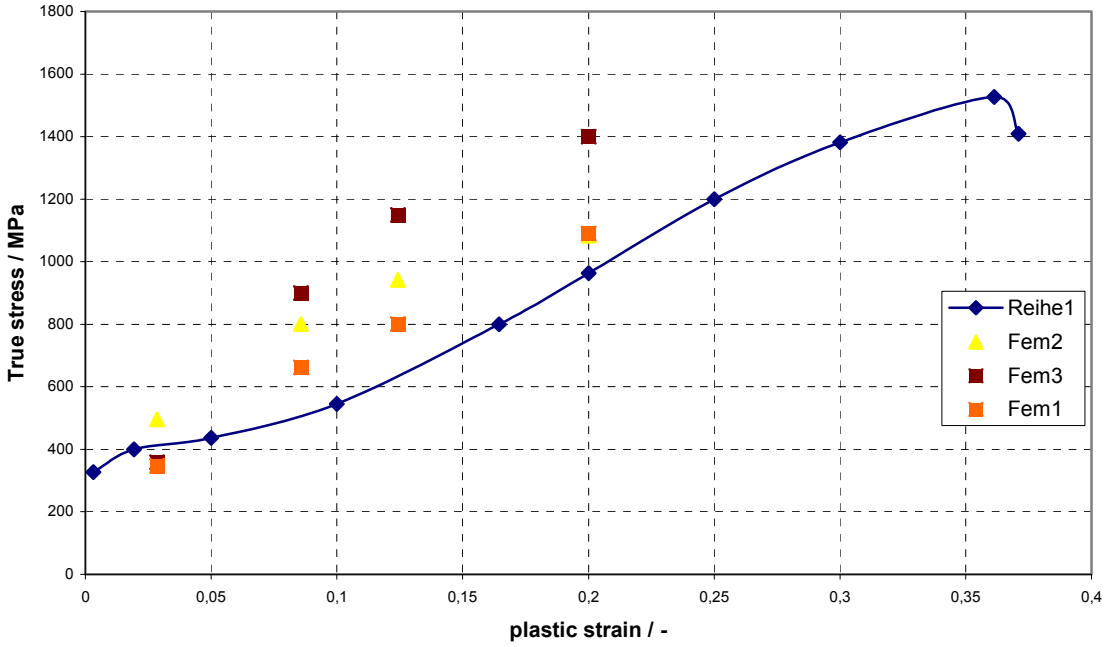

Figure 6.11 True stress-plastic strain curves for the steel X6CrNiTi18.10 (H3) at -80°C, experimental data [Wei01].

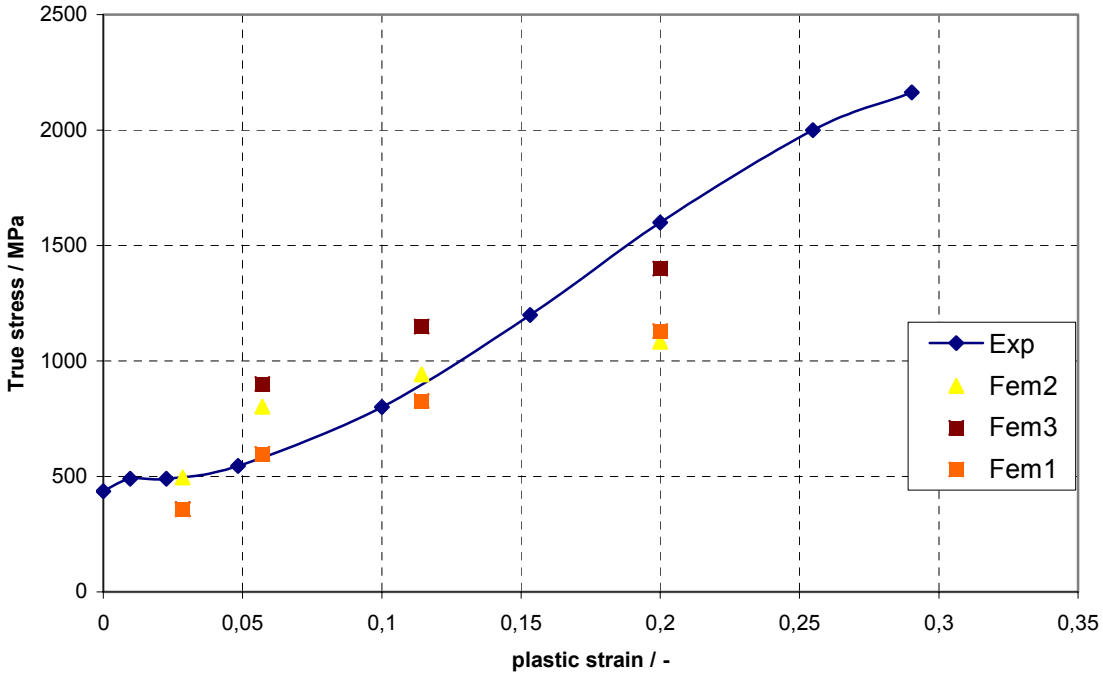

Figure 6.12 True stress-plastic strain curves for the steel X6CrNiTi18.10 at -196°C, experimental data [Wei01].

Figures 6.4 and 6.5 shows that the calculated true stress values closely approximates the experimental values if the stress-strain relationship for the individual phases are approximated by Equation (6.2) (Fem1), and when the hardening rates between the phases are in the ratio of 1:1.5 (Fem0). However, when the simple power law relationship (Fem2) is used to estimate the stress-strain relationship, the calculated values lies below the experimental curve. For the steel X6CrNiTi18.10 (H3), the calculated values tend to lie below the experimental values for temperatures 0°C, 20°C, and 40°C depending on the material parameters and the type of stress-strain relation as shown in Figures 6.8-6.10. For temperatures -80°C and -196°C, the calculated values lies above the experimental curves as depicted in Figures 6.11 and 6.12 for steel X6CrNiTi18.10 (H3) depending on the material parameters and stress-strain relations. It should also be noted that the volume fraction of martensite versus true strain curves for the this steel (see Figure 6.3) did not conform to our experimental results.

For plastic strains up to 10%, the martensite volume formed seemed to have a marked effect on the increase of strength for temperatures below 0°C for the steels X5CrNi18.10 and X6CrNiTi18.10 (H3). Doubling the strength of martensite in the range of plastic strains up to 10% does not necessarily double the predicted stresses in this plastic region. The yield strength of martensite in Fem3 was taken as 2498 MPa and for the others (Fem0, Fem1, and Fem2) the yield strength was taken as 1000 MPa. This behaviour can be attributed to very high local strain hardening and work hardening rate at the start of the plastic deformation and a very high rate of austenite to martensite transformation in this region [Bou83, Wak77]. Beyond 10% plastic deformation, the effect of martensite strength increases. This increase is much more pronounced at -40°C, the effect decreasing as one approaches temperature -196°C. For example, at a plastic strain of 10%, and a temperature of -60°C, twice the amount of martensite was formed compared to the amount formed at temperature of -40°C. The same trend is observed as the plastic strain increases. Given that the same deformation gradient tensor was applied for both cases but different amount of martensite, it can be concluded that in addition to the amount of martensite formed, other factors starts playing important roles in the final stress attained [Dav78].

Above 10% plastic strain, for temperatures below 0°C for the two steels, the deviation in true stresses versus true strain curves may give an indication of the effect and magnitude of $\gamma \rightarrow \alpha'$ direct transformation accompanied by $\gamma \rightarrow \varepsilon \rightarrow \alpha'$ transformation as well as may be $\varepsilon \rightarrow \alpha'$ transformation. At temperatures above 0°C, there was a general improvement in the predicted values that was necessitated by an assumed gradual transformation to α'-martensite. In reality this gradual transformation must have been due to the ε-martensite which later transformed to α'-martensite.

The amount of stress that can be sustained by austenite seems to contribute uniquely to the final stress attained. It is important to note that in finite element code employed, it was not possible to take into consideration the partition or sharing of strain or stress at micro-level. It is a known physical fact that there is some partitioning of strain or stress [Fis77]. The difference in the values of predicted and experimental values could give an indication on the degree of partitioning or sharing between the two phases. This difference may also give the degree of redundant deformations or internal shearing [Bol95]. The rate of austenite-martensite transformation and the subsequent amount of martensite generated varies with temperature, history of deformation, and the level of plastic strain. It is known that this affects the overall work hardening rate, strain hardening and the stress-strain partition or sharing between the phases.

The question of martensite distribution could lead to errors in the composite true stresses computed. The distribution has an influence on the direct mechanical action of surfaces and interfaces through the surface or interface stress during deformation [Spa00]. In our analysis, at each increment, the same “average” strain history was assumed which in reality is not the case. This procedure ignores the critical effects of interactions between disparate regions in the evolution of deformation fields.

The error introduced in these assumptions may be significant depending on temperature, volume of martensite considered and the level of strain. Important aspects like the rate of transformation, temperature and level of strain are expected to influence the accuracy [Coh53, Ros59]. It can be concluded that though the composite true stress is uniquely influenced by the amount of α'-martensite other factors may play also significant roles. The rate of formation of α'-martensite and interphase interaction may be important in determining the final stresses attained.

6.2.2 STRESS DISTRIBUTION

Selected stress distribution contour maps are shown for the steel, X5CrNi18.10 in Figures 6.13-6.18. Figures 6.16-6.18 shows stress distributions for a constant displacement or constant deformation gradient tensor (true strain 0.15), but different constitutive relationships between the phases. As can be observed, the stress distribution depends on stress-strain relationship of the individual phases. It would naturally be expected that the stress distribution is also affected by the boundary conditions and the distribution of the phases. These two aspects have been clearly demonstrated in the past [Jin78, Ank82, Leg98], and therefore were not tested in our case. There seem to be an orientation effect on the stress distribution as can be seen from Fig 6.13. In the vicinity of the martensite phase, the stresses are not necessarily high nor do we have unusual multicontours showing high intensity of stress concentration points. Each finite element was assumed to be either an austenite or martensite grain. As expected, the stress inhomogeneities are accompanied by strain inhomogeneities. Stress gradients can be seen both in the martensite and austenite phases.

Stress distributions are highly influenced by the topology of the phase distribution, yield stress ratio and volume fraction as demonstrated by the contour maps [Bol95]. Given that we are dealing with a real physical phenomenon the stress distribution should be unique. This does not, however, diminish the practical relevance of information that can be extracted from stress distribution contour maps such points of stress concentrations, but the focus will be on the calculation of average quantities able to guide macroscopic constitutive equation development.

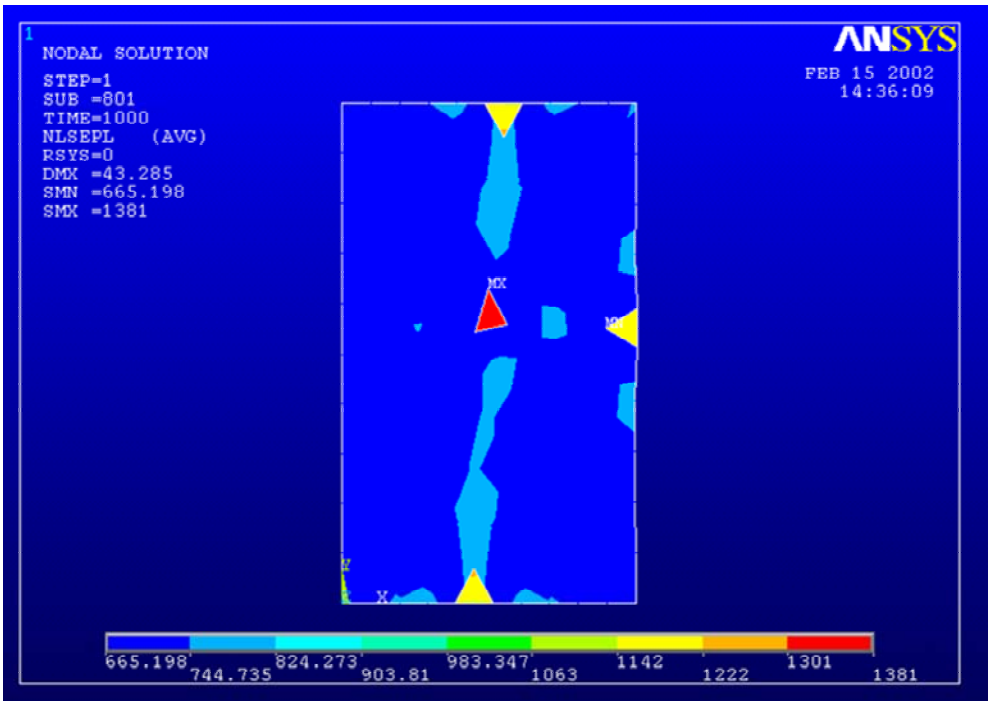

Figure 6.13 FEM nodal solutions at 40°C for the steel X5CrNi18.10 showing stress distribution and an orientation effect in the direction of loading (true strain 0.3). Volume fraction of deformation induced martensite 1% (Fem0).

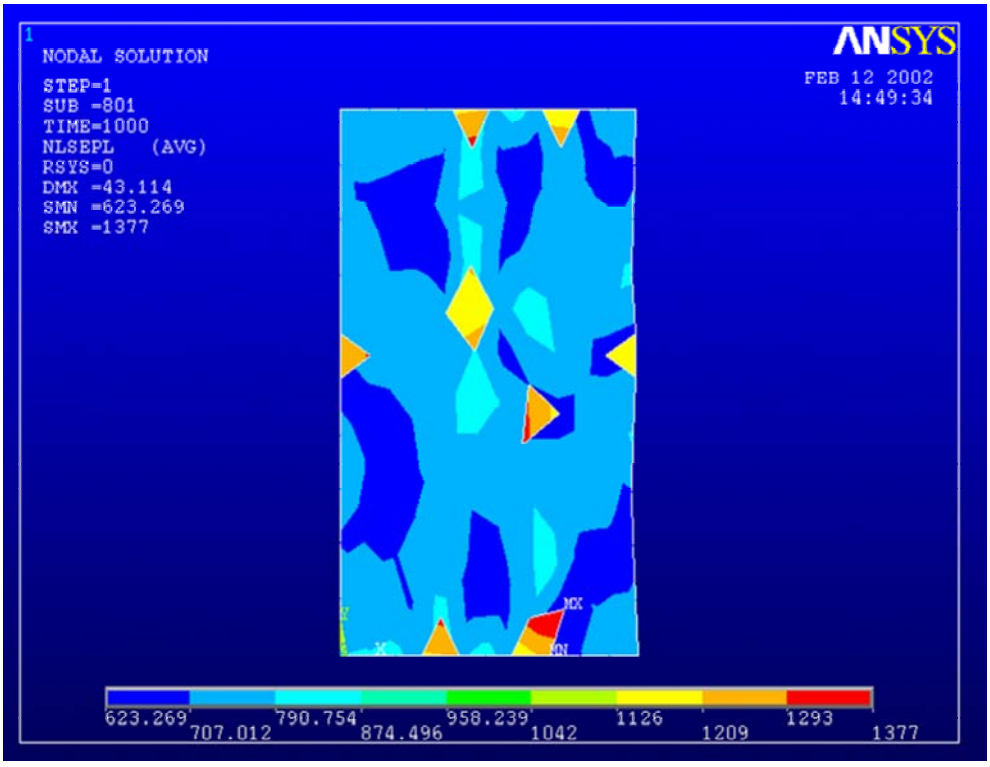

Figure 6.14 FEM nodal solutions for the steel X5CrNi18.10 at 20°C (true strain 0.25).Volume fraction of deformation induced martensite 3% (Fem0).

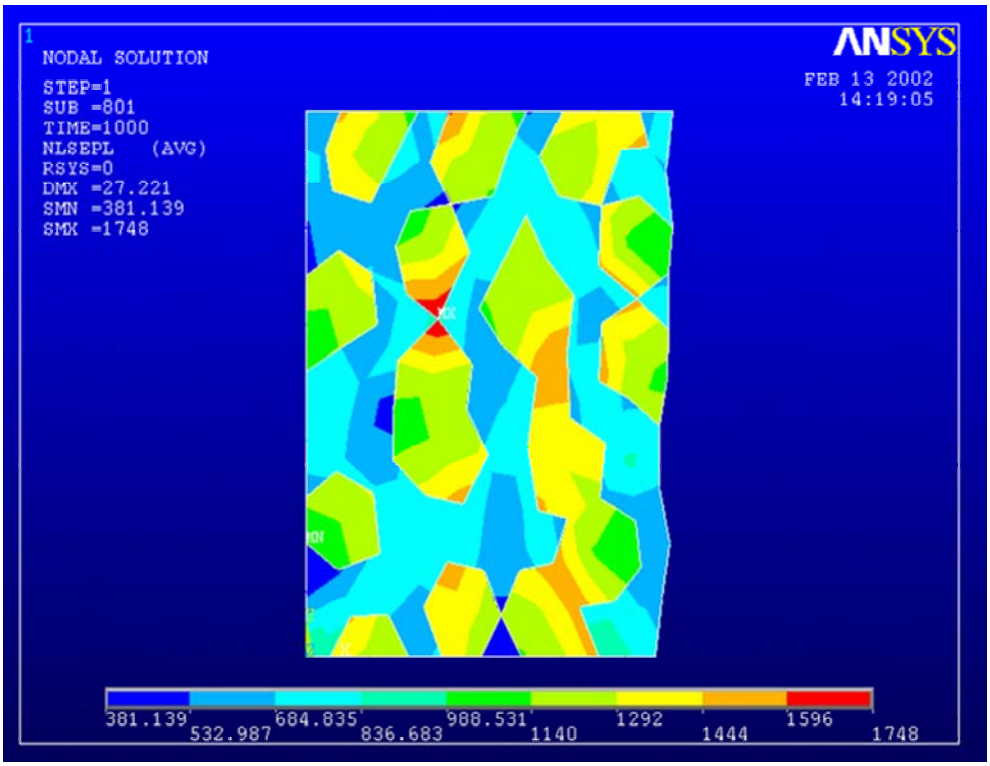

Figure 6.15 FEM nodal solutions showing stress distribution at -40°C (true strain 0.2), volume fraction of deformed martensite 47% (Fem0).

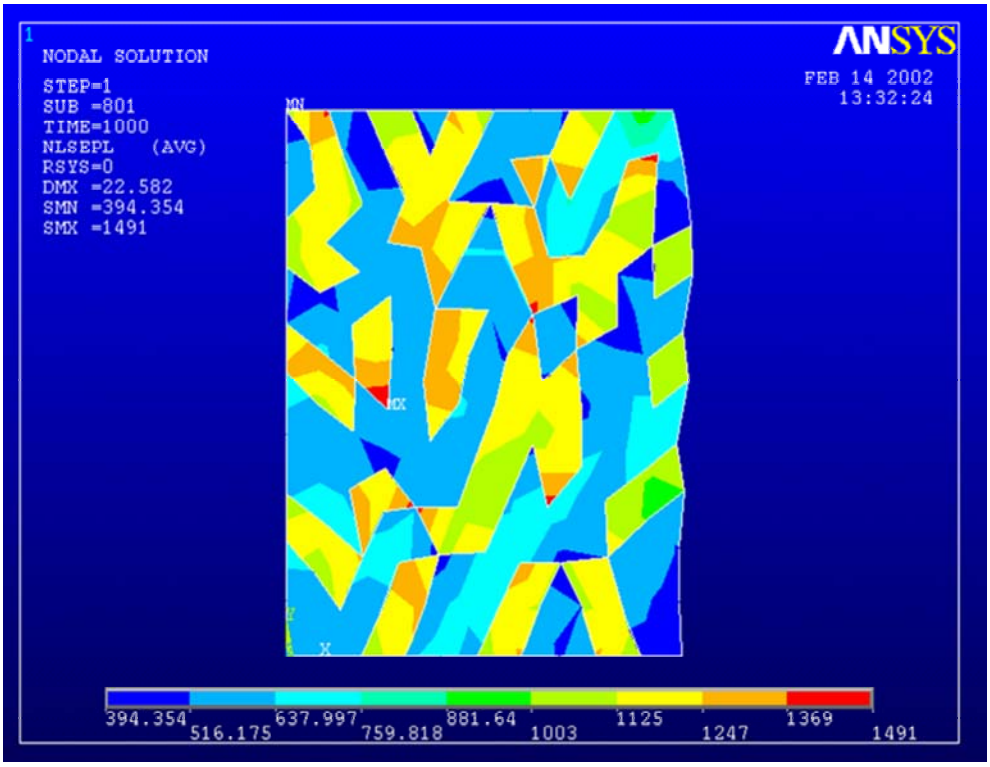

Figure 6.16 FEM nodal solution showing stress distribution at -60°C (true strain 0.15), Volume fraction of deformation induced martensite 39% (Fem0).

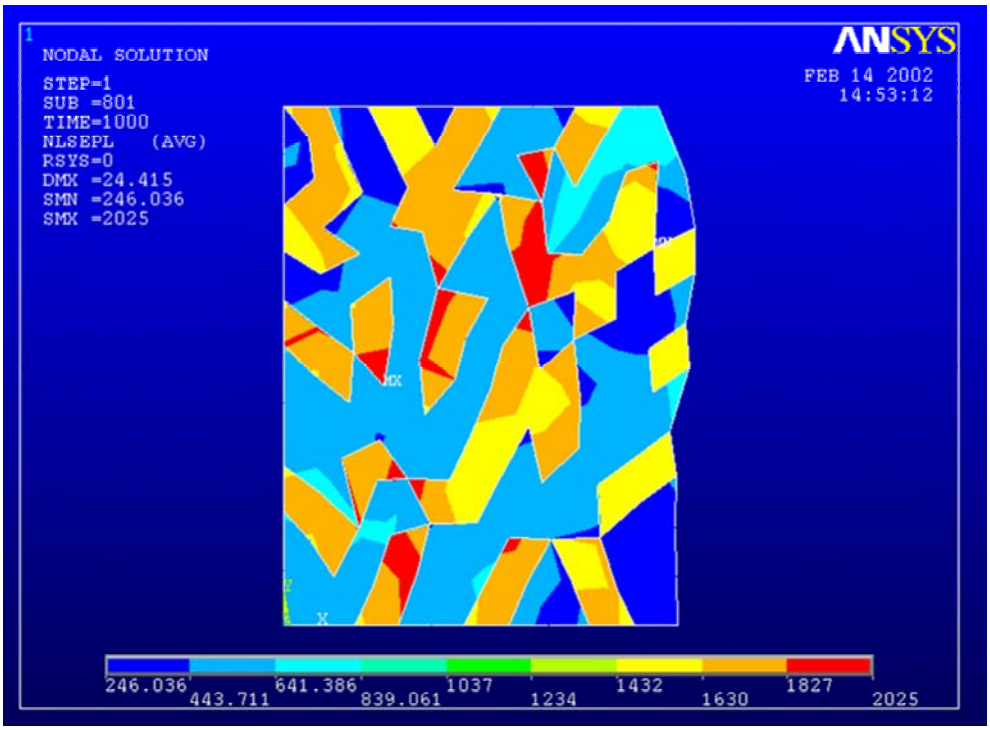

Figure 6.17 FEM nodal solution showing stress distribution at -60°C (true strain 0.15), Volume fraction of deformation induced martensite 39% (Fem2).

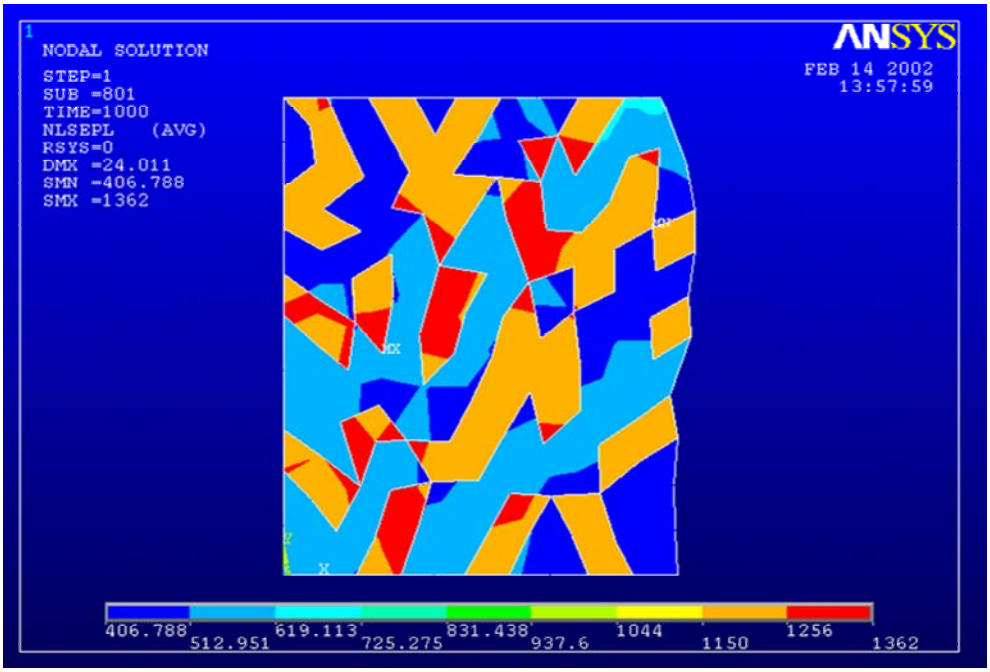

Figure 6.18 FEM nodal solution showing stress distribution at -60°C (true strain 0.15), Volume fraction of deformation induced martensite 39% (Fem3).

6.2.3 EFFECT OF HARDENING

The work-hardening seems to increase with increased plastic deformation as the temperature decreases. At low temperatures, there are high work-hardening rates in the early stages of deformation followed by a faster decay. The rate of austenite to martensite transformation is much higher at low temperatures. As the temperature increases, the rate of transformation decreases i.e. there is more progressive transformation as plastic deformation increases. In the FEM simulation, the global increment of martensite was part of the input information. Transformation kinetics itself was taken from experiments. The increment of martensite was evenly distributed on grain-per-grain basis (the finite elements) and the corresponding displacement imposed at the end of the transformation step. This procedure assumes that transformation starts simultaneously at the selected positions and continue at the same rate till the transformation is completed. This implies that the properties are calculated from a completely transformed and stable volume.

FEM assumed that hardening is continuously increasing as the deformation increased in proportion to the volume fraction of the individual phases. The effect of hardening seems to be temperature sensitive and more effective at low volume fractions of martensite. At higher temperatures taking into consideration the hardening of the phases leads to lower predicted values while at lower temperatures this leads to higher predicted values. This leads to the hypothesis that at higher temperatures, the effects of others factors which are not captured by FEM may start playing a vital role in enhancing or reducing the hardening of both phases. Factors like the amount of ε-martensite and the rate of $\varepsilon \rightarrow \alpha'$ transformation must have played crucial roles. It has been reported that several ε-martensite variants can be obtained from $\gamma \rightarrow \varepsilon$-martensitic transformation [Yan92]. Energetically, one ε band is an obstacle for other ε bands and one may cross another only if the local shear stress is sufficiently large. Thus, additional energy is necessary leading to significant strain hardening effects [Yan92]. The inability to consider ε-martensite could have led to deviation observed in considering only the hardening of austenite and α'-martensite.

It has been reported that different micromechanisms act at different volume fractions and temperatures [Bol95]. At the interfaces, the normal and tangential strain components are expected to be continuous. The shear component, however, is not continuous. The way this component interacts with both phases at the interface determines how the deformation and hardening proceeds [Bol95]. It is well known that deformation can be caused by movement of interfaces and that the mechanism of deformation is sensitive to the atomic structure of the interfaces [Chr82]. At high deformations, the martensite regions start contacting one another and this may lead to some rotation being imposed on some areas [Bol95]. Grain shape effects have also been reported to influence creep properties [Leg98].

6.3 SIMULATION OF DEFORMATION BEHAVIOUR BY LAW OF MIXTURE

A semi-mechanistic modified Goel model that predicts the flow behaviour of a commercial metastable austenitic, and low alloy Mn-Si-Al steel, has been presented in chapter three. The expressions developed and again given below will be used to calculate the flow curves for our investigated metastable austenitic steel X5CrNi18.10.

The composite flow stress for metastable austenitic steel (see Equation (3.52))is given as:

$$\sigma_C = V_{\gamma R}^0 \left\{ 1 - \left(1 + \frac{e_C^{-B}}{A} \right)^{-1} \right\} k_{\gamma R} \varepsilon_I^{n_{\gamma R}} + k_{\alpha'} \left\{ V_{\gamma R}^0 \left(1 + \frac{e_C^{-B}}{A} \right)^{-1} \right\} \varepsilon_\alpha^{n_{\alpha'}}$$

where $\varepsilon_T = \varepsilon_{\gamma R} + \varepsilon_\gamma^T$ and austenite as the matrix.

The composite flow strain (see Equation (3.53)) is given as:

$$\varepsilon_c = V_{\gamma R} \varepsilon_T + V_{\alpha'} \varepsilon_{\alpha'}$$

The stress-strain partition (see Equation (3.54)) is given as:

$$q = \left(\frac{k_{\alpha'} \varepsilon_{\alpha'}^{n_{\alpha'}} - \sigma_m}{\varepsilon_{\alpha'} - \varepsilon_m} \right)$$

The composite flow stress (see Equation (3.55)) for low alloy high strength multiphase steel is given as:

$$\sigma_C = \left(V_\alpha + V_b + V_{\gamma R} \right) \sigma_m + k_{\alpha'} \left\{ V_{\gamma R}^0 \left(1 + \frac{e_C^{-B}}{A} \right)^{-1} \right\} \varepsilon_\alpha^{n_{\alpha'}}$$

The composite strain (see Equation (3.56)) is given as:

$$\varepsilon_c = \left(V_\alpha + V_b + V_{\gamma R}\right)\varepsilon_m + V_{\alpha'}\varepsilon_{\alpha'}$$

The stress-strain partition is given by Equation (3.54) with ferrite, bainite and retained austenite as matrix.

Total contribution of martensite (see Equation (3.57)) to the flow stress in multiphase steels is given as:

$$V_{\alpha'}\sigma_{\alpha'} = k_{\alpha'}\left\{V_{\gamma R}^0\left(1+\frac{e_C^{-B}}{A}\right)\right\}\varepsilon_\alpha^{n_{\alpha'}}$$

Contribution by the matrix (see Equation (3.58)) is given as:

$$\left(V_\alpha + V_b + V_{\gamma R}\right)\sigma_m = \left(V_\alpha + V_b\right)k_\alpha\left\{\varepsilon_m + \varepsilon_\alpha^T\right\}^{n_\alpha} + V_{\gamma R}^0 k_{\gamma R}\left\{1-\left(1+\frac{e_C^{-B}}{A}\right)^{-1}\right\}\bullet\left\{\varepsilon_m^{n_{\gamma R}}\right\}$$

CALCULATION OF FLOW CURVES

The above equations have been used to generate the flow curves for the steel X5CrNi18.10. Other appropriate expressions for the calculation of the extra strain due to extra dislocations generated as a result of austenite to martensite transformation during the deformation are given in Chapter 3 and in the paper from Bourell [Bou83].

Representative values of Holloman constants for pure austenite, martensite, ferrite phase and other constant shown in Table 6.6 were obtained from literature [Bou83, Goe85] because they studied deformation induced martensite transformation or derived from curve fitting the appropriate expressions with the experimental data (see Figure 5.29 and Table 5.6). Plastic strain values and the amount of martensite formed during deformation were obtained from the experimental data, and the values used as input to calculate the matrix stress. The total matrix strain was calculated from the plastic strain values from the experimental data and the extra strain was estimated using the appropriate expressions and the experimental determined martensite volumes.

It is important to note that the value of constants for pure austenite and martensite can be a source of error. From Figure 6.2, the value of constants used for the simple power law (Fem2) gave reasonable values compared to experimental results at 150°C. It can be assumed that the values of the constants are reasonable from experience, experiments, and literature.

The procedure was as follows;

- Matrix strain was defined following the experimental results.
- The extra strain due to dislocations was estimated using the appropriate expressions and data from Bourell [Bou83].
- The matrix stress was calculated.
- Newton-Raphson method was used to estimate martensite strain.
- The martensite stress was calculated.
- The composite stress was calculated
- The partition parameter of 4500 MPa was found to give the best fit between the experimental and calculated values.

Table 6.6 Parameters used for modified rule of mixtures model

Parameter	Value
k_{α}	450 MPa
$k_{\gamma R}$	689 MPa
$k_{\alpha'}$	1496 MPa
n_{α}	0.24
$n_{\gamma R}$	0.18
$n_{\alpha'}$	0.08
σ_y	350
E	200000 MPa
G (Equation 3.50)	80800 MPa
k (Equation 3.50)	$1.91\times10\text{-}6$ MPa^{-1}
C (Equation 3.51)	2×10^{9} cm^{-2}
g (Equation 3.51)	0.7
a/a_o	1.01
c/a	2.0
A (below 0°C)	1310.56
B (below 0°C)	4.17
A (above 0°C)	0.85
B (above 0°C)	2.5

6.3.1 COMPOSITE STRESS-STRAIN CURVES

The calculated and experimental composite stress-composite strain curves are depicted in Figures 6.19-6.22. For plastic strains of up to 10% there was good agreement between the calculated curve and the experimental curve. Above 10% plastic strain, there was better agreement between the calculated curve and the experimental curve for -60°C as compared to -40°C. For 20°C, Figure 6.20, there was good agreement below 10% plastic strain. Above 10% plastic strain, the model curves lies below the experimental curves. The deviation from the experimental curves seems constant.

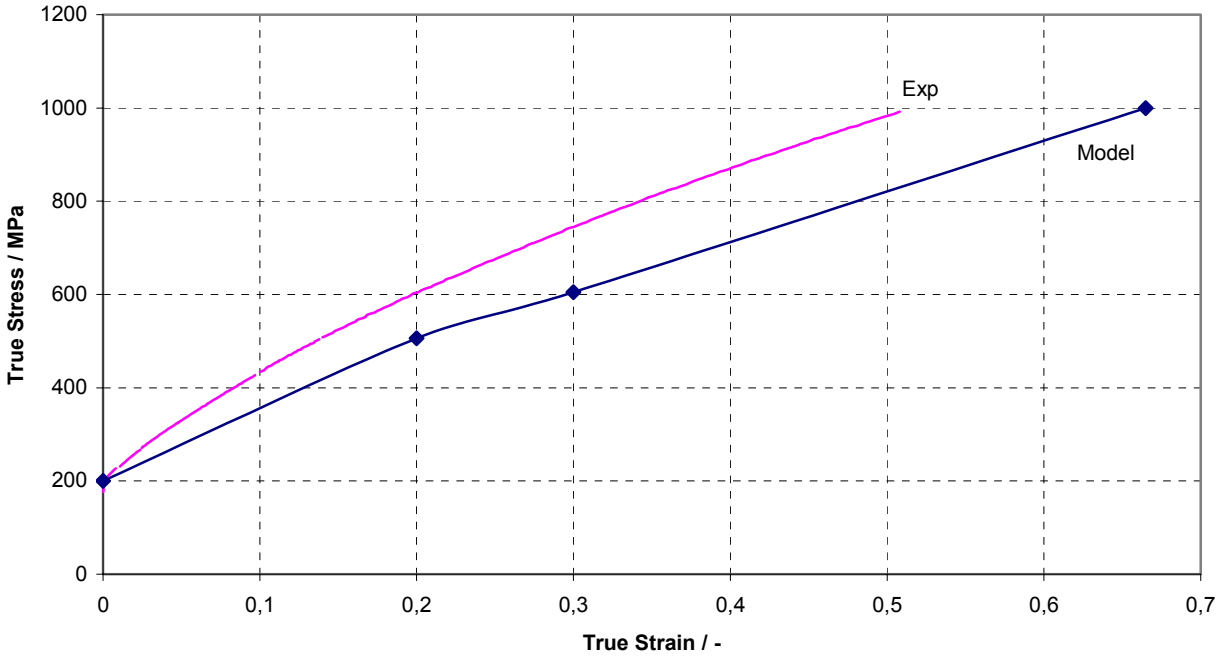

Figure 6.19 True stress-strain curves for the steel X5CrNi18.10 at 40°C; predicting the experimental values with the modified law of mixtures.

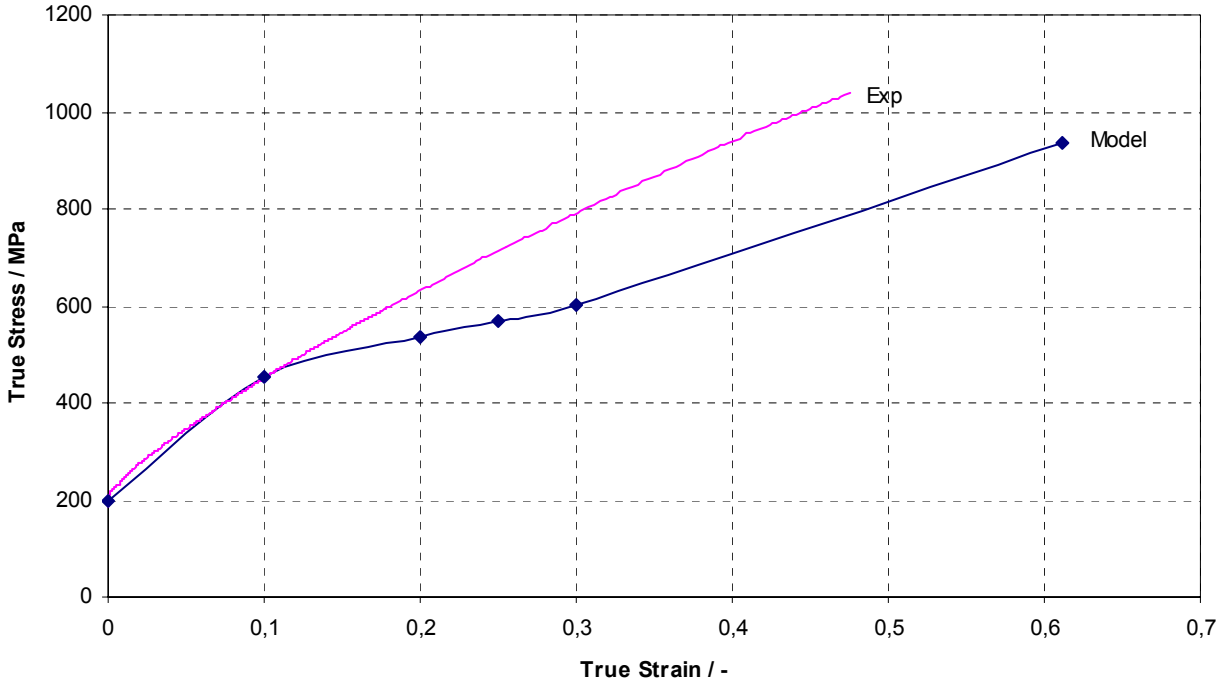

Figure 6.20 True stress-strain curves for the steel X5CrNi18.10 at 20°C; predicting the experimental values with the modified law of mixtures.

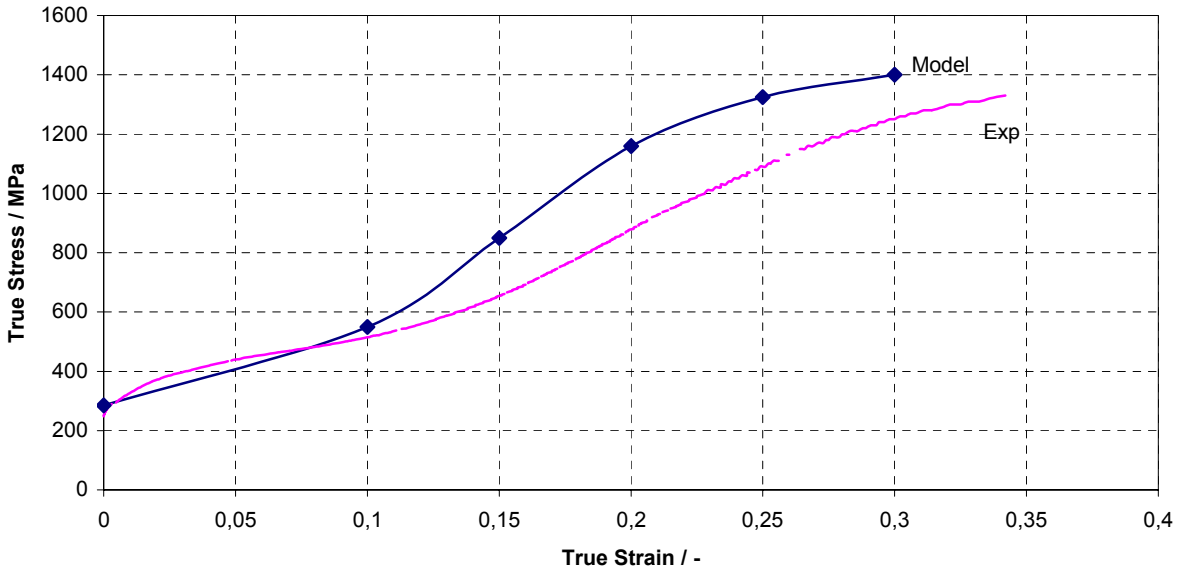

Figure 6.21 True stress-strain curves for the steel X5CrNi18.10 at -40°C; predicting the experimental values with the modified law of mixtures.

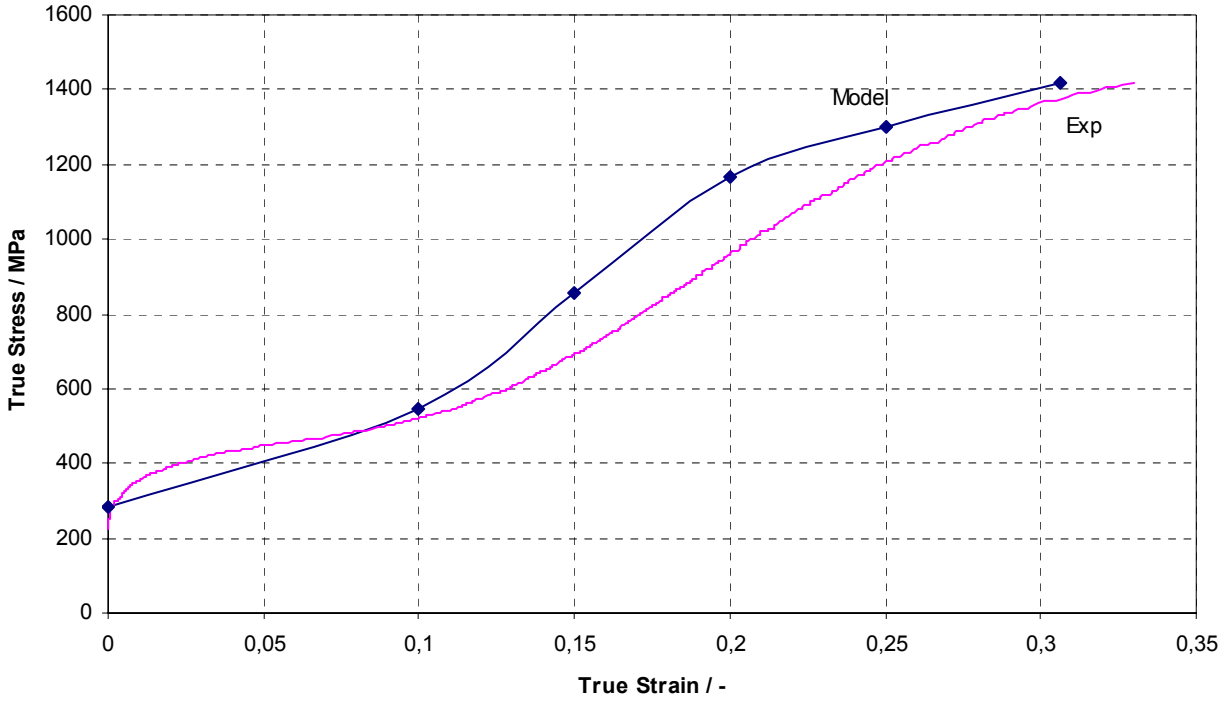

Figure 6.22 True stress-strain curves for the steel X5CrNi18.10 at -60°C; predicting the experimental values with the modified law of mixtures.

At 40°C, Figure 6.19, there is a general deviation in the whole plastic range between the calculated and the experimental curves. The composite stress deviation is small compared to the deviation at 20°C (Figure 6.20). This modified Goel model presented here enforces a “self-consistency” by requiring that the macroscopic strains are equal to the volume averages of the local strain due to each phase plus the phase transformation strain.

At maximum uniform elongation, twice the amount of martensite was formed at 20°C compared to the amount formed at 40°C. In this temperature range, ε-martensite formation, quantity and hardening effects are very important. The model did not consider the amount and effect of ε-martensite phase. At temperatures where the transformation $\varepsilon \rightarrow \alpha'$ plays an important role, failure to consider its effect could have led to the deviations observed. At low temperatures (-40°C and -60°C), the possibilities of phase transformations $\gamma \rightarrow \alpha', \varepsilon \rightarrow \alpha', \gamma \rightarrow \varepsilon, \gamma \rightarrow \varepsilon \rightarrow \alpha'$ which could not be separated and their individual effect taken into account could lead to errors. The model presented does not capture this high rate of phase transformation, nor does it consider the extra dislocations generated due to each individual transformation.

The failure to consider transformation softening below 0°C, could have also contributed to the model predictions being higher than the experimental values in the true stress versus true strain curves. Another source of error could be the stress-strain partition. A constant partition coefficient of 4500 was assumed which may vary with temperature, the amount of martensite, and the level of plastic strain. However, the decomposition of strain is qualitatively correct: the harder phase has a lower strain than the softer phase.

Evolution of martensite volume fraction is generally viewed as function of temperature, plastic strain, and stress state [Str92]. In our analysis, the influence of dislocation hardening caused by strain induced martensitic transformation was considered, but stress state effect was ignored. The flow behaviour of these steels normally involves a complex interaction of slip and transformation effects [Fis00] (orientation and dilatation effects) and the effect of stress-state especially as it impacts on transformation kinetics could lead to errors and thus discrepancy from the experimental values [Ols75, Ols82, Str92]. There is the fact that martensite formed at different levels of plastic strain have different characteristics depending on the dislocation substructure of its parent austenite [Hen83, Kli82]. This implies that the contribution of martensite to the composite stress may vary depending on the level of plastic strain. The complex nature of stress-strain partition and the influence of interphase boundaries may influence the accuracy of the predicted flow stresses.

CHAPTER 7

7 SUMMARY

A study has been made of deformation behaviour accompanying deformation induced martensite transformation in metastable austenitic steel and low alloy Mn-Si-Al steel. The steels were tested in uniaxial tension to different strain levels and at different temperatures. The evolved microstructures were examined using different methods to help in understanding the mechanism of transformation plasticity effect and the underlying factors affecting its occurrence. The flow curves obtained for the steel AISI 304 were simulated using FEM and a modified law of mixtures. The underlying questions were: can the flow curves of steels exhibiting transformation induced plasticity phenomenon be predicted? What are the underlying physical mechanisms?

1. **STEEL AISI 304 (X5CrNi18.10)**

This steel was first austenitised at 1050°C for 30 minutes and then quenched in water. The specimens were then tested in uniaxial tension at different temperatures. After testing, metallographical, magnetic, and TEM specimens were prepared for microstructural characterisation. Microstructural changes were followed using magnetic measurements and optical micrography.

The transformation of austenite to martensite was found to be both a function of strain and temperature. Ludwigson and Berger's transformation kinetics equation was modified to explicitly include the effect of temperature. It is hoped this equation would help the development of coupled constitutive equations and hence the modelling effort in metastable austenitic steels and low alloy high strength multiphase steels.

Temperature-true stress and temperature-true strain transformations diagrams have been constructed and presented for this steel. From these diagrams, possible occurrences of various martensitic variants can be read directly. The formation of α'-martensite was construed to form through the following possible transformation paths: $\gamma \rightarrow \alpha'$, $\gamma \rightarrow \varepsilon \rightarrow \alpha'$.

ε-martensite was found to be stable at high temperatures and could be identified easily but only qualitatively using optical microscopy. However, it was hardly possible to distinguish ε-martensite and α'-martensite in the microstructure at low temperatures. Attempt to quantify ε-martensite using X-ray diffraction or optical microscopy was not successful. The extremely thin ε-martensite lamellas lead to remarkable broadening of the X-ray profiles.

The formation of α'-martensite during deformation leads to formation of inflection points on the flow curves and work-hardening rate versus true strain curves. The ultimate tensile strength and strain attained at maximum uniform elongation was found to be influenced by the rate of transformation of austenite-to-martensite, the hardening behaviour of the various martensitic variants, and the effect the transformations have on structural damage.

The ε-martensite hypothesis first mentioned by Schumann [Schu69] and applied by Weiss [Wei90, Wei95, Wei01, Wei02a, Wei02b] could explain the gradual transformation that was observed at 20°C and 40°C. The gradual rate of austenite transformation may have been due to the formation of metastable ε-martensite variants which later transformed to α'-martensite. ε-martensite was optically identified at all levels of straining except at maximum uniform elongation at these temperatures. At lower temperatures, the high rate of austenite to martensite transformation, $\gamma \rightarrow \alpha'$, resulted in high strength due to martensite but to reduced ductility.

A simple energy hypothesis has been proposed in this work to explain the values of ultimate strength and strain attained at maximum uniform elongation. The hypothesis states that the plastic work that can be sustained by a material before instability remains constant. The main thrust of this hypothesis rest on the premise that internal stored energy at a critical damage state in a material is proportional to the plastic work. This implies that at maximum uniform elongation, a critical damage state in the material has been reached. However, if phase transformation takes place, the amount of plastic work will depend on how the different types of transformations affect the structural damage. Increased hardening results in decreased maximum uniform elongation.

Orientation and accommodation effects which result from austenite-martensite transformation cannot account for the observed maximum uniform elongation normally observed in these steels. Therefore, TRIP-Effect was construed to be as a result of reduction of local stress concentrations due to formation of α'-martensite at these places. Maximum reduction of critical stresses occurs when the α'-martensite is about 10-20%.

An attempt was made to simulate the flow curves using commercially available FEM software (ANSYS). The agreement between calculated and experimental values was strongly dependent on the stress-strain relations, temperature and the material constants used. Deviations observed may have been due to the fact that the rate of austenite-martensite transformation, and the different types of martensite variants formed was not automatically coupled to the software. Loading was done on a completely transformed volume which in reality is not the case.

Attempt was also made to simulate the flow curves of AISI 304 using a modified law of mixture (Goel model) during deformation as it undergoes phase transformations. The modified Goel model proposed here takes into consideration the extra dislocation generated during austenite-martensite phase transformation. The deviations observed were attributed to different rates of phase transformations and the different martensite variants formed that were not considered. It is also possible that the parameters used were not appropriate.

2. Mn-Si-Al STEEL

This steel belongs to a new generation of low alloy high strength multiphase steels. The application of this new generation of high-strength steels with a 25 percent greater strength–to–weight ratio in the transportation industry promises high energy savings. This work was therefore designed to increase understanding between microstructure and mechanical properties with the accompanying transformation induced plasticity.

A laboratory prepared steel sample was investigated for this case. A deformation dilatometer was used to simulate controlled heating and cooling in order to obtain adequate retained austenite at room temperature.

From the microstructural observations and dilatometer curves, a continuous cooling transformation diagram (CCT) diagram and a corresponding time temperature transformation (TTT) diagram was constructed for this steel. Based on the overall transformation behaviour represented in the CCT diagram, two heat treatment routes were selected for the tensile specimens before uniaxial testing. Before uniaxial testing, the initial microstructures of the two heat treatments routes were investigated using optical micrography, X-ray diffraction and transmission electron microscopy.

Colour etching enabled the optical identification of exact location of retained austenite and the identification of other phases that constitute the microstructure of these steels. TEM microscopy revealed that retained austenite appears as thin films or in lamellar form inside the bainitic areas and as globules or islands at the grain boundaries.

An improvement of strain of about 4-8% over the entire temperature range was obtained. This performance is quite remarkable and the increase in ductility was attributed to the effect of phase transformations on fracture kinetics as well as the composite deformation behaviour of the phases which constitute these high strength low alloy multiphase steels.

A cooling rate of 50 K/s from the austenite region and austempering at 330°C for 10 minutes and finally cooling at 50 K/s yielded the best final microstructure and retained austenite of moderate stability that enabled enhanced of ductility to take place. Retained austenite of moderate stability (controlled by the carbon content) for the austempered specimens resulted in a slower rate of strain hardening, gradual transformation of $\gamma \rightarrow \alpha'$ and because the phases harden as deformation progresses, there is a combined enhancement of ductility due to same mechanism as for the steel AISI 304.

The composite deformation behaviour of the constituent phases and in addition to retained austenite plays an important role in enhancing the mechanical properties of multiphase high-strength steels for low alloy multiphase steels. The presence of martensite (a sign of insufficient austenite stability) in the initial microstructure was found to negatively influence the enhancement of ductility.

Highly unstable retained austenite in the continuously cooled specimens which transforms very fast and completely to martensite leads to increased strain hardening in the early stages of deformation resulting in higher strength but poor enhancement of ductility.

Retained austenite with moderate stability which transforms gradually or hardly transforms during straining with accompanied strain hardening is responsible for enhanced strength and ductility for the low alloy high strength multiphase steels. From the results of AISI 304, the critical volume fraction of retained austenite that could simultaneously improve the mechanical properties in terms of strength and ductility should be about 15-20%.

3. FUTURE WORK

The development of optimised multiphase steels with improved strength and formability combinations offers the potential for significant weight reduction in many applications, including automobiles. Due to their complex microstructures, the development and utilisation of these steels is still not as widespread as expected. Further microstructural characterisation work on these steels would further improve understanding thus aiding design and production.

Deformation induced martensite formation in metastable austenitic steels is complex. Important would be investigations on metastable austenitic steels with the aim of quantifying and understanding the mechanisms of TRIP-effect. This should focus in particular on the microstructural investigations on martensitic nucleation, growth and kinetics especially as it impacts on damage behaviour of the material using transmission electron microscopy (TEM).

The differentiation and quantification of various martensite variants (ε, α') which normally form simultaneously is still not adequately addressed.

The influence of strain rate and multiaxial stress state on deformation induced martensite formation needs to be further investigated.

The transformation kinetic equation proposed in this work needs to be modified to take into account multiaxial stress state.

The extraction of macroscopic properties of microscopically heterogeneous media has taken varied paths in literature. As demonstrated in this work, the use of Representative Volume Element (RVE) with appropriate constitutive equations could yield reasonable results. It is important that the mechanical behaviour of martensite phase be investigated as a precondition of successful modelling work for the steel AISI 304.

Further work on development of appropriate constitutive equations which take into consideration phase transformations and can easily be applied in FEM in both uniaxial and multiaxial stress systems would substantially aid the modelling effort in these steels especially in the framework of RVE.

The plastic work hypothesis proposed in this work could act as sound basis for the development of damage model that describes the critical condition at the point of instability (Necking Phenomenon) taking into consideration the phase transformations.

BIBLIOGRAPHY

[ANS01] ANSYS Theory Reference, 001242, Eleventh Edition, SAS IP, Inc., 1999.

[Ang54] Angel, T., Formation of Martensite in Austenitic Stainless Steels, Journal of Iron and Steel Institute (1954), 165-174.

[Ank82] Ankem, S., Margolin, H., Finite Element Method (FEM) Calculations of Stress-Strain Behaviour of Alpha-Beta Ti-Mn Alloys: Part I. Stress-Strain Relations.

[Bae00] Bae, J.H., Park, S.J., Oh, K.H., Lee, C.G., Kim, J.J., Prediction of mechanical properties of TRIP steels by FEM and micromechanics, Proc. Of the 5TH Asia-Pacific Symposium on Advances in Engineering Plasticity and Its Applications (AEPA 2000), Hong Kong, 12-16 June, 2000, Trans. Tech. Pub., Switzerland, 449-454.

[Ber97] Bergeon, N., Guenin, G., Esnouf, C., Characterization of the stress-induced ε-martensite in a Fe-Mn-Si-Al-Cr-Ni Shape memory alloy: microstructure observation at different scales, mechanisms of formation and growth, Mater. Sci. Eng. A238 (1997), 309-316.

[Ble98] Bleck, W., Kranz, S., Ohlert, J., TRIP-Stähle-Eine neue klasse hochfeste, kaltformbare Stähle, Anwendungsforschung 4 (1998), Studiengesellschaft Anwendung e.V.

[Bol95] Bolmaro, R.E., Browning, R.V., Guerra, F.M., Rollett, A.D., Finite element method simulations of two-phase material plastic strain, Mater. Sci. Eng. A 196 (1995), 53-63.

[Bou83] Bourell, D.L., Rizk, A., Influence of martensite transformation strain on the ductility of dual-phase steels, Acta metall. 31 (1983), 609-617.

[Che00] Cherkaoui, M., Berveiller, M., Mechanics of Materials undergoing phase change: A micro-macro approach for Transformation Induced Plasticity, Zeitschrift für Angw. Math. Mech. 80 (2000), 219-232.

[Chi97] Chiro, A., Root, J.H., Yue, S., Hot Workability of Steels and Light Alloys-composites, Proc. Of the Internat. Symp., Montreal, CDN, AUG 24-28,1997, 515.

[Chr82] Christian, J.W., Deformation by moving Interfaces, Metall.Trans. A 13 (1982), 509-536.

[Cut99] Cuttino, J.F., Andrew, J.R., Piwonka, T.S., Developments in Thin-Wall Iron Casting technology, AFS Transactions 99-189 (1999), 363-372.

[Dav78a] Davies, R.G., Mechanical Properties of Zero-Carbon Ferrite-Plus-Martensite Structure, Metall. Trans. A 9 (1978), 451-455.

[Dav78b] Davies, R.G., Influence of Martensite Composition and Content on the Properties of Dual Phase Steels, Metall. Trans. A 9 (1978), 671-679.

[Ebe98] Eberle, K., Harlet, Ph., Cantinieaux, P., Populiere, M.V., New thermomechanical strategies for the realization of multiphase steels showing a transformation induced plasticity(TRIP) effect, 40TH Mechanical Working and Steel Processing Conference, PROC., ISS, Vol. XXVI, Pittsburgh, PA, USA, Oct 25-28, 1998, Iron and Steel Society, ISBN 1-886362-28-9, 251-258.

[Eck95] Eckstein, C., Weiß, A., Eckstein, H.J., Der Einfluß martensitischer Gefügeausbildung in Cr-Ni-Stählen auf das Lochfraßverhalten, Materials and Corrosion 46 (1995), 76-82.

[Ehr99] Ehrhardt, B., Verbesserung der Umformeigenschaften von hochfestem Warm- und Kaltband aus niedrig legierten Stählen durch Restaustenit, Dissertation, RWTH Aachen, 1999.

[Fis96] Fischer, F.D., Sun, Q.P., Tanaka, K., Transformation-induced plasticity (TRIP), Appl. Mech. Rev. 49 (1996), 317-364.

[Fis97] Fischer, F.D., Berveiler, M., Mechanics of Solids with Phase Change, Springer Wien, New York, (1997).

[Fis00] Fischer, F.D., Reisner, G., Werner, E., Tanaka, K., Cailletaud, G., Antretter, T., A New View on transformation induced plasticity(TRIP), International Journal of Plasticity 16 (2000), 723-748.

[Fis77] Fischmeister, H., Karlsson, B., Plastizitätseigenschaften grob-zweiphasiger Werkstoffe, Z. Metallkund. Bd. 68 (1977), 311-327.

[Fro98] Frommeyer, G., Grässel, O., High strength TRIP/TWIP and superplastic steels: development, properties, application, La Revue de Metallurgie-CIT (1998), 1299-1310.

[Gan92] Ganghoffer, J.F., Dennis, S., Gautier, E., Simon, A., Simonsson, K., Sjöström, S., Micromechanical simulation of martensitic transformation by finite elements, in: H. Fujwara, T. Abe, K. Tanaka (Ed), Proc. Int. Conf. Residual stresses, Tokushima, Japan, July 23-26, 1991, Elsevier Applied Science Publishers, London-New York, 1992, 1215-1220.

[Goe85] Goel, N.C., Sangal, S., Tangri K., A Theoretical Model for the Flow Behaviour of Commercial Dual-Phase Steels Containing Metastable Retained Austenite: Part I Derivation of Flow Curve Equations, Metall. Tans. A 16 (1985), 2013-2021.

[Gre65] Greenwood, G.W., Johnson, R.H., The deformation of metals under small stresses during phase transformation, Proc. Roy. Soc. A 283 (1965), 403-422.

[Hen83] Hensger, K.E., Klimanek, P., Texturänderungen bei der hochtemperaturthermomechanischen Behandlung von Federstahl, Freiberger Forschungshefte B 236 (1982), 68-108.

[Han97a] Hanzaki, A.Z., Yue, S., Ferrite Formation Characteristics in Si-Mn TRIP Steels, ISIJ International 37(1997), 583-589.

[Han97b] Hanzaki, A.Z., Hodgson, P.D. Yue S., Retained Austenite Characteristics in Thermomechanically processed Si-Mn Transformation-Induced Plasticity Steels, Metall. Trans. A 28(1997), 2405-2414.

[Iwa01] Iwamoto, T., Kawagishi, Y., Tsuta, T., Morita, S., Identification of constitutive equation for TRIP steel and its application to improve mechanical properties, JSME International Journal, A 44 (2001), 443-453.

[Jac98] Jacques, P., Eberle, K., Harlet, Ph., Delannay F., Development and Characterization of a Cold-Rolled Low Silicon TRIP-Assisted Multiphase Steel: a New Opportunity for the Automotive Steel Industry, 40TH Mechanical Working and Steel Processing Conference, PROC., ISS, Vol. XXVI, Pittsburgh, PA, USA, Oct 25-28, 1998, Iron and Steel Society, ISBN 1-886 362-28-9, 239-250

[Jin78] Jindrich, J., Calculation of stress-strain curve and stress and strain distributions for an α-β Ti-8 Mn Alloy, Mater. Sci. Eng. 34 (1978), 203-211.

[Kli82] Klimanek, P., Große, G., Hensger, K.E., Martin, U., Untersuchungen zum Einfluß einer HTMB auf die Realstruktur von Federstählen, Freiberger Forschungshefte B 225 (1982), 6-63.

[Kou01] Kouznetsova, V., Brekelmans, A.M., Baaijens, F.P.T., An approach to micro-macro modelling of heterogeneous materials, Computational Mechanics 27 (2001), 37-48.

[Kra99] Kranz, W.S., Mechanish-technologische Eigenschaften metastabiler austenitischer Edelstähle und deren Beeinflussung durch den TRIP-Effekt, Dr-Ing. Dissertation, Aachen, 1999.

[Kru02] Kruijver, S., Zhao, L., Sietsma, J., Offerman, E., Dijk, N., Margulies, L., Lauridsen, E., Grigull, S., Poulsen, H., Zwaag, S., In situ observations on the austenite stability in TRIP-steel during tensile testing, Steel research 73 (2002), 236-241.

[Kuj02] Kujanpää, A, Anelli, E., Nunzio, P.E., Wade, B., Ferritic-bainitic and TRIP steels for improved combinations of strength and ductililty, European Commission, technical steel research, No. 7210-PR/092.

[Leg98] Leggoe, J.W., Mammoli, A.A., Bush, M.B., Hu, X.Z., Finite element modelling of deformation in particulate reinforced metal matrix composites with random local microstructures variations, Acta metal. 17 (1998), 6075-6088.

[Lud69] Ludwigson, D.C., Berger J.A., Plastic behaviour of metastable austenitic stainless steels, Journal of the Iron and Steel Institute (1969), 63-69.

[Lun02] Lung, T., Drillet, J., Couturier, A., Olier, C., Detailed study of the transformation mechanism in ferrous TRIP aided steels, Steel research 73 (2002), 218-224.

[Mah02] Mahieu, J., Dooren, D., Liesbeth, B., Cooman, B., Influence of Al, Si and P on the kinetics of intercritical annealing of TRIP-aided steels: thermodynamical prediction and experimental verification, Steel research 73 (2002), 267-273.

[Mar97] Marketz, F., Computational micromechanics studies of Martensitic Transformations, VDI Fortschrittsberichte, Reihe 5 Nr. 491 (1997).

[Mat02] Matsuda, H., Kitano, F., Hasegawa, K., Urabe, T., Hosoya, Y., Metallurgy of continuously annealed high strength TRIP steel sheet, steel research 73 (2002), 211-217.

[Min96] Minota, T., Torizuka, S., Ogawa, A., Nikura, M., Modelling of Transformation Behaviour and Compositional Partitioning in TRIP Steel, ISIJ International, 36 (1996), 201-207.

[Oll88] Ollilainen, V., The Influence of Structure and Alloying on the Cold-formability of Ferritic steels and the Utility of Uniaxial Tensile Testing in its Assessments, Dissertation, Helsinki University of Technology, (1988).

[Ols75] Olson, G.B., Cohen, M., Kinetics of Strain-induced Martensitic Nucleation, Metall. Trans. A 6 (1975), 791-795.

[Ols78] Olson, G.B., Azrin, M., Transformation Behaviour of TRIP steels, Metall. Trans. A 9 (1978), 713-721.

[Ols82] Olson, G.B., Cohen, M., Stress-Assisted Isothermal Martensitic Transformation: Application to TRIP Steels, Metall. Trans. A 13 (1982), 1907-1913.

[Par97] Park, S.H., Choo, W.Y., Ko, H.J., Kim, N.J., Hot Workability of Steels and Light Alloys-composites, Proc. Of the Internat. Symp., Montreal, CDN, AUG 24-28,1997, 493, ISBN 0-919086-66-7.

[Par98] Park, S.H., Han, H.N., Lee, J.K., Lee, K.J., Microstructural Evolution of Hot Rolled TRIP Steels During Cooling Control, 40TH Mechanical Working and Steel Processing Conference, PROC., ISS, Vol. XXVI, Pittsburgh, PA, USA, Oct 25-28, 1998, Iron and Steel Society, ISBN 1-886 362-28-9, 283-291.

[Pat53] Patel, J.R., Cohen, M., Criterion for the action of applied stress in the martensitic transformation, Acta Metall. 1 (1953), 531-537.

[Pic98] Pichler, A., Stiaszny, P., Potzinger, R., Tikal, R., Werner, E., TRIP Steels with Reduced Si content, 40TH Mechanical Working and Steel Processing Conference, PROC., ISS, Vol. XXVI, Pittsburgh, PA, USA, Oct 25-28, 1998, Iron and Steel Society, ISBN 1-886 362-28-9, 259-274

[Rei97] Reisner, G., Micromechanical Modelling of Strain Induced Martensitic Transformation in Cu-Fe-Alloys and in Low Alloyed TRIP-Steels, VDI Fortschrittsberichte, Reihe 18 Nr.214 (1997).

[Rem77] Remy, L., Kinetics of Strain-Induced fcc-hcp Martensitic Transformation, Metall. Trans. A 8 (1977), 253-258.

[Ros59] Rosenthal, P.C., Porter, L.F., Effect of applied tensile stress on phase transformation in steel, Acta Metall. 7 (1959), 504-514.

[Sch00] Schoß, V., Martensitische Umwandlung und Ermündung austenitische Edelstähle, Gefügeveränderungen und Möglichkeiten der Früherkennung von Ermüdungsschädigungen, Dissertation, TU Bergakademie Freiberg (2000).

[Sin89] Sinha, A.K., Ferrous Physical Metallurgy, Butterworth Publishers, MA, USA (1989), ISBN 0409901393.

[Shu69] Shumann, H., Fircks, H.J., Die martensitische Umwandlungen in kohlenstoffarmen austenitischen Chrom-Nickel-Stählen, Arch. Eisenhüttenwesen, 7 (1969), 561-568.

[Spa00] Spaepen, F., Interfaces and stresses in thin films, Acta mater. 48 (2000), 31-42.

[Str92] Stringfellow, R.G., Parks, D.M., Olson, G.B., A Constitutive Model for Transformation Plasticity accompanying Strain-induced Martensitic Transformations in Metastable Austenitic Steels, Acta Metall. Mater. 40 (1992), 1703-1716.

[Sug93] Sugimoto, K., Misu, M., Kobayashi, M., Shirasawa, H., Effects of Second Phase Morphology on Retained Austenite Morphology and Tensile Properties in a TRIP-aided Dual-phase Steel Sheet, ISIJ International 33 (1993), 775-782.

[Sug99] Sugimoto, K., Nagasaka, A., Kobayashi, M., Hashimoto, S., Effects of Retained Austenite Parameters on Warm Stretch-flangeability in TRIP-aided Dual-phase Sheet Steels, ISIJ International, 39 (1999), 56-63.

[Sun73] Sundström, B.O., Elastic-Plastic Behaviour of WC-Co Analysed by Continuum Mechanics, Mater. Sci. Eng. 12 (1973), 265-276.

[Tam82] Tamura, I., Deformation-induced martensitic transformation and transformation-induced plasticity in steels, Metals science 16 (1982), 245-253.

[Tim02] Timokhina, B., Hodgson, P.D., Pereloma, E.V., Effect of alloying elements on the microstructure-property relationship in thermomechanically processed C-Mn-Si-Al TRIP steels, Steel research 73 (2002), 274-279.

[Tra02] Traint, S., Andreas, P., Hauzenberger, K., Stiaszny, P., Werner, E., Influence of silicon, aluminium, phosphorus and copper on the phase transformations of low alloyed TRIP-steels, Steel research 73 (2002), 259-266.

[Tsu93] Tsuta, T., Cortes, R., Jorge, A., Flow stress and phase transformation analyses in austenitic stainless steel under cold working (Part2, Incremental theory under multiaxial stress state by the Finite element method), JSME International Journal, A 36 (1993), 63-72.

[Tsu00] Tsuchida, N., Tomota, Y., A micromechanic modelling for transformation induced plasticity in steels, Mater. Sci. Eng. A285 (2000), 345-352.

[Vas02] Vasilakos, A.N., Ohlert, J., Giasla, K., Hademenopoulos, G.N., Bleck, W., Low-alloy TRIP steel: a correlation between mechanical properties and the retained austenite stability, steel research 73 (2002), 249-252.

[Vil85] Villars P., Cluert, L.D., Pearson's Handbook of Crystallographic Data for Intermetallic phases (volume 3), American Society for Metals, (1985).

[Vog90] Vogt, J.B., Foct, J., Nilssion, J.O., Scandinavian Journal of Metallurgy (1990), 273-277.

[Wak77] Wakasa, K., Nakamura, T., Transformation-induced plasticity in two-phase Fe-Cr-Ni alloys, Journal of Material Science 12 (1977), 1438-1442.

[Wei90] Weiß, A., Eckstein, H.J., Martensitbildung in Korrosionsbeständiger Stähle, In; Eckstein, H.J. (Hrg.), Korrosionsbeständige Stähle, Deutscher Verlag für Grundstoffindustrie GmbH, Leipzig, 1990, 89-98.

[Wei92] Weiß, A., Eckstein, H.J., Der Einfluß äußerer Spannungen auf die spannungs- und verformungsinduzierte Martensitbildung in austenitischen und austenitisch-ferritischen Cr-Ni-Stählen, Neue Hütte 12 (1992), 438-450.

[Wei95] Weiß, A., Fang, X., Eckstein, J.H., Eckstein, C., Dahl, W., Effect of Cryoforming of austenitic Cr-Ni-Steels at 77K on martensitic transformation and work-hardening characteristics, Steel Research 66 (1995), 495-500.

[Wei01] Weiß, A., Entwicklung von Spannung-Temperatur-Umwandlungs-diagrammen zur Beschreibung der verformungsinduzierten Martensitbildung in metastabilen austenitischen CrNi-Stählen, Abschlußbericht zum Forschungsvorhaben PE 579/3-1/3-2.

[Wei02a] Weiß, A., Peisker, D., Tranta, F., Einfluss von Zugspannungen auf die Martensitbildung in metastabiler austenitischen CrNi-Stählen, UTF Science III (2002), 25-30.

[Wei02b] Weiß, A., Peisker, D., Tranta, F., Gutte, H., Einfluss von Nickel auf die Martensitbildung metastabiler austenitische CrNi-Stählen unter Zugbeanspruchung, UTF Science IV (2002), 18-25.

[Wer87] Werner, M., Umwandlungsplastizität und ihre Berücksichtigung bei der Berechnung von Eigenspannungen, Materialkundlich-Technische Reihe 7, Gebrüder Borntraeger Berlin-Stuttgart (1987).

[Wer94] Werner, D., Mikro- und makromechanische Simulation des Deformationsverhaltens von Stählen unter Berücksichtigung von Umwandlungs-und Diffusionsvorgängen, VDI Fortschrittsberichte, Reihe 18 Nr. 141 (1994).

[Yan92] Yang, J.H., Wayman, C.,M., Intersecting-shear mechanisms for the formation of secondary ε martensite variants, Acta Metall. Mater. 40 (1992), 2025-2031.

[Yok96] Yokoi, T., Kawasaki, K., Takahashi, M., Koyama, K., Mizui, M., JSAE Review 17 (1996), 210-212.

[Zac67] Zackay, F.V., Parker, E.R., Fahr, D., Busch, R., The Enhancement of Ductility in High-Strength Steels, Trans. ASM 60 (1967), 252-259.

APPENDIX A

ANSYS IMPLEMENTATION

Below is the procedure for implementation in ANSYS [ANSYS 99]

1. σ_y is determined
2. Stresses are computed based on the trial strain $\{\varepsilon^{tr}\}$

$$\{\varepsilon_n^{tr}\} = \{\varepsilon_n - \{\varepsilon_{n-1}^{pl}\}\}$$
$$\{\sigma^{tr}\} = [D]\{\varepsilon^{tr}\}$$

3. The equivalent stress σ_e is evaluated and compared with σ_y
4. The plastic multiplier λ is determined by a local Newton-Raphson iteration procedure
5. $\Delta\varepsilon^{pl}$ is computed using,

$$\{d\varepsilon^{pl}\} = \lambda\left\{\frac{\partial Q}{\partial \sigma}\right\}$$

6. The current plastic strain is updated using,

$$\{\varepsilon_n^{pl}\} = \{\varepsilon_{n-1}^{pl}\} + \{\Delta\varepsilon^{pl}\}$$

and the elastic strain computed,

$$\{\varepsilon^{pl}\} = \{\varepsilon^{tr}\} - \{\Delta\varepsilon^{pl}\}$$
$$\{\sigma\} = [D]\{\varepsilon^{pl}\}$$

7. The increments in the plastic work $\Delta\kappa$ and the centre of the yield surface $\{\Delta\alpha\}$ are computed and the current values updated,

$$\kappa_n = \kappa_{n-1} + \Delta\kappa$$
$$\{\alpha_n\} = \{\alpha_{n-1}\} + \{\Delta\alpha\}$$

8. For output purposes, an equivalent plastic strain $\hat{\varepsilon}^{pl}$, equivalent plastic strain increment $\Delta\hat{\varepsilon}^{pl}$, equivalent stress parameter σ_e^{pl} and stress ratio are computed.

APPENDIX B

CONSTITUTIVE RELATIONSHIPS

Material nonlinearities are due to the nonlinear relationship between stress and strain, that is, the stress is a nonlinear function of the strain. The stress depends on the strain history as well as the strain itself. We assumed a Rate-independent plasticity characterized by the irreversible straining that occurs in a material once a certain level of stress is reached. The plastic strains are assumed to develop instantaneously, that is, independent of time.

B.1 YIELD CRITERION

The yield criterion determines the stress level at which yielding is initiated and is given as:

$$\sigma_y = f(\sigma)$$

B.2 FLOW RULE

The flow rule determines the direction of plastic straining:

$$\left(d\varepsilon^{pl}\right) = \lambda\left\{\frac{\partial Q}{\partial \sigma}\right\}$$

Where

λ - Plastic multiplier (which determines the amount of plastic straining)

Q - Function of stress termed the plastic potential (which determines the direction of plastic straining)

B.3 HARDENING RULE

The hardening rule describes the changing of the yield surface with progressive yielding, so that conditions for subsequent yielding can be established. The main issue is how to determine the functional dependence of yield stresses on the plastic loading history in a simple and realistic manner. Several models called hardenings rules have been proposed to describe this relationship.

Isotropic hardening rule; the loading function is given as:

$$f(\sigma,\kappa)=\sigma^2-\kappa^2$$

Kinematic hardening rule; the loading function is given as:

$$f(\sigma,\alpha)=(\sigma-\alpha)^2-\sigma_0^2$$

Mixed hardening rule; the loading function is given as:

$$f(\sigma,\alpha,\kappa)=\{\sigma-(1-M)\alpha\}^2-\{(1-M)\sigma_0+M\kappa\}^2$$

We assumed a kinematic hardening, where the yield surface remains constant in size but translates in stress space with progressive yielding.